Universidade do Minho
Escola de Ciências

Carlos Miguel da Silva Costa

Electroactive polymer based porous membranes for energy storage applications

Junho de 2014

Universidade do Minho
Escola de Ciências

Carlos Miguel da Silva Costa

Electroactive polymer based porous membranes for energy storage applications

Tese de Doutoramento
Doutoramento em Ciências, Especialidade em Física

Trabalho efectuado sob a orientação do
Professor Doutor Senentxu Lanceros-Méndez
Professor Doutor José Gerardo Rocha
Doutor Vitor Sencadas

Junho de 2014

To my parents for everything

To my wife for existing

"E quando à tua frente se abrirem muitas estradas e não souberes a que hás-de escolher, não metas por uma ao acaso, senta-te e espera. Respira com a mesma profundidade confiante com que respiraste no dia em que vieste ao mundo, e sem deixares que nada te distraia, espera e volta a esperar. Fica quieta, em silêncio, e ouve o teu coração. Quando ele te falar, levanta-te, e vai onde ele te levar".

Susanna Tamaro, *Vai Aonde Te Leva o Coração*

Acknowledgements

To the Foundation for Science and Technology-FCT (grant SFRH/BD/68499/2010) by the financial support for the realization of this work.

To my supervisor Professor Senentxu Lancers-Méndez, I appreciate the opportunity to work with him again, all transmitted scientific knowledge and friendship built over the years of working together.

To my co-supervisors Professor Gerardo and Vitor, thank you for all the support and helping me whenever I needed.

To Professora Manuela for her availability and support.

To Professor José Luis Gómez Ribelles at Polytechnic University of Valencia and Professor Bruno Scrosati and Giovanni B. Appetecchi at "La Sapienza" University of Rome by the reception in their universities, scientific support and friendship. My stay in both cities was memorable.

To all the colleagues of the ESM group who helped me and encouraged. I have only these words: thank you very much.

To my family and friends who directly or indirectly contributed to this work and are not mentioned, my inlaws (Sr. Manuel and D. Conceição) and D. Rosinda.

To My Parents, João and Conceição and My wife Teresa for all that signify to me: you are the reason of my life.

Abstract

In the field of mobile applications the efficient storage of energy is one of the most critical issues. Lithium ion batteries are lighter, cheaper, show higher energy density (210Wh kg^{-1}), no memory effect, longer service-life and higher number of charge/discharge cycles than other battery solutions. The separator membrane is placed between the anode and cathode and serves as the medium for the transfer of charge, being a critical components for the performance of the batteries.

Polymers such as PVDF and its copolymers poly(vinylidene fluoride-co-trifluoroethylene), P(VDF-TrFE), poly(vinylidene fluoride-co-hexafluoropropylene), P(VDF-HFP), and poly(vinylidene fluoride-co-chlorotrifluoroethylene), P(VDF-CTFE) are increasingly investigated for their use as battery separators due to their high polarity, excellent thermal and mechanical properties, controllable porosity and wettability by organic solvents, being also chemically inert and stable in cathodic environment.

Despite previous works in some of the PVDF co-polymers, there is no systematic investigations on poly(vinylidene fluoride-trifluoroethylene), P(VDF-TrFE), despite its large potential for this specific application.

The objective of this work is thus establish the suitability of P(VDF-TrFE) for battery separators and to control of its structure, stability and ionic conductivity in order to increase performance of the material as battery separators. It is shown that solvent evaporation at room temperature allows the preparation of membranes with degrees of porosity from 70% to 80% leading to electrolyte solution uptakes from 250% up to 600%.

The preparation of composites of P(VDF-TrFE) with lithium salts allows ionic conductivity values of the electrolytes of 2.3×10^{-6} S/cm at 120 °C. These composites show good overall electrochemical stability.

A novel type of polymer blend based on poly(vinylidene fluoride-trifluoroethylene)/poly(ethylene oxide), P(VDF-TrFE)/PEO, was prepared and it was found that the microstructure, hydrophilicity and electrolyte uptake strongly depend on PEO content within the blend. For this blend, the best value of ionic conductivity at room temperature was 0.25 mS cm^{-1} for the 60/40 membrane.

It was also verified that the ionic conductivity of the membrane is depend on the anion size of the salts present in the electrolyte solution, affecting also the electrolyte uptake value.

Batteries fabricated with the separators developed in this work within Li/$LiFePO_4$ and Li/Sn-C cells revealed very good cycling performance even at high current rates and 100% of depth of discharge (DOD), approaching the results achieved in liquid electrolytes. Good rate capability was observed in Li/$LiFePO_4$ cathode cells, being able to deliver at 2C more that 90% of the capacity discharged at 0.1C. These results, in conjunction with the approximately 100% coulombic efficiency, indicate very good electrolyte/electrode compatibility.

Thus, the developed materials showed suitable thermal, mechanical and electrochemical characteristics as well as high performance in battery applications, indicating the possibility of fabricating lithium-ion batteries with the battery separators developed in this work.

Resumo

Na área dos dispositivos móveis, tais como telemóveis e computadores, o armazenamento eficiente de energia é um dos problemas críticos a resolver.

As baterias de ião-lítio são mais leves, mais baratas, com maior densidade de energia (210Wh kg^{-1}), sem efeito de memória, tempo de vida prolongado e maior número de ciclos de carga / descarga do que outras baterias, tais como as de níquel-cádmio.

Um dos componentes essenciais para o desempenho das baterias é a membrana de separador, colocada entre o ánodo e o cátodo.

Polímeros como o poli (fluoreto de vinilideno) (PVDF) e seus co-polímeros: poli (fluoreto de vinilideno-co-trifluoroetileno), P(VDF-TrFE), poli (fluoreto de vinilideno-co-hexafluoropropileno), P(VDF-HFP), e poli (fluoreto de vinilideno-co-clorotrifluoroetileno), P(VDF-CTFE) são investigados quanto à sua utilização como separador de bateria devido à sua elevada polaridade; excelentes propriedades mecânicas e térmicas; porosidade controlável; molhabilidade por solventes orgânicos; ser quimicamente inertes e estáveis em ambiente catódico. Existem trabalhos com alguns co-polímeros de PVDF, mas não há investigações sistemáticas sobre poli (fluoreto de vinilideno-trifluoroetileno), P(VDF-TrFE), apesar do seu grande potencial para esta aplicação específica.

O objetivo deste trabalho é, determinar a performance do P(VDF-TrFE) para a sua utilização em separadores de baterias, controlando a sua estrutura, a estabilidade e a condutividade iónica, a fim de aumentar o desempenho do material.

Mostra-se que a evaporação do solvente à temperatura ambiente permite a preparação das membranas com diferentes graus de porosidade desde 70% até 80%, e com absorção de electrólito entre 250% e 600%. A preparação de compósitos de P(VDF-TrFE) com sais de lítio permitiu obter uma condutividade iónica dos electrólitos de $2{,}3\times10^{-6}$ $S.cm^{-1}$ à 120ºC com boa estabilidade electroquímica.

Um novo tipo de misturas de polímeros à base de poli (fluoreto de vinilideno - trifluoroetileno) / poli (óxido de etileno), P(VDF-TrFE)/PEO, foram preparadas tendo em conta que a microestrutura, hidrofilicidade e absorção de eletrólitos dependem fortemente do teor de PEO dentro da mistura. Para esta mistura, o melhor valor de condutividade iónica à temperatura ambiente foi de 0,25 $mS.cm^{-1}$ para a membrana com composição 60/40. Verificou-se que a condutividade iónica da membrana depende do

tamanho do anião do sal presente na solução de electrólito, afetando também o valor de absorção do electrólito.

Baterias fabricadas com os separadores desenvolvidos neste trabalho foram avaliadas em células de Li/$LiFePO_4$ e Li/Sn-C revelando muito bom desempenho cíclico, mesmo para taxas altas de varrimento e 100% de “depth of discharge”, DOD, aproximando-se dos resultados obtidos em eletrólitos líquidos. Igualmente, em células de cátodo Li/$LiFePO_4$ foi obtido a 2C mais de 90% da capacidade descarregada à 0.1C. Estes resultados, em conjunto com a eficiência coulombica aproximadamente de 100%, indicam uma muito boa compatibilidade entre o electrólito e o eléctrodo.

Assim, os materiais desenvolvidos neste trabalho apresentam características térmicas, mecânicas e eletroquímicas apropriadas para a fabricação de baterias de ião-lítio baseados nestes separadores.

List of Symbols and Abbreviations

13TFSI	N-methyl-N-propylpiperidinium Bis(trifluoromethanesulfonyl) Amide
Al_2O_3	Aluminum Oxide
$AlO[OH]_n$	Aluminum Oxyhydroxide
AN	Acetonitrile
$BaTiO_3$	Barium Titanate
BMIBF4	1-Butyl-3- Methylimidazolium Tetrafluoroborate
BMITFSI	1-butyl-3-methylimidazolium bis(trifluoromethanesulfonyl)imide
BMPyrTFSI	1-Butyl-3-Methypyrrolidinium Bis (trifluoromethanesulfonyl)imide
CNF	Carbon Nanofibres
CNT	Carbon Nanotubes
CoO	Cobalt Oxide
CTFE	Chlorotrifluoroethylene
DEC	Diethyl Carbonate
DIOX	1,3-Dioxolane
DMBITFSI	1,2-dimethyl-3-n-butylimidazolium-bis-trifluoromethanesulfonylimide
DMC	Dimethyl Carbonate
$DMOImPF_6$	2,3-Dimethyl-1-octylimidazolium Hexafluorophosphate
EC	Ethylene Carbonate
EMC	Ethyl Methyl Carbonate
EMITf:	1-ethyl-3-methylimidazolium trifluoromethanesulfonate
Fe_2O_3	Iron Oxide
GBL	γ-butyrolactone
HFP	Hexafluoropropene
ILs	Ionic Liquid
Li	Lithium
$LiAlO_2$	Lithium Aluminate
$LiAsF_6$	Lithium Hexafluoroarsenate
$LiBF_4$	Lithium Tetrafluoroborate)
LiBETI	Lithium Bis(perfluoroethanesulfonyl)imide
$LiCF_3SO_3$	Lithium Trifluoromethanesulfonate
$LiClO_4$	Lithium Perchlorate
$LiClO_4 \cdot 3H_2O$	Lithium Perchlorate Trihydrat
$LiCoO_2$	Lithium Cobalt Oxide
$LiFePO_4$	Lithium Iron Phosphate
$LiPF_6$	Lithium Hexafluorophosphate
$LiMnO_2$	Lithium Manganese Dioxide
$LiNiO_2$	Lithium Nickel Oxide
$LiNi_{0.5}Mn_{0.5}O_4$	Lithium Nickel Manganese Oxide
LiTFSI	Lithium Bis(Trifluoromethanesulfonyl)Imide
$Li_4Ti_5O_{12}$	Lithium Titanium Oxides
MCM-41	Molecular Sieves
$Mg(CF_3SO_3)_2$	Magnesium Triflate
$Mg(ClO_4)_2$	Magnesium Perchlorate
MgO	Magnesium Oxide
NH_4PF_6	Ammonium Hexafluorophosphate

MMT	Montmorillonite
MnO_2	Manganese Dioxide
$NaClO_4$	Sodium Salt
NaTf	Sodium Triflate
NaY	Molecular Sieves
PAN	Poly(acrylonitrile)
PC	Propylene Carbonate
PDPA	Polydiphenylamine
PDMS	Poly(dimethylsiloxane)
PE	Poly(ethylene)
PEG	Poly(ethylene glycol)
PEGDA	Poly(ethylene glycol diacrylate)
PEGDMA	Poly(ethylene glycol dimethacrylate)
PEO	Poly(ethylene oxide)
P(EO-EC)	Poly(ethylene oxide-*co*-ethylene carbonate)
PEO-PPO-PEO	Polyethylene oxide-*co*-polypropylene oxide-*co*-polyethylene oxide
PET	Poly(ethylene terephthalate)
PMAML	Poly(methyl methacrylate-*co*-acrylonitrile-*co*-lithium methacrylate)
PMMA	Poly(methyl methacrylate)
PMMITFSI	1,2-dimethyl-3-propylimidazolium bis(trifluoromethanesufonyl)imide
PP	Poly(propylene)
PPG-PEG-PPG	Poly(propylene glycol)-co-poly(ethylene glycol)-co-poly(propylene glycol)
PVA	Poly(vinyl alcohol)
PVC	Poly(vinyl chloride)
PVDF	Poly(vinylidene fluoride)
P(VDF-CTFE)	Poly(vinylidene fluoride-*co*- chlorotrifluoroethylene)
P(VDF-HFP)	Poly(vinylidene fluoride-*co*-hexafluoropropene)
P(VDF-TrFE)	Poly(vinylidene fluoride-*co*-trifluoroethylene)
PVK	Poly(N-vinylcarbazole)
PVP	Poly(vinyl pyrrolidone)
SBA-15	Molecular Sieves
SiO_2	Silicon Dioxide
SN	Succinonitrile
Sn-C	Sn nanoparticles within a carbon matrix
SnO_2	Tin Dioxide
$TEABF_4$	Tetraethylammonium Tetrafluoroborate
TEGDMA	Tetraethylene Glycol Dimethyl Ether
TEGDME	Tetra(ethylene glycol) Dimethyl Ether
TiO_2	Titanium Dioxide
TrFE	Trifluoroethylene
VDF	Vinylidene Fluoride
ZnO	Zinc Oxide
ZrO_2	Zirconium Dioxide

Table of contents

List of figures

List of tables

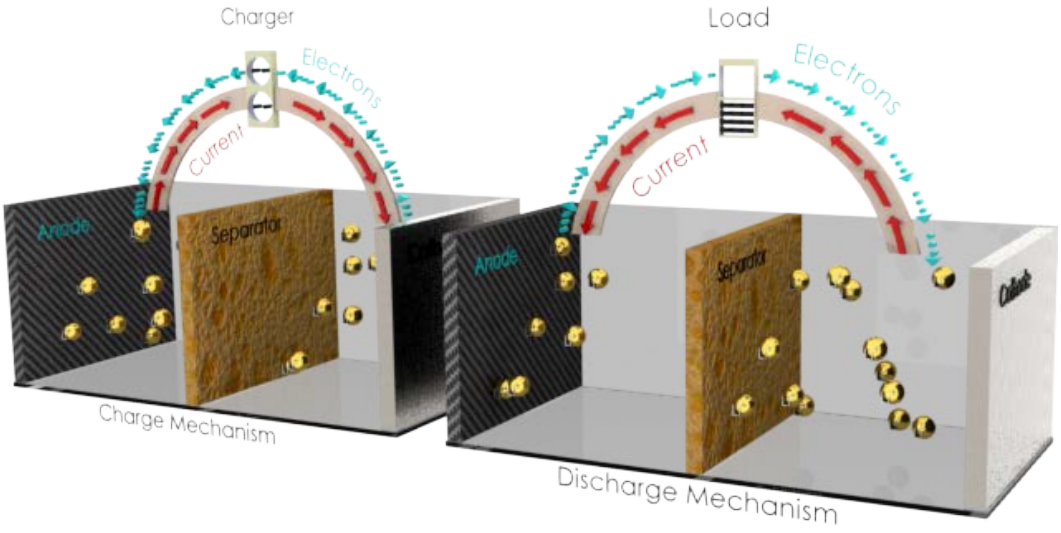

1. Introduction

This chapter describes the main properties of separator membranes for lithium-ion battery application, being a critical factor which affects the performance of the battery. The developments and main characteristics of poly(vinylidene fluoride), PVDF, and its copolymers for battery separator membranes is presented. Finally, the main objectives of the study are defined and the structure of the document presented.

This chapter is based on the following publication:

"Battery separators based on vinylidene fluoride (VDF) polymers and copolymers for lithium ion battery applications", C. M. Costa, M. M. Silva, S. Lanceros-Méndez, RSC Advances 3 (2013) 11404-11417

1.1. Battery separators

After Pike Research Consulting, the market of portable batteries will reach $30.5 billion dollars in 2015 with an annual growth rate of 8.5% [1]. The most used type of portable batteries are lithium-ion batteries as they are light, cheap, show high energy density, low charge lost, no memory effect, prolonged service-life and high number of charge/discharge cycles. The market for lithium-ion (Li-ion) cells is mainly focused in portable electronic devices such as notebook computers and mobile phones. The first Li-ion batteries were commercialized 1991 [2, 3]. This commercialization was preceded by several scientific achievements, including the pioneering work of Yazami [4] regarding the use of lithium-graphite as a negative electrode. A Li-ion battery is an electrochemical cell that converts chemical energy into electrical energy [5, 6]. The basic constituents of an electrochemical cell are the anode, cathode and the separator, as illustrated in figure 1.1.

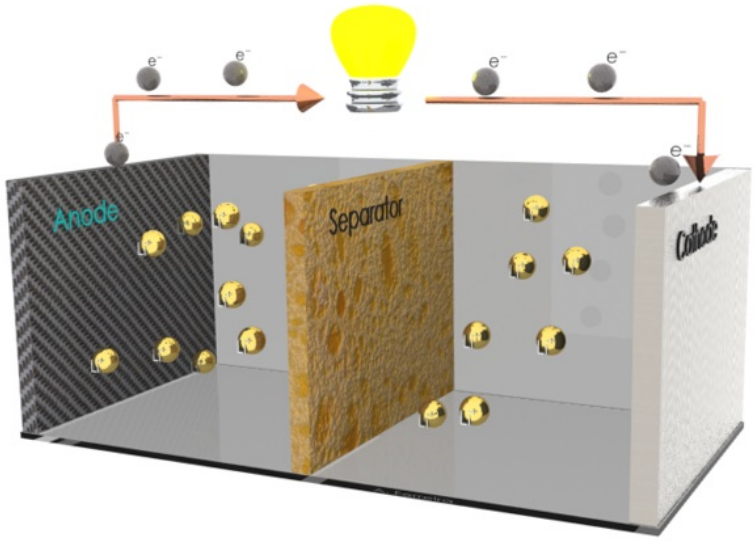

Figure 1.1 - Schematic representation of the main components of a lithium-ion battery

The separator membrane separates the anode and the cathode and it is essential in all electrochemical devices [7, 8]. The role of the separators is to the serve as the medium for the transfer of the lithium ions between both electrodes and to control the number of lithium ions and their mobility [9]. The separator is constituted by a polymer matrix soaked by the electrolyte solution, i.e, a liquid electrolyte where salts are dissolved in a solvent, water or organic molecules. Most commonly, the liquid electrolyte solution is composed by a lithium salt in a mixture of one or more solvents. The solvents present in the electrolyte solution must meet a combination of

requirements for battery applications, which are, in some cases, not easy to achieve, as for example, high fluidity vs. high dielectric constant [10]. The characteristics of an ideal solvent are high dielectric constant, for dissolving high salt concentrations; low viscosity, for improving ion transportation; to be inert to all cell components and to be in the liquid state in a wide temperature range. The nonaqueous solvents most used in electrolyte solutions belong to organic esters and ethers classes [11]. In both classes, the most used solvents are ethylene carbonate (EC), propylene carbonate (PC), dimethyl carbonate (DMC), diethyl carbonate (DEC) and ethyl methyl carbonate (EMC). Other possibility for the fabrication of polymer electrolyte separators is by incorporating the lithium salts directly into the polymer matrix [12].

A large diversity of requirements determine the performance of separator membranes for battery applications, such as low ionic strength, mechanical and dimensional stability, physical strength to allow easy handling, resistance to thermal and chemical degradation by electrolyte impurities and chemical reagents, to be easily wetted by liquid electrolytes and to show uniform thickness [9, 12, 13]. Table 1.1 summarizes the typical values and the relevance of the main requirements of lithium-ion battery separators, adapted from [12, 13].

Table 1.1 - Ideal value and relevance of the typical parameters for lithium-ion battery separators

Parameter	Ideal Value	Relevance
Thickness (μm)	<25	Determines the mechanical strength of the membrane and the risk of inner battery electrical shorting.
Electrical resistance (MacMullin no.,)	<8	Describes the relative contribution of a separator to cell resistance.
Gurley (s)	~25/mil	Expresses the time necessary for a specific amount of air to pass through a specific area of the separator with a specific pressure.
Porosity (%) / Pore Size (μm)	40 / <1	Determines the permeability required for battery separators.
Shrinkage (%)	< 5% in both MD and TD	Dimensional stability. The separator should not shrink when exposed to the electrolyte solution.
Tensile strength (%)	<2% offset at 1000psi	The separator should stand mechanical stress between the electrodes.
Shutdown temperature (ºC)	130	The temperature safety range of the battery that is provided by the separator.
High-temperature melt integrity	>150	Separators with good mechanical properties at high temperatures may provide a larger safety margin for batteries
Skew (mm/m)	<0.2	When a separator is laid out, the separator should be straight and not bowed or skewed.

The materials used as separators for batteries are mainly polymers or polymer composites with dispersed fillers of various types. The most used polymers are poly(ethylene) (PE) [14, 15], poly(propylene) (PP) [16], poly(ethylene oxide) (PEO) [17-19], poly(acrylonitrile) (PAN) [20-22] and poly(vinylidene fluoride) (PVDF) and its copolymers [22-26]. The most used fillers incorporated into the polymer hosts are inert oxide ceramics (Al_2O_3, SiO_2, TiO_2), molecular sieves (zeolites), ferroelectric materials ($BaTiO_3$) and carbonaceous fillers, among others, with the main function of increasing the mechanical stability and/or ionic conductivity of the

separator [27].

Figure 1.2 illustrates the increasing number of published scientific articles related to lithium ions battery separators and polymer electrolytes.

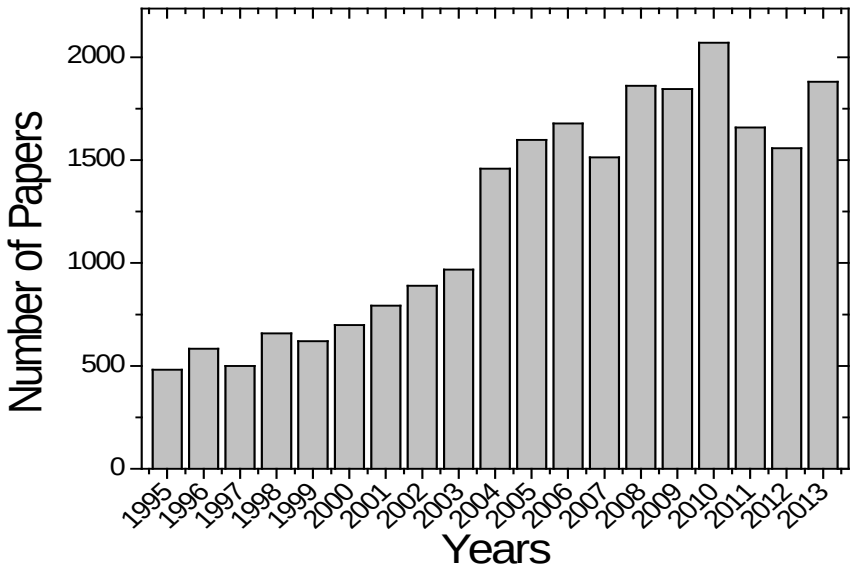

Figure 1.2 - Research articles published on battery separators and polymer electrolytes for lithium ion battery applications. Search performed in Scopus database with the keywords “battery separators” and “polymer electrolytes”.

The strong growth of work in this field in the past decade results from the development of new materials and processing techniques, which allows rapid and efficient technology transfer of the novel developed materials.

PVDF is semi-crystalline polymer in which the amorphous chains are embedded between the lamellar crystalline structures with a degree of crystallinity ranging from 40% to 60%. It exhibits four polymorphs called α, β, γ, δ [28, 29]. The most common and important polymorphs of PVDF are the α- and β-phases. The α-phase is non-polar, it is the phase thermodynamically more stable when the material is obtained from the melt and when the solvent is evaporated at temperatures above 80 ºC [30]. The β-phase is the most interesting phase for technological applications due to its electroactive properties: piezoelectric, pyroelectric and ferroelectric [31]. The β-phase is obtained with a porous microstructure directly by solution at crystallization temperatures below 70 ºC [32] or by mechanical stretching of the α-phase at temperatures between 70 ºC and 100 ºC [33]. The dielectric constant of the

β-phase ranges between 10 at 13 and the conformational repeating unit (planar zigzag, all-trans) has a dipolar moment of $7x10^{-30}$ Cm [34].

The semi-crystalline copolymer poly(vinylidene fluoride-*co*-trifluoroethylene), P(VDF-TrFE), shows, for specific molar ratios of VDF and TrFE, a polar ferroelectric transplanar chain conformation similar to the one of the β-phase of PVDF [35]. P(VDF-TrFE) exhibits the ferroelectric (FE)-paraelectric (PE) phase transition at a Curie temperature, Tc, below the melting temperature, Tm. Both temperatures depend on the crystallization conditions and molar ratio of VDF and TrFE [36-38]. The copolymer poly(vinylidene fluoride-*co*-hexafluoropropene), P(VDF-HFP), is also a semi-crystalline polymer with a degree of crystallinity significantly reduced due to the addition of hexafluoropropylene (HFP) [39]. Therefore, it shows high flexibility as compared to PVDF [40] and a dielectric constant of 8.4.

In the copolymer poly(vinylidene fluoride-*co*-chlorotrifluoroethylene), P(VDF-CTFE), the amount of chlorotrifluoroethylene, CTFE is essential for determining properties and applications [41]. For 25-70 % mol of VDF, the P(VDF-CTFE) is amorphous [42] being for the remaining concentrations a semicrystalline copolymer with a hexagonal structure [43]. The dielectric constant of P(VDF-CTFE) is 13 [44] and shows high electromechanical response for 9 and 12 mol % CTFE content [45].

PVDF and its copolymers poly(vinylidene fluoride-*co*-trifluoroethylene), P(VDF-TrFE), poly(vinylidene fluoride-*co*-hexafluoropropylene), P(VDF-HFP), and poly(vinylidene fluoride-*co*-chlorotrifluoroethylene), P(VDF-CTFE) show strong advantages for their use as separator membranes in comparison to polyolefins [46] and other used materials due to their strong polarity (high dipolar moment) and high dielectric constant for a polymer material, which can assist ionization of lithium salts. It is also possible to control the porosity of the materials through binary and ternary polymer/solvent systems. Further, they are wetted by organic solvents, chemically inert, show good contact between electrode and electrolyte and are stable in cathodic environment [47-55]. Different processing techniques, such as solvent casting, electrospinning and hot-press have been used for the development for battery separators from these materials [56-61].

This chapter focused on battery separators and polymer electrolytes based on PVDF and its copolymers, P(VDF-HFP), P(VDF-TrFE) and P(VDF-CTFE), for lithium-ion battery application due to the recent advances and their large potential for energy

storage applications. A summary of the obtained results will allow establishing the maturity of these materials for the intended purpose as well as to reflect on the future steps to be taken both in research and technology transfer.

The information is structured in three sections devoted to the state of the art in single polymers, composites and polymer blends, respectively. For each section, the materials and electrolyte solutions will be presented as well as the main characteristics of the materials, such as porosity, ionic conductivity and related properties. Some remarks on the electrodes of batteries based on the aforementioned separators will be provided.

1.2.Polymer electrolytes based on poly(vinylidene fluoride) and its copolymers

1.2.1. Single polymer and copolymers

Fluorinated polymers such as PVDF and its copolymer show advantages when compared to commercial polyolefine separators (PE) due to their high polarity and dielectric permittivity, which provides larger affinity with polar liquid electrolytes. The characteristics of the developed PVDF and copolymer membranes are summarized in Table 1.2 as achieved in chronological order. The porous battery separators of fluorinated polymers are most commonly obtained by phase inversion processes such as thermal induced phase separation (TIPS), using solvent and non-solvent system and electrospinning [26, 62-64]. The achieved porosity of the battery separators ranges between 0 to 90% and the pore size from 0.5 μm to 16 μm [62]. Porous membranes with controlled porosity and pore sizes of 2 μm [65] and 1 μm [66] were also obtained by adding urea and salicylic acid, respectively, as foaming agents for PVDF or P(VDF-HFP).

In 1996, Tarascon *et al* produced the first Li-ion battery with a fluorinated polymer (P(VDF-HFP)) as battery separator [67]. The performance of such a battery compares favourably in terms of gravimetric or volumetric energy density, life cycle, power rate and self-discharge with its liquid counterparts, while having enhanced safety characteristics, larger shape flexibility and scale ability. One of the main advantages of fluorinated polymers is their ability to be tailored in different geometries, including very thin cells.

Kataoka *et al* [26] showed that the ionic conductivity depends on the immersion time of the polymer membrane in the electrolyte solution and on the aging time after removal from the solution. PVDF for polymer electrolytes is optimized with 1:1 EC:PC plasticizer in salts such as $LiAsF_6$ (lithium hexafluoroarsenate), $LiPF_6$ (Lithium hexafluorophosphate) and $LiBF_4$ (Lithium tetrafluoroborate). Nevertheless, $LiAsF_6$ gives better results for ionic conductivity than $LiBF_4$ and $LiPF_6$, irrespective of the nature of the polymer and the amount of plasticizer [68]. Salts with a polarizing cation and a large anion with a well delocalized charge, and therefore with low lattice energy, are the most suitable for polymer electrolytes [69].

Modifications of the properties of PVDF have been achieved by radiation grafting for improving adhesion to electrodes, leading to good rate performance and stable cycle life [70].

Table 1.2 – Developed polymer electrolytes based on PVDF and co-polymers and their main properties in chronological order

Material	Electrolyte solution/ lithium ions	Porosity (%) / Fiber Diameter* (electrospun) (nm)	Uptake / %	σ_i / (S/cm) at 25ºC	Ref.
P(VDF-HFP)	1M $LiPF_6$ in EC/PC	-----	60	0.8×10^{-3}	[67]
PVDF	1M $LiPF_6$ + PC/EC/3DMC	70	65	3.7×10^{-3}	[62]
PVDF	1M LiTFSI in EC/DEC (2/3 in volume ratio)	-----	-----	6.7×10^{-3}	[26]
PVDF	10% $LiBF_4$ in EC/PC (1:1)	-----	-----	3.4×10^{-4}	[68]
PVDF	10% $LiPF_6$ in EC/PC (1:1)	-----	-----	4.7×10^{-4}	[68]
PVDF	10% $LiAsF_6$ in EC/PC (1:1)	-----	-----	6.6×10^{-4}	[68]
PVDF	1 M LiTFSI in EC/DEC	0	20	5.6×10^{-8}	[71]
PVDF	1 M LiTFSI in EC/DEC	23	32	2.7×10^{-6}	[71]
PVDF	1 M LiTFSI in EC/DEC	30	41	1.0×10^{-6}	[71]
PVDF	1 M LiTFSI in EC/DEC	70	60	9.8×10^{-5}	[71]
PVDF	1 M LiTFSI in EC/DEC	75	65	1.3×10^{-4}	[71]
P(VDF-HFP)	1 M $LiPF_6$ in 1/1 w/w (EC/DEC)	-----	-----	$1.5\text{-}2.0 \times 10^{-3}$	[72]
PVDF	1 M $LiPF_6$ in 1/1 w/w (EC/DEC)	23	33	2.2×10^{-5}	[73, 74]
PVDF	1 M $LiPF_6$ in 1/1 w/w (EC/DEC)	30	39	2.4×10^{-5}	[73, 74]
PVDF	1 M $LiPF_6$ in 1/1 w/w (EC/DEC)	38	45	1.5×10^{-4}	[73, 74]
PVDF	1 M $LiPF_6$ in 1/1 w/w (EC/DEC)	71	77	1.0×10^{-3}	[73, 74]
P(VDF-HFP)	1M $LiClO_4$ – EC/PC (1:1)	83	220	1.5×10^{-3}	[75]
PVDF	1M $LiPF_6$ – EC/PC	-----	-----	2.0×10^{-3}	[76]
PVDF	1M $LiPF_6$ – EC/DMC/DEC (2/2/1)	70	142	5.0×10^{-2}	[77]
P(VDF-HFP)	1M $LiPF_6$ – EC/DMC (1/1)	23	76.4	0.3×10^{-3}	[78]

PVDF	1M LiTFSI in distilled water	100–800*	50-73	1.6-2.0 × 10^{-3}	[63]
P(VDF-HFP)	1 M $LiBF_4$ in 1/3 w/w (EC/GBL)	-----	120	3.4 × 10^{-3}	[79]
PVDF	1M $LiPF_6$ – EC/DMC/DEC (2/2/1)	-----	-----	3.5 × 10^{-3}	[80]
PVDF	20wt% $LiClO_4$	-----	-----	8.7 × 10^{-4}	[81]
PVDF	1M $LiPF_6$ – EC/DMC/DEC (2/2/1)	70	-----	3.1 × 10^{-3}	[82]
P(VDF-HFP)	1M $LiPF_6$ – EC/DEC (1/1)	70-90	-----	1.2 × 10^{-3}	[83]
PVDF	$LiBF_4$ – PC:EC	-----	-----	1.0 × 10^{-3}	[84]
PVDF	EC/PC/$LiPF_6$ = 43/43/7 (in wt%)	-----	-----	1.0 × 10^{-3}	[85]
PVDF	15 wt% of $LiFePO_4$	-----	-----	6.7 × 10^{-6}	[86]
PVDF	1 M $LiPF_6$-EC/DMC/DEC (1/1/1).	750-1630*	300-400	6.7 × 10^{-2}	[87]
P(VDF-HFP)	0.5M LiTFSI in BMITFSI	<1000*	750	2.3 × 10^{-3}	[64]
P(VDF-HFP)	0.5M $LiBF_4$ in $BMIBF_4$	<1000*	600	2.3 × 10^{-3}	[63]
P(VDF-HFP)	1M $LiPF_6$ in EC/DMC	59	165	9.1 × 10^{-2}	[88]
P(VDF-HFP)	1M $LiCF_3SO_3$ in TEGDME	59	210	1.8 × 10^{-2}	[88]
PVDF	1 M $LiPF_6$-EC/DMC/EMC (1/1/1)	70	230	1.4 × 10^{-3}	[49]
PVDF	1M $LiCF_3SO_3$ in TEGDME/DIOX (1/1)	-----	250	0.6 × 10^{-3}	[89]
P(VDF-HFP)	1 M $LiPF_6$-EC/DMC/EMC (1/1/1)	-----	-----	1.8 × 10^{-3}	[90]
P(VDF-HFP)	1 M $LiPF_6$-EC/DMC (1/1)	78	321	3.4 × 10^{-4}	[91]
P(VDF-HFP)	1 M $LiPF_6$-EC/DMC/DEC (1/1/1)	70	-----	1.4 × 10^{-3}	[65]
PVDF	1 M $LiPF_6$-EC/DMC/EMC (1/1/1)	-----	230	4.8 × 10^{-3}	[66]
P(VDF-HFP)	0.3 M $Mg(CF_3SO_3)_2$ in EMITf	-----	-----	4.8 × 10^{-3}	[92]
PVDF	1 M $LiPF_6$-EC/DMC	77	-----	1.9 × 10^{-3}	[55]

	(1/1)				
P(VDF-CTFE)	1 M $LiPF_6$-EC/DMC (1/1)	230*	800	2.0×10^{-3}	[93]
PVDF	50wt% LiTFS	-----	-----	1.7×10^{-2}	[94]
P(VDF-HFP)	40wt% LiTf	-----	-----	7.8×10^{-5}	[95]
P(VDF-HFP)	0.8M LiTFSI in 1g 13TFSI	-----	670	3.2×10^{-4}	[96]
P(VDF-HFP)	LiTFSI-PC (0.15/0.3 wt%)	-----	-----	1.0×10^{-5}	[97]
PVDF	1M $TEABF_4$ in AN	80	117	1.8×10^{-3}	[52]
PVDF	1 M $LiPF_6$-EC/DEC (4/6)	48	142	-----	[98]

From table 1.2 it is observed that PVDF and P(VDF-HFP) with $LiPF_6$ and $LiCF_3SO_3$ in different organic solvents lead to the best values of ionic conductivity ($1.8 – 5 \times 10^{-2}$ S/cm).

PVDF polymer as battery separator was found to be effective in enhancing the lithium transport number due to selective interactions with the anion. The ionic conductivity of PVDF is associated to the total solution uptake, which depends on the gelation process related to porosity and pore size. The solution introduced in the polymer is stored in the pores and then penetrates into the polymer, swelling the polymer network [71]. Other possibility for obtaining polymer electrolytes taking advantage of the properties of PVDF is by coating a microporous polyolefin membrane with a fluorinated polymer [72]. The cells with these polymer electrolytes showed good electrochemical and rate performance during cycling. Ideal membranes for porous polymer electrolytes based on PVDF for battery applications should present high porosity and small pore diameters with a narrow distribution. Experimental results show that porosity should be > 80% and pore diameter should be < 1 μm [75]. This porous structure has been also achieved with electrospun nanofiber webs [63].

The effect of the liquid organic solvents in PVDF microporous membranes was studied by Saunier *et al* [80]. It was observed that the affinity of PVDF for the liquid electrolyte may affect its mechanical strength and compromise battery safety. This indicates that the thermal and mechanical stability are affected when too much

solvent is incorporated into the polymer. The reversible modifications can also affect the membrane properties, as the glass transition and melting temperature are lowered [80]. The ionic conductivity of the PVDF microporous membranes is also affected by solvent/polymer and solvent/salt interactions, ionic dissociation and tortuosity value [82]. It was proven also that interactions between PVDF and PC mainly occur in the surface area of the PVDF crystalline phase, whereas interactions between PC, PVDF, and lithium salt mainly occur in the amorphous area [48].

It was also observed that ionic conductivity decreases in the order EC/DEC > EC/EMC > EC/DMC among the electrospun PVDF fiber-based polymer electrolytes with the same weight fraction of EC [87]. For P(VDF-HFP)-based solid polymer electrolytes, lithium triflate salt effectively reduces the degree of crystallinity of the polymer and increases the ionic conductivity of the membrane [95]. The ionic conductivity depends not only on the characteristics of the electrolyte solution but also on the properties of the membrane -porosity and pore size- as shown in figure 1.3.

In figure 1.3, it is observed that for the same porosity are obtained different uptake ratios and ionic conductivities (table 1.2) due to the interactions with the cations and anions produced from the Li salts by the solvation process. The viscosity of the solvent also influences the transport and the transference numbers of the ions [99, 100].

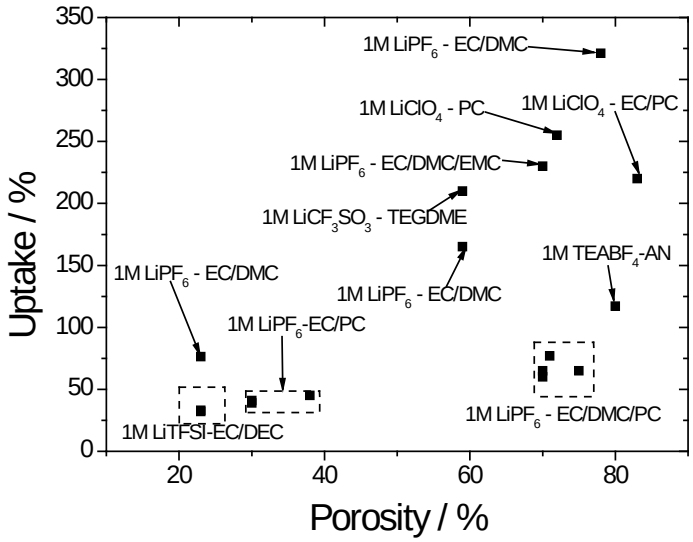

Figure 1.3 - Porosity vs uptake for various electrolyte solutions incorporated into PVDF membranes

Therefore, the main problem still to be optimized for battery separators persists: to obtain a combination of good ionic conductivity with high uptake ratio and excellent mechanical properties without deterioration of the ionic conductivity in the temperature range of the lithium-ion battery operation.

PVDF was proven to battery separator by Yamamoto *et al* in a 4.4 V Li-ion polymer battery. The discharge capacity reached 520 Whl^{-1} and the capacity retention ratio was 91.4% at 3C [85].

1.2.2. Polymer and copolymer composites

To solve some of the problems existing in single polymer membranes, battery separators have been developed by the incorporation of suitable fillers into the host polymer for improving mechanical strength, thermal stability and ionic conductivity. Among these fillers are oxide ceramic, zeolites, ferroelectric ceramics, carbon, etc [27, 101]. These fillers can be divided into two groups: the fillers that participate in the ionic conduction process and the fillers that are not involved in the lithium transport process [27].

The characteristics of PVDF and copolymer composites for separator membranes are summarized in Table 1.3 in chronological order.

From table 1.3 it is observed that separator membranes with the different fillers increase the ionic conductivity with respect to the pristine polymer matrix (table 1.2), the characteristics/properties of fillers playing an important role in the conduction mechanism of separator membranes.

Du Pasquier *et al* showed that the combination of a phase-inversion process and the presence of finely divided silica in the separator results in the formation of a stable porous structure, in which the pores are mechanically reinforced by the silica particles at their inner surface and the ionic conductivity of the P(VDF-HFP) membrane increases [102].

The addition of MgO fillers increases the compatibility between separator and electrodes (anode and cathode) and batteries with these membranes exhibit high power density (at 3C rate was > 280 W kg^{-1}) [103].

Some authors verified that the presence of Montmorillonite (MMT) fillers have an effect on the nano-scale microenvironment for composite materials and a positive

increment of the charge carriers and its mobility, the membranes exhibiting high electrochemical characteristics for Li-ion battery applications [104]. Further, this filler is adequate for battery separators as it enhances the uptake of liquid electrolyte due to the excellent affinity of clays towards electrolyte molecules [105].

The effect of powder particle size on battery separator was studied by Takemura *et al*. It was observed that composites with 0.01 μm ceramic powders (Al_2O_3) showed excellent cycling properties [106].

The addition of molecular sieves has expanded the electrochemical stability window of polymer electrolytes, enhanced the interfacial stability of polymer electrolyte with lithium electrodes, and inhibited the crystallization of the PVDF-HFP matrix [107].

Table 1.3 - Polymer electrolytes based on PVDF based composite materials and their properties in chronological order.

Material	**Fillers**	**Electrolyte solution / lithium ions**	**Porosity / %**	**Uptake / %**	**σ_i / (S/cm) at 25ºC for maximum amount**	**Ref**
P(VDF-HFP)	SiO_2	1M $LiPF_6$ in EC/DMC (1:1)	-----	100-250	0.87 - 3.1 × 10^{-3}	[102]
P(VDF-HFP)	MgO	1M $LiPF_6$ in EC/DMC (1:1)	-----	40	4.0 × 10^{-4}	[103]
PVDF	SiO_2	1M$LiPF_6$ in EC/PC (1/1)	-----	-----	-----	[108]
PVDF	SiO_2	1M $LiClO_4$ in EC–PC (1/1)	-----	-----	-----	[108]
PVDF	SiO_2	1M $LiPF_6$ in EC–PC (1/1)	-----	-----	3.5 × 10^{-2}	[109]
P(VDF-HFP)	MMT	$LiCF_3SO_3$ in PC	-----	-----	1.0 × 10^{-3}	[104]
P(VDF-HFP)	SiO_2	1M LiTFSI in EC/DEC (1/1)	77	-----	2.7 × 10^{-2}	[110]
P(VDF-HFP)	SBA-15	1M $LiPF_6$ in EC/DMC/EMC (1/1/1)	59	76	0.8 × 10^{-3}	[107]
P(VDF-HFP)	MCM-41	1M $LiPF_6$ in EC/DMC/EMC (1/1/1)	14	30	4.6 × 10^{-2}	[107]
P(VDF-HFP)	NaY	1M $LiPF_6$ in EC/DMC/EMC (1/1/1)	9	39	3.0 × 10^{-3}	[107]
P(VDF-HFP)	TiO_2	DMBITFSI / $LiPF_6$	-----	-----	1.3 × 10^{-3}	[111]
P(VDF-HFP)	AlO[OH]n	5wt% of	-----	-----	1.1 × 10^{-2}	[112]

		$LiN(CF_3SO_2)_2$				
P(VDF-HFP)	TiO_2	$LiClO_4$ in EC/PC	26	110	4.1×10^{-2}	[113]
P(VDF-HFP)	MgO	$LiClO_4$ in EC/PC	27	62	3.7×10^{-2}	[113]
P(VDF-HFP)	ZnO	$LiClO_4$ in EC/PC	23	61	5.5×10^{-2}	[113]
P(VDF-HFP)	MCM-41	$LiClO_4$ in EC/PC	42	93	6.1×10^{-2}	[113]
P(VDF-HFP)	SBA-41	$LiClO_4$ in EC/PC	52	82	5.0×10^{-2}	[113]
P(VDF-HFP)	MMT	1M $LiPF_6$ in EC:DMC (1/1)	-----	40	2.5×10^{-3}	[114]
P(VDF-HFP)	$LiAlO_2$	1M $LiClO_4$ in EC:DEC (1/1)	87	121	8.1×10^{-3}	[115]
P(VDF-HFP)	ZrO_2	1M $LiClO_4$ in EC:DEC (1/1)	86	91	11×10^{-3}	[116]
P(VDF-HFP)	TiO_2	1M $LiPF_6$ in EC/DMC/DEC (1/1/1)	67	-----	0.9×10^{-3}	[117]
P(VDF-HFP)	SiO_2	1M $LiClO_4$ in EC/ PC (1:1)	-----	-----	4.3×10^{-3}	[118]
P(VDF-HFP)	SiO_2	$LiClO_4$+PC+DEC	-----	-----	1.0×10^{-2}	[119]
P(VDF-HFP)	TiO_2	1M $LiPF_6$ in EC/DMC (1/1)	-----	125	1.0×10^{-3}	[120]
P(VDF-HFP)	TiO_2	1M $LiPF_6$ in EC/DMC (1/1)	60	359	1.7×10^{-3}	[93]
P(VDF-HFP)	MgO	1M $Mg(ClO_4)_2$ in EC/PC (1/1)	-----	-----	8.0×10^{-3}	[121]
P(VDF-HFP)	DMOImP F6	0.5M NH_4PF_6	-----	-----	3.0×10^{-5}	[122]
PVDF	SiO_2	-----	136	-----	-----	[123]
P(VDF-HFP)	$BaTiO_3$	LiBETI+EC+PC	-----	-----	0.8×10^{-3}	[124]
P(VDF-HFP)	Al_2O_3	1M $LiPF_6$ in EC/DEC (1/1)	-----	-----	-----	[125]
P(VDF-HFP)	effervescent disintegrant	1M $LiPF_6$ in DMC/EC/EMC (1/1/1)	55	-----	1.2×10^{-3}	[126]
P(VDF-HFP)	α-MnO_2	1M LiTFSI-PMMITFSI	-----	-----	1.3×10^{-3}	[127]
PVDF	MCM-41 + SO_4^{2-} /ZrO_2	1M $LiPF_6$ in EC/DMC/DEC (1/1/1)	62	161	1.0×10^{-3}	[128]
P(VDF-HFP)	SiO_2	1M $LiPF_6$ in EC/DEC (1/1)	68	-----	0.61	[129]
PVDF	Fe_2O_3, SnO_2 and CoO	1M $LiPF_6$ in EC/DMC (2/1)	-----	-----	-----	[130]
PVDF	Organic clays	-----	75	-----	-----	[131]
PVDF	MMT	1M $LiClO_4$ in PC/DEC (1/1)	-----	177	2.3×10^{-3}	[105]
PVDF	TiO_2	1 M $LiPF_6$ in	65-79	-----	-----	[132]

		EC/DMC (1/1)				
P(VDF-HFP)	SiO_2	1M NaTf in EC/PC (1:1)	-----	-----	4.1×10^{-3}	[133]
PVDF	SiO_2	1 M $LiPF_6$ in EC/DMC (1/1)	75	-----	1.4×10^{-3}	[134]
P(VDF-HFP)	SiO_2	1 M $LiPF_6$ in EC/DEC (1/1)	61	-----	0.9×10^{-3}	[135]
P(VDF-HFP)	Cellulose	1 M LiTFSI in BMPyrTFSI	58	712	4.0×10^{-4}	[136]
P(VDF-TrFE)	MMT	1M $LiClO_4.3H_2O$-PC	90	335	8.0×10^{-7}	[137]
P(VDF-TrFE)	NaY	1M $LiClO_4.3H_2O$-PC	36	233	2.0×10^{-6}	[138]
P(VDF-TrFE)	CNT	1M $LiClO_4.3H_2O$-PC	82	275	2.0×10^{-6}	[139]
P(VDF-TrFE)	BaTiO3	1M $LiClO_4.3H_2O$-PC	71	----	6.4×10^{-5}	[140]

Stephan *et al*, verified that the incorporation of inert fillers reduces the crystallinity of the polymer host, acts as 'solid plasticizer' capable of enhancing the transport properties and provides better interfacial properties towards lithium metal anodes [112].

The uptake of electrolyte solution is not related directly to the surface area or dielectric constant of the oxides. It may be due to the affinity of the metal oxide toward the electrolyte solution [113]. The incorporation of fillers such as SiO_2 and Al_2O_3 in the PVDF membrane promotes amorphicity, explaining the conductivity enhancement in PVDF-based electrolytes [141].

P(VDF-HFP) with SiO_2 nanoparticles has been prepared for Na/S batteries with a first discharge capacity of 165 mAh g^{-1} [133].

Galvanostatic cycling experiments of PVDF membranes with SiO_2 showed that these membranes have behaviour similar to the corresponding liquid electrolyte, without significant differences in capacity [108].

Miao *et al* showed that TiO_2 added to the composite electrolyte membranes helps to improve mechanical strength, electrolyte uptake, ionic conductivity, and the electrode/electrolyte interfacial stability [91].

Composite polymer electrolytes containing ionic liquids have been found to be thermally stable up to 300°C and show results adequate to be used as battery separators [122].

The nature of the filler and the filler content play therefore a very delicate role in the ionic conductivity of the composite materials [124]. The maximum amount of fillers found in the different works was 32 wt%. The ionic conductivity of the composite materials as battery separators depends on the nature of the fillers, the characteristics of the membrane (porosity) and the electrolyte solution type (lithium salts and solvent). For ionic conductivity improvement, the Lewis acid-base interactions between filler surface groups, polymer matrix and cations/anions play an essential role.

Different fillers also incorporate complementary characteristics to the separator membranes. The molecular sieves produce a specific conducting pathway on the membranes and improve mechanical strength [128, 138]. The MMT particles do not affect the morphology of the polymer matrix and increase of electrochemical behaviour of the battery separator [104, 114, 137]. The inert oxide ceramics (Al_2O_3, TiO_2, ZrO_2) reduce the degree of crystallinity and promotes of Li^+ transport at the boundaries of the filler particles [142]. Ferroelectric ceramic fillers ($BaTiO_3$) increase the polarity of the battery separator due of the high dielectric constant of the fillers and due to the charge separation [27]. The interfacial stability between electrodes and battery separators as well as the ionic conductivity are improved with fillers based of carbon (CNT, CNF) [143].

Figure 1.4 shows the best ionic conductivity of the composite materials obtained with the different fillers.

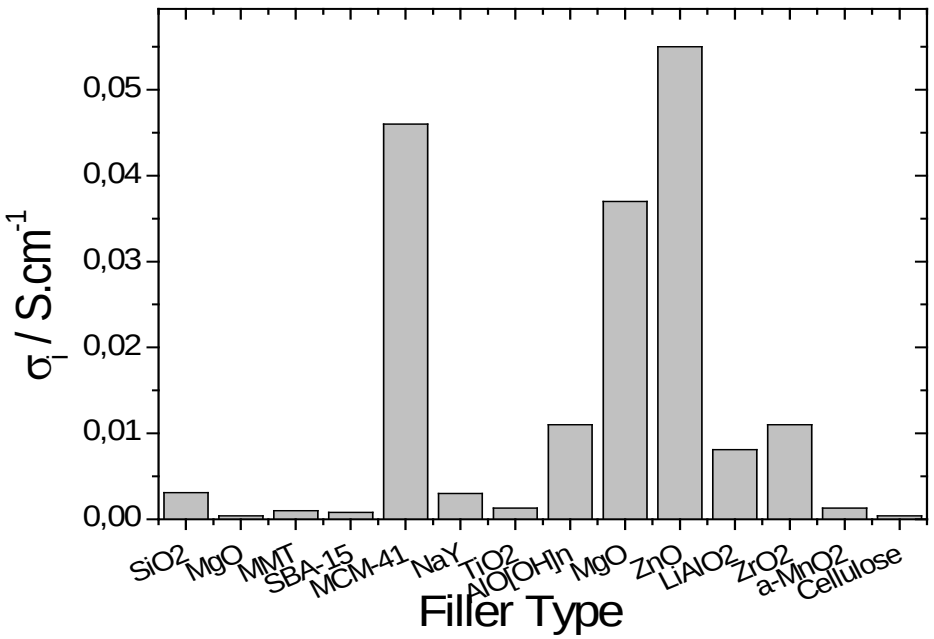

Figure 1.4 - Ionic conductivity for different filler types.

Figure 1.4 shows that the best ionic conductivities are achieved for MgO, ZnO and MCM-41 fillers. The MgO and ZnO are inert oxide ceramics that change the dynamics of the polymer chains and MCM-41 are molecular sieves with strong Lewis acid centers in their frameworks and increase the Li^+ transference number.

1.2.3. Poly(vinylidene fluoride) and copolymer based polymer blends

Another strategy for enhancing the ionic conductivity and other relevant properties of battery separator membranes such as mechanical and thermal properties is the fabrication of polymer blends. In the polymer blends for battery separators the strategy has been the following: one polymer should show a very good affinity with the liquid electrolyte and the other polymer must show excellent mechanical properties. The dimensional and electrochemical stability are also necessary requirements for polymer blends.

The developed PVDF and copolymers based polymer blend membranes are summarized in Table 4 in chronological order.

Table 1.4 shows that the polymer blends show high ionic conductivity and the

polymers more used with PVDF and its copolymers are PMMA and PEO due to the increased adhesion of electrodes and battery separators as well as to the ability to solvate a wide variety of salts, respectively.

P(VDF-HFP)/PAN polymer blend membranes were prepared by Kim *et al* and high ionic conductivity and good mechanical properties were observed for the gel polymer electrolytes [144].

P(VDF-HFP)/PE blend membranes show that PE particles dispersed in P(VDF-HFP) form a continuous film with 23 wt% of PE. The continuous PE film exhibits the ability to cut off the ion diffusion between cathode and anode and induces high ionic conductivity and good mechanical strength [145].

Rajendran *et al* determined that the resulting ionic conductivity of the blend membranes is determined by the overall mobility of ion and polymer, which depends on the free volume around the polymer chain [146]. In the PMMA/PVDF (25-75) polymer blend with $LiClO_4$ an ionic conductivity of 3.14×10^{-5} S/cm was obtained at room temperature.

PMAML/P(VDF-HFP) is a promising electrolyte candidate for rechargeable lithium ion polymer batteries as it shows high ionic conductivity (2.6 $mS.cm^{-1}$ at room temperature and electrochemical window around 4.6V) and good electrochemical stability [147].

Michael *et al* demonstrated that P(VDF–HFP)/PVK with $LiBF_4$ offers the room temperature ionic conductivity of 0.72 mS/cm with an ionic transference number of 0.49 [148].

A new type of separator was introduced by Lee *et al* [149] by coating poly(vinyl alcohol) (PVAc) on the surface of a PVDF/PE non-woven matrix. The coated separator exhibits smoother surface morphology and better adhesion properties toward electrodes.

Table 1.4 - Polymer electrolyte blends based on PVDF and copolymers and their properties in chronological order.

Material	Blends	Electrolyte solution/ lithium ions	Porosity / %	Uptake / %	σ_i / (S/cm) at 25ºC	Ref
P(VDF-HFP)	PAN	1 M $LiPF_6$ in EC/DMC (1/1)	76	82	1.9×10^{-3}	[144]
P(VDF-HFP)	PAN	1 M $LiBF_4$ in EC/DMC (1/1)	76	80	1.2×10^{-3}	[144]
P(VDF-HFP)	PE	1 M $LiClO_4$ / PC + EC	-----	-----	0.2×10^{-3}	[145]
PVDF	PMMA	10 mol % $LiClO_4$	-----	-----	3.1×10^{-5}	[146]
P(VDF-HFP)	PVP	1 M $LiBF_4$ in EC/DMC (1/1)	-----	62	0.4×10^{-3}	[150]
PVDF	PAN	$LiClO_4$ – PC - EC	-----	-----	-----	[151]
P(VDF-HFP)	PEG	LiTFSI	-----	-----	1.0×10^{-5}	[152]
P(VDF-HFP)	PMAML	1 M $LiBF_4$ in EC/DMC (1/1)	76	75	2.6×10^{-3}	[147]
PVDF	PMMA-PEGDA	1 M $LiPF_6$ in EC/DMC/EMC (1/1/1)	-----	600	4.5×10^{-3}	[153]
P(VDF-HFP)	PEG-PEGDMA	1 M $LiPF_6$ in EC/DEC (1/1)	15	98	1.0×10^{-3}	[154]
P(VDF-HFP)	PVK	1.5M $LiBF_4$ in EC	-----	-----	0.7×10^{-3}	[148]
PVDF	PEGDA-PMMA	$LiPF_6$/$LiCF_3SO_3$ in EC/DMC/EMC (1/1/1)	-----	-----	1.0×10^{-3}	[155]
PVDF	PE	1 M $LiPF_6$ in EC/DEC/PC (35/60/5, w/w/w)	48	302	1.1×10^{-3}	[156]
PVDF	PE	1 M $LiPF_6$ in EC/DEC/PC (35/60/5, w/w/w)	53	290	8.9×10^{-4}	[149]
P(VDF-HFP)	PEO	1M LiTFSI in EC/PC	-----	-----	-----	[157]
P(VDF-HFP)	PEO	1M LiTFSI in EC/PC (1/1)	-----	-----	-----	[158]
PVDF	PEO	1M $LiClO_4$ in PC	84	210	2.0×10^{-3}	[159]
P(VDF-HFP)	PAN	1M $LiClO_4$ in EC/DEC (1/1)	-----	-----	3.4×10^{-3}	[160]

P(VDF-HFP)	PVP-PEG	1 M $LiPF_6$ in DMC/EMC/EC (1/1/1)	49	125	0.5×10^{-3}	[161]
P(VDF-HFP)	P(EO-EC)	$LiCF_3SO_3$	65	61	3.7×10^{-5}	[162]
PVDF	PMMA	1 M $LiPF_6$ in DMC/EMC/EC (1/1/1)	-----	-----	-----	[163]
P(VDF-HFP)	PEG	1 M $LiPF_6$ in DEC/ EC (1/1)	90	100	1.0×10^{-4}	[164]
PVDF	PVC	$NaClO_4$+PC	-----	-----	1.5×10^{-4}	[165]
P(VDF-HFP)	PVA	1M $LiClO_4$ in EC/DEC (1/1)	86	90	7.9×10^{-3}	[166]
PVDF	PVC	$LiClO_4$ +EC/PC	-----	-----	3.7×10^{-3}	[167]
PVDF	PAN	1M $LiClO_4$ in PC	85	300	7.8×10^{-3}	[20]
P(VDF-HFP)	PAN	1M $LiPF_6$ in EC:EMC (1:3)	83	-----	6.7×10^{-3}	[168]
PVDF	PMMA	1M $LiPF_6$ in EC:DMC (1:1)	-----	260	7.9×10^{-3}	[54]
PVDF	PDPA	1M $LiClO_4$ in PC	-----	280	3.6×10^{-3}	[23]
P(VDF-HFP)	PEGDMA	1M $LiClO_4$ in EC/DEC	-----	125	3.8×10^{-4}	[169]
PVDF	PEGDA-PEO-PPO-PEO	1M $LiClO_4$ in EC/PC (1/1)	32	63	1.9×10^{-3}	[170]
PVDF	PMMA	1M $LiClO_4$ in EC/PC (1/1)	-----	292	1.9×10^{-3}	[171]
P(VDF-HFP)	SN	$LiClO_4$	-----	-----	1.0×10^{-3}	[172]
P(VDF-HFP)	PE	1M $LiPF_6$ in EC/ DEC (1/1)	-----	-----	$0.8\text{-}1.2 \times 10^{-3}$	[173]
P(VDF-HFP)	PMMA	1M $LiPF_6$ in EC:DMC (1:1)	-----	377	2.0×10^{-3}	[174]
P(VDF-HFP)	PET	1M $LiPF_6$ in EC:DMC (1:1)	-----	-----	0.8×10^{-3}	[175]
P(VDF-HFP)	PVA	8wt% $LiBF_4$ + 67wt% EC	-----	-----	1.2×10^{-3}	[176]
PVDF	PDMS	1M $LiPF_6$ in EC:DMC:EMC (1:1:1)	55	250	1.2×10^{-3}	[177]

P(VDF-HFP)	PPG-PEG-PEG	1M $LiClO_4$ in EC/PC (1/1)	-----	259	1.3×10^{-2}	[178]
P(VDF-HFP)	PMMA	1M $LiClO_4$ in EC/DEC (1/1)	50	403	1.7×10^{-3}	[179]

Sannier *et al*, produced a polymer blend of P(VDF-HFP)/PEO and also highlighted the role of the macroscopic blend interfaces toward dendrite in bi-layered separators [158].

For PVDF/PEO or P(VDF-HFP)/PEG blends, the addition of PEO or PEG in the PVDF matrix improves the pore configuration (connectivity) of the PVDF microporous membranes and increases ionic conductivity [159, 164].

Electrospun membranes based on PVDF were prepared and modified via pre-irradiation grafting with PMMA. PMMA possesses good affinity for the liquid electrolyte and gelled PMMA could substitute nonconductive PVDF for being in contact with the electrodes [54].

Sohn *et al* prepared a P(VDF-HFP)/PEGDMA coated PE separator for lithium ion battery applications by electron beam irradiation (EB). The EB treatment of the blend membranes containing PEGDMA was found to strongly improve the thermal shrinkage of the separators by the formation of crosslinked networks, enhancing also electrolyte uptake and ionic conductivity [169].

The ionic conductivity of the polymer blends for battery separators depends on the affinity between polymers and the characteristics of the membrane (e.g. porosity, crystallinity, etc), which also depends on the processing technique such as thermal induced phase separation (TIPS). Figure 1.5 shows the best ionic conductivity for each developed polymer blend type.

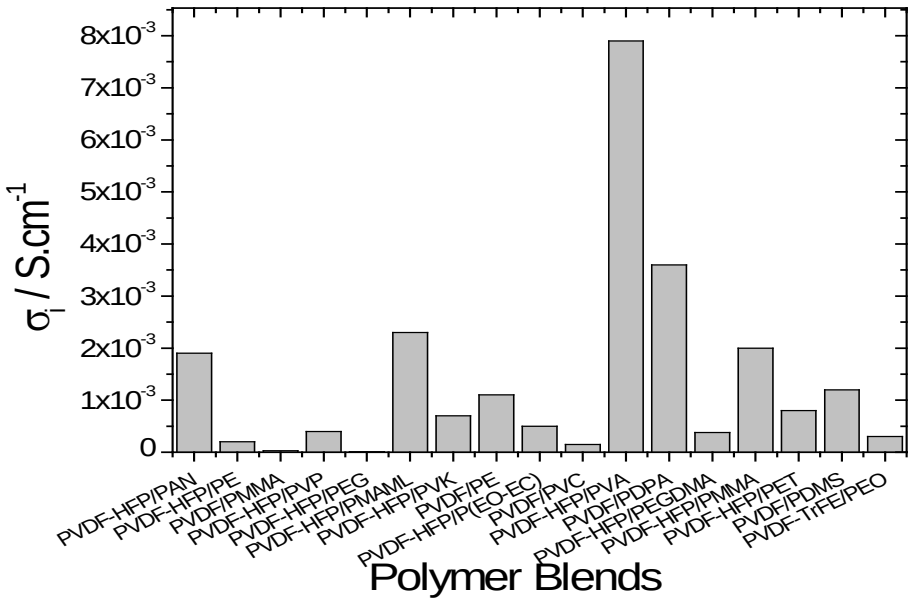

Figure 1.5 - Best ionic conductivity for the different polymer blends

The common element for the polymer blends with the best ionic conductivity is the presence of P(VDF-HFP) (Figure 1.5) due to the lower degree of crystallinity, its dielectric constant, ε=8.4, and strong electron withdrawing functional groups (-C-F-).

1.3. Anode and cathode electrodes used with PVDF based separators

The two different types of electrodes, anode and cathode, immersed in the electrolyte solution create the electrical potential, i.e. the electrochemical cell.

During charging process, electrons move from the cathode to the anode (figure 1.6, left) and during discharge the electrons move from the anode to the cathode (figure 1.6, right) [180].

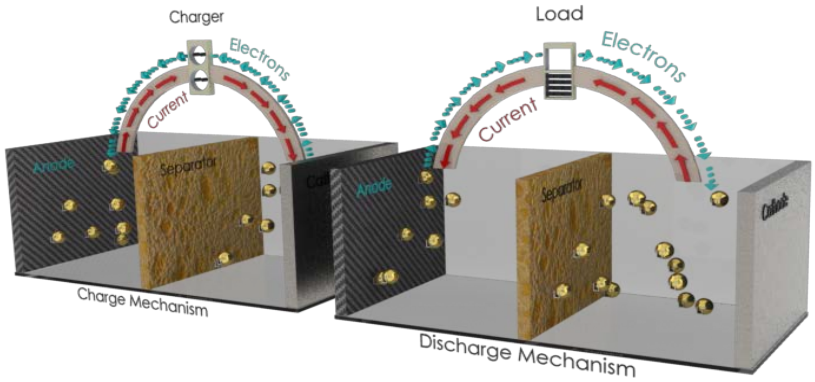

Figure 1.6 – Representation of the charge and discharge modes of the electrochemical cell

The anode is the negative active material. It is commonly based on carbonaceous materials and non carbon alloys where reversion reaction occurs [181]. Examples of carbonaceous materials used as anode materials are graphites, carbon nanotubes (CNT), carbon nanofibres (CNF) and lithium titanium oxides ($Li_4Ti_5O_{12}$).

Carbonaceous materials show the largest potential for improving the lithium ion cells and versatile, strong and highly conductive electrodes have been obtained to be used as anodes in batteries systems [182].

The cathode is the positive active material. It is based on transition metal oxides and it is the main responsible for the cell capacity and cycle life.

Lithium cobalt oxide ($LiCoO_2$), lithium manganese dioxide ($LiMnO_2$), Lithium nickel oxide ($LiNiO_2$) and lithium iron phosphate ($LiFePO_4$) are some examples of materials used as cathodes.

For batteries with separator membranes based on PVDF and copolymers, the most used materials for the anode electrodes are Sn nanoparticles within a carbon matrix (Sn-C),

graphite and lithium foil and for the cathode electrode are $LiFePO_4$, $LiCoO_2$ and lithium nickel manganese oxide ($LiNi_{0.5}Mn_{0.5}O_4$) [66, 93, 96].

The abovementioned electrodes are of general use for different separator membranes and some work still remains to be developed in this area in order to optimize electrodes for PVDF based separators. Further, it is to notice that electrodes are typically formed by an active material, additives and a polymer binder. The polymer binder used both as anode and cathode for lithium-ion batteries can be also based on PVDF polymer due to its electrochemical, thermal and chemical stability as well as its easy processing.

Finally, the state of art reflects the suitable characteristics of PVDF and co-polymers for the intended purpose but that there is a lack of research on poly(vinylidene fluoride-trifluoroethylene), P(VDF-TrFE), despite its large potential.

Thus, it is essential to investigate the characteristics of P(VDF-TrFE) co-polymer for battery separator membranes applications and to tune its microstructure, stability and ionic conductivity in order to increase performance of the material as battery separators.

1.4. Objectives

The main objective of my work is the processing, characterization and optimization of polymer separator membranes based on poly(vinylidene fluoride-trifluoroethylene), P(VDF-TrFE), for energy applications.

Electroactive polymers allow tailoring dielectric constant and ionic conductivity, which is one of the main requirements of energy related applications. This work is thus focused on tailoring of the porous structures of the polymer accomplishing also the requirements of mechanical stability and ionic mobility, among others.

The main specific objectives of this work are:

1) Produce the porous membranes of poly(vinylidene fluoride-trifluoroethylene), (P(VDF-TrFE)), in order to tailor the microstructure and the electrical response of the materials.

2) Study the performance of the materials with the inclusion of the lithium salts ($LiClO_4.3H_2O$).

3) Obtain fundamental knowledge on the materials through the relationship between, processing, structural properties and morphology of the materials.

4) Produce a new type of polymer blend based on P(VDF-TrFE) and PEO in order to modify electrolyte uptake and ionic conductivity

5) Study the influence of the different salts in the electrolyte solution in the electrical, thermal and mechanical response of the materials.

6) Select the best materials and microstructures from the point of view of the selected applications.

7) Fabricate and test cells with the developed battery separators.

1.5. Thesis structure and methodology

The present thesis is divided into nine chapters showing the evolution of the work during this investigation.

Seven of those chapters are based on published or submitted scientific articles.

Chapter 1 shows a state of art for polymer electrolyte membranes based on poly(vinylidene fluoride) and its copolymers. Also in this chapter, the objectives of the study as well as the structure of the thesis are provided.

The experimental procedures used in the diverse chapters, i.e, preparation procedures of the materials and characterizations techniques (morphological, thermal, mechanical and electrochemical behavior) are described in chapter 2.

The effect of pore size and overall porosity in the characteristics of microporous membranes of P(VDF-TrFE) are studied and presented in chapter 3. The thermal, mechanical and electrical properties of the membranes were evaluated before and after liquid uptake of an electrolyte solution of 1 M $LiClO_4$–PC.

Chapter 4 reports on the main characteristics of P(VDF-TrFE) membranes doped with different lithium perchlorate trihydrate contents.

Some of the main parameters affecting separator performance such as porosity, dehydration of lithium ions and processing technique (Li-ion uptake versus composite formation) are presented and discussed in chapter 5.

Chapter 6 reports on the effect of PEO content and molecular weight in polymer blends based on poly(vinylidene fluoride-trifluoroethylene)/poly(ethylene oxide), P(VDF-TrFE)/PEO.

The effect of different salts in the electrolyte solution of poly(vinylidene fluoride-co-trifluoroethylene) battery separator membranes is provided in chapter 7.

Chapter 8 reports on the physicochemical properties and cycling tests performed on Li/$LiFePO_4$ and Li/Sn-C half cells of the novel electrolyte membranes based on P(VDF-TrFE) and poly(vinylidene fluoride-hexafluoropropylene), P(VDF-HFP), and the P(VDF-TrFE)/poly(ethylene oxide) blend.

Finally, chapter 9 provides the general conclusions as well as suggestions for future work.

1.6. References

1. Consulting, P.R., *Advanced Batteries for Portable Power Applications,* 2011.
2. Nagaura, T. and K. Tozawa, Progress in Batteries and Solar Cells, 1990. 209.
3. Colin A, V., *Lithium batteries: a 50-year perspective, 1959–2009.* Solid State Ionics, 2000. 134(1-2): p. 159-167.
4. Yazami, R. and P. Touzain, *A reversible graphite-lithium negative electrode for electrochemical generators.* Journal of Power Sources, 1983. 9(3): p. 365-371.
5. Li, J., C. Daniel, and D. Wood, *Materials processing for lithium-ion batteries.* Journal of Power Sources, 2011. 196(5): p. 2452-2460.
6. Besenhard, J.O., ed. *Handbook of Battery Materials*. 1999, Wilcy-VCH.
7. Balbuena, P.B. and Y. Wang, eds. *Lithium-Ion Batteries: Solid-Electrolyte Interphase*. 2004, Imperial College Press: London.
8. Hikmet, R.A.M., *Organic Electrolytes and Electrodes for Batteries,* in *Encyclopedia of Materials: Science and Technology,* K.H.J. Buschow, et al., Editors. 2001, Elsevier: Oxford. p. 6534-6545.
9. Stephan, M.A., *Review on gel polymer electrolytes for lithium batteries.* European Polymer Journal, 2006. 42(1): p. 21-42.
10. Xu, K., *Nonaqueous Liquid Electrolytes for Lithium-Based Rechargeable Batteries.* Chemical Reviews, 2004. 104(10): p. 4303-4418.
11. Janz, G.J. and R.P.T. Tomkins, *Nonaqueous Electrolytes Handbook*1972: Academic Press.
12. Arora, P. and Z. Zhang, *Battery Separators.* Chemical Reviews, 2004. 104(10): p. 4419-4462.
13. Huang, X., *Separator technologies for lithium-ion batteries.* Journal of Solid State Electrochemistry, 2011. 15(4): p. 649-662.
14. Chung, Y.S., S.H. Yoo, and C.K. Kim, *Enhancement of Meltdown Temperature of the Polyethylene Lithium-Ion Battery Separator via Surface Coating with Polymers Having High Thermal Resistance.* Industrial & Engineering Chemistry Research, 2009. 48(9): p. 4346-4351.
15. Gao, K., et al., *PE-g-MMA polymer electrolyte membrane for lithium polymer battery.* Electrochimica Acta, 2006. 52(2): p. 443-449.
16. Venugopal, G., et al., *Characterization of microporous separators for lithium-ion batteries.* Journal of Power Sources, 1999. 77(1): p. 34-41.

17. Choi, B.K., K.H. Shin, and Y.W. Kim, *Lithium ion conduction in PEO-salt electrolytes gelled with PAN.* Solid State Ionics, 1998. 113-115: p. 123-127.
18. Kang, Y., et al., *Photocured PEO-based solid polymer electrolyte and its application to lithium-polymer batteries.* Journal of Power Sources, 2001. 92(1-2): p. 255-259.
19. Laik, B., et al., *Ion-ion interactions and lithium stability in a crosslinked PEO containing lithium salts.* Electrochimica Acta, 1998. 44(5): p. 773-780.
20. Gopalan, A.I., et al., *Development of electrospun PVdF-PAN membrane-based polymer electrolytes for lithium batteries.* Journal of Membrane Science, 2008. 325(2): p. 683-690.
21. Huang, B., et al., *Lithium ion conduction in polymer electrolytes based on PAN.* Solid State Ionics, 1996. 85(1-4): p. 79-84.
22. Sekhon, S.S., N. Arora, and S.A. Agnihotry, *PAN-based gel electrolyte with lithium salts.* Solid State Ionics, 2000. 136-137: p. 1201-1204.
23. Gopalan, A.I., et al., *Poly(vinylidene fluoride)–polydiphenylamine composite electrospun membrane as high-performance polymer electrolyte for lithium batteries.* Journal of Membrane Science, 2008. 318(1-2): p. 422-428.
24. Kim, J.R., et al., *Electrospun PVdF-based fibrous polymer electrolytes for lithium ion polymer batteries.* Electrochimica Acta, 2004. 50(1): p. 69-75.
25. Manuel Stephan, A. and Y. Saito, *Ionic conductivity and diffusion coefficient studies of PVdF–HFP polymer electrolytes prepared using phase inversion technique.* Solid State Ionics, 2002. 148(3–4): p. 475-481.
26. Kataoka, H., et al., *Conduction Mechanisms of PVDF-Type Gel Polymer Electrolytes of Lithium Prepared by a Phase Inversion Process.* The Journal of Physical Chemistry B, 2000. 104(48): p. 11460-11464.
27. Srun Jung, et al., *Fillers for Solid-State Polymer Electrolytes: Highlight.* Bull. Korean Chem. Soc, 2009. 30(10).
28. Nalwa, H.S., *Recent Developments in Ferroelectric Polymers.* Journal of Macromolecular Science, Part C, 1991. 31(4): p. 341-432.
29. Bassett, D.C., *Developments in Crystalline Polymers*1982: Applied Science Publishers.
30. Gregorio, J.R. and M. Cestari, *Effect of crystallization temperature on the crystalline phase content and morphology of poly(vinylidene fluoride).* Journal of Polymer Science Part B: Polymer Physics, 1994. 32(5): p. 859-870.

31. Silva, M.P., et al., *Degradation of the dielectric and piezoelectric response of β-poly(vinylidene fluoride) after temperature annealing.* Journal of Polymer Research, 2011. 18(6): p. 1451-1457.
32. Magalhães, R., et al., *The Role of Solvent Evaporation in the Microstructure of Electroactive β-Poly(Vinylidene Fluoride) Membranes Obtained by Isothermal Crystallization.* Soft Materials, 2010. 9(1): p. 1-14.
33. Sencadas, V., R. Gregorio, and S. Lanceros-Méndez, *α to β Phase Transformation and Microestructural Changes of PVDF Films Induced by Uniaxial Stretch.* Journal of Macromolecular Science, Part B, 2009. 48(3): p. 514-525.
34. Sencadas, V., et al., *Poling of β-poly(vinylidene fluoride): dielectric and IR spectroscopy studies.* e-Polymers, 2005. 2: p. 12.
35. Nalwa, H.S., *Ferroelectric Polymers: Chemistry, Physics, and Applications*1995: Marcel Dekker.
36. Lovinger, A.J., et al., *Crystallographic changes characterizing the Curie transition in three ferroelectric copolymers of vinylidene fluoride and trifluoroethylene: 2. Oriented or poled samples.* Polymer, 1983. 24(10): p. 1233-1239.
37. Furukawa, T., et al., *Ferroelectric phase transition in a copolymer of vinylidene fluoride and trifluoroethylene.* Ferroelectrics, 1981. 32(1): p. 61-67.
38. Li, W., et al., *Crystalline morphologies of P(VDF-TrFE) (70/30) copolymer films above melting point.* Applied Surface Science, 2008. 254(22): p. 7321-7325.
39. Abbrent, S., et al., *Crystallinity and morphology of PVdF–HFP-based gel electrolytes.* Polymer, 2001. 42(4): p. 1407-1416.
40. Jiang, Z., B. Carroll, and K.M. Abraham, *Studies of some poly(vinylidene fluoride) electrolytes.* Electrochimica Acta, 1997. 42(17): p. 2667-2677.
41. Ameduri, B., *From Vinylidene Fluoride (VDF) to the Applications of VDF-Containing Polymers and Copolymers: Recent Developments and Future Trends†*. Chemical Reviews, 2009. 109(12): p. 6632-6686.
42. Wang, Z., Z. Zhang, and T.C.M. Chung, *High Dielectric VDF/TrFE/CTFE Terpolymers Prepared by Hydrogenation of VDF/CTFE Copolymers: Synthesis and Characterization.* Macromolecules, 2006. 39(13): p. 4268-4271.

43. Kalfoglou, N.K. and H.L. Williams, *Mechanical relaxations of poly(vinylidene fluoride) and some of its copolymers.* Journal of Applied Polymer Science, 1973. 17(11): p. 3367-3373.
44. Chu, B., et al., *A Dielectric Polymer with High Electric Energy Density and Fast Discharge Speed.* Science, 2006. 313(5785): p. 334-336.
45. Li, Z., Y. Wang, and Z.-Y. Cheng, *Electromechanical properties of poly(vinylidene-fluoride-chlorotrifluoroethylene) copolymer.* Applied Physics Letters, 2006. 88(6): p. 062904.
46. Sarada, T., L.C. Sawyer, and M.I. Ostler, *Three dimensional structure of celgard® microporous membranes.* Journal of Membrane Science, 1983. 15(1): p. 97-113.
47. Yoshio, M.B., Ralph J; Kozawa, Akiya, *Lithium-Ion Batteries: Science and Technologies*2009: Springer.
48. Tian, L.-y., X.-b. Huang, and X.-z. Tang, *Study on morphology behavior of PVDF-based electrolytes.* Journal of Applied Polymer Science, 2004. 92(6): p. 3839-3842.
49. Ji, G.-L., et al., *PVDF porous matrix with controlled microstructure prepared by TIPS process as polymer electrolyte for lithium ion battery.* Polymer, 2007. 48(21): p. 6415-6425.
50. Su, Y., et al., *PVDF Membrane Formation via Thermally Induced Phase Separation.* Journal of Macromolecular Science, Part A, 2007. 44(1): p. 99-104.
51. Cheng, L.-P., et al., *PVDF membrane formation by diffusion-induced phase separation-morphology prediction based on phase behavior and mass transfer modeling.* Journal of Polymer Science Part B: Polymer Physics, 1999. 37(16): p. 2079-2092.
52. Karabelli, D., et al., *Poly(vinylidene fluoride)-based macroporous separators for supercapacitors.* Electrochimica Acta, 2011. 57(0): p. 98-103.
53. Kim, K.M., J.-C. Kim, and K.S. Ryu, *Physical and Electrochemical Properties of PVdF-HFP/SiO2-Based Polymer Electrolytes Prepared Using Dimethyl Acetamide Solvent and Water Non-Solvent.* Macromolecular Chemistry and Physics, 2007. 208(8): p. 887-895.
54. Li, Z., et al., *High ionic conductive PVDF-based fibrous electrolytes.* Journal of Solid State Electrochemistry, 2008. 12(12): p. 1629-1635.

55. Djian, D., et al., *Macroporous poly(vinylidene fluoride) membrane as a separator for lithium-ion batteries with high charge rate capacity.* Journal of Power Sources, 2009. 187(2): p. 575-580.
56. Kim, S.S. and D.R. Lloyd, *Microporous membrane formation via thermally-induced phase separation. III. Effect of thermodynamic interactions on the structure of isotactic polypropylene membranes.* Journal of Membrane Science, 1991. 64(1–2): p. 13-29.
57. Raghavan, P., et al., *Preparation and electrochemical characterization of gel polymer electrolyte based on electrospun polyacrylonitrile nonwoven membranes for lithium batteries.* Journal of Power Sources, 2011. 196(16): p. 6742-6749.
58. Jacob, M.M.E., S.R.S. Prabaharan, and S. Radhakrishna, *Effect of PEO addition on the electrolytic and thermal properties of PVDF-LiClO4 polymer electrolytes.* Solid State Ionics, 1997. 104(3–4): p. 267-276.
59. Chandra, A., R.C. Agrawal, and Y.K. Mahipal, *Ion transport property studies on PEO–PVP blended solid polymer electrolyte membranes.* Journal of Physics D: Applied Physics, 2009. 42(13): p. 135107.
60. Rao, M., et al., *Preparation and performance of gel polymer electrolyte based on electrospun polymer membrane and ionic liquid for lithium ion battery.* Journal of Membrane Science, 2012. 399–400(0): p. 37-42.
61. Kumar, A. and M. Deka, *PEO/P(VdF-HFP) blend based Li^+ ion-conducting composite polymer electrolytes dispersed with dedoped (insulating) polyaniline nanofibers.* Journal of Solid State Electrochemistry, 2012. 16(1): p. 35-44.
62. Boudin, F., et al., *Microporous PVdF gel for lithium-ion batteries.* Journal of Power Sources, 1999. 81–82(0): p. 804-807.
63. Choi, S.-S., et al., *Electrospun PVDF nanofiber web as polymer electrolyte or separator.* Electrochimica Acta, 2004. 50(2–3): p. 339-343.
64. Cheruvally, G., et al., *Electrospun polymer membrane activated with room temperature ionic liquid: Novel polymer electrolytes for lithium batteries.* Journal of Power Sources, 2007. 172(2): p. 863-869.
65. Li, Z.H., et al., *A foaming process to prepare porous polymer membrane for lithium ion batteries.* Electrochimica Acta, 2009. 54(18): p. 4403-4407.

66. Zhang, H.P., et al., *A porous poly(vinylidene fluoride) gel electrolyte for lithium ion batteries prepared by using salicylic acid as a foaming agent.* Journal of Power Sources, 2009. 189(1): p. 594-598.
67. Tarascon, J.M., et al., *Performance of Bellcore's plastic rechargeable Li-ion batteries.* Solid State Ionics, 1996. 86–88, Part 1(0): p. 49-54.
68. Muniyandi, N., et al., *Optimisation of PVdF-based polymer electrolytes.* Journal of Power Sources, 2001. 96(1): p. 14-19.
69. Vincent, C.A., *Polymer electrolytes.* Progress in Solid State Chemistry, 1987. 17(3): p. 145-261.
70. Jarvis, C.R., et al., *Use of grafted PVdF-based polymers in lithium batteries.* Journal of Power Sources, 2001. 97–98(0): p. 664-666.
71. Saito, Y., et al., *Carrier Migration Mechanism of Physically Cross-Linked Polymer Gel Electrolytes Based on PVDF Membranes.* The Journal of Physical Chemistry B, 2002. 106(29): p. 7200-7204.
72. Wang, Y., J. Travas-Sejdic, and R. Steiner, *Polymer gel electrolyte supported with microporous polyolefin membranes for lithium ion polymer battery.* Solid State Ionics, 2002. 148(3–4): p. 443-449.
73. Magistris, A., et al., *PVDF-based porous polymer electrolytes for lithium batteries.* Solid State Ionics, 2002. 152–153(0): p. 347-354.
74. Quartarone, E., P. Mustarelli, and A. Magistris, *Transport Properties of Porous PVDF Membranes.* The Journal of Physical Chemistry B, 2002. 106(42): p. 10828-10833.
75. Shi, Q., et al., *Structure and performance of porous polymer electrolytes based on P(VDF-HFP) for lithium ion batteries.* Journal of Power Sources, 2002. 103(2): p. 286-292.
76. Croce, F., et al., *Advanced electrolyte and electrode materials for lithium polymer batteries.* Journal of Power Sources, 2003. 119–121(0): p. 399-402.
77. Saunier, J., et al., *Thin and flexible lithium-ion batteries: investigation of polymer electrolytes.* Journal of Power Sources, 2003. 119–121(0): p. 454-459.
78. Song, J.M., et al., *Electrochemical characteristics of phase-separated polymer electrolyte based on poly(vinylidene fluoride–co-hexafluoropropane) and ethylene carbonate.* Electrochimica Acta, 2003. 48(10): p. 1339-1346.
79. Zhang, S.S., et al., *Microporous gel electrolyte Li-ion battery.* Journal of Power Sources, 2004. 125(1): p. 114-118.

80. Saunier, J., et al., *Plasticized microporous poly(vinylidene fluoride) separators for lithium-ion batteries. III. Gel properties and irreversible modifications of poly(vinylidene fluoride) membranes under swelling in liquid electrolytes.* Journal of Polymer Science Part B: Polymer Physics, 2004. 42(12): p. 2308-2317.
81. Shen, Y.J., M.J. Reddy, and P.P. Chu, *Porous PVDF with LiClO4 complex as 'solid' and 'wet' polymer electrolyte.* Solid State Ionics, 2004. 175(1–4): p. 747-750.
82. Saunier, J., et al., *NMR Study of Cation, Anion, and Solvent Mobilities in Macroporous Poly(vinylidene fluoride).* The Journal of Physical Chemistry B, 2005. 109(7): p. 2487-2492.
83. Pu, W., et al., *Preparation of PVDF–HFP microporous membrane for Li-ion batteries by phase inversion.* Journal of Membrane Science, 2006. 272(1–2): p. 11-14.
84. Ward, I.M., et al., *Separator-free rechargeable lithium ion cells produced by the extrusion lamination of polymer gel electrolytes.* Journal of Power Sources, 2006. 162(2): p. 818-822.
85. Yamamoto, T., et al., *4.4 V lithium-ion polymer batteries with a chemical stable gel electrolyte.* Journal of Power Sources, 2007. 174(2): p. 1036-1040.
86. Subba Reddy, C., et al., *Characterization of (PVDF + $LiFePO_4$) solid polymer electrolyte.* Journal of Applied Electrochemistry, 2007. 37(5): p. 637-642.
87. Choi, S.W., et al., *Characterization of Electrospun PVdF Fiber-Based Polymer Electrolytes.* Chemistry of Materials, 2006. 19(1): p. 104-115.
88. Li, X., et al., *Polymer electrolytes based on an electrospun poly(vinylidene fluoride-co-hexafluoropropylene) membrane for lithium batteries.* Journal of Power Sources, 2007. 167(2): p. 491-498.
89. Choi, J.-W., et al., *Rechargeable lithium/sulfur battery with suitable mixed liquid electrolytes.* Electrochimica Acta, 2007. 52(5): p. 2075-2082.
90. Li, G.C., et al., *A porous polymer electrolyte based on P(VDF-HFP) prepared by a simple phase separation process.* Electrochemistry Communications, 2008. 10(12): p. 1883-1885.
91. Miao, R., et al., *PVDF-HFP-based porous polymer electrolyte membranes for lithium-ion batteries.* Journal of Power Sources, 2008. 184(2): p. 420-426.

92. Pandey, G.P. and S.A. Hashmi, *Experimental investigations of an ionic-liquid-based, magnesium ion conducting, polymer gel electrolyte.* Journal of Power Sources, 2009. 187(2): p. 627-634.
93. Croce, F., et al., *A safe, high-rate and high-energy polymer lithium-ion battery based on gelled membranes prepared by electrospinning.* Energy & Environmental Science, 2011. 4(3): p. 921-927.
94. Zhou, J., et al., *Development of all-solid-state mediator-enhanced supercapacitors with polyvinylidene fluoride/lithium trifluoromethanesulfonate separators.* Journal of Power Sources, 2011. 196(23): p. 10479-10483.
95. Ramesh, S. and S.-C. Lu, *Effect of lithium salt concentration on crystallinity of poly(vinylidene fluoride-co-hexafluoropropylene)-based solid polymer electrolytes.* Journal of Molecular Structure, 2011. 994(1–3): p. 403-409.
96. Li, M., et al., *Li/LiFePO4 batteries with gel polymer electrolytes incorporating a guanidinium-based ionic liquid cycled at room temperature and 50 °C.* Journal of Power Sources, 2011. 196(15): p. 6502-6506.
97. Alcock, H.J., et al., *New high-throughput methods of investigating polymer electrolytes.* Journal of Power Sources, 2011. 196(6): p. 3355-3359.
98. Hwang, K., B. Kwon, and H. Byun, *Preparation of PVdF nanofiber membranes by electrospinning and their use as secondary battery separators.* Journal of Membrane Science, 2011. 378(1–2): p. 111-116.
99. Chagnes, A., et al., *Modeling viscosity and conductivity of lithium salts in γ-butyrolactone.* Journal of Power Sources, 2002. 109(1): p. 203-213.
100. Hayamizu, K. and Y. Aihara, *Ion and solvent diffusion and ion conduction of PC-DEC and PC-DME binary solvent electrolytes of LiN(SO2CF3)2.* Electrochimica Acta, 2004. 49(20): p. 3397-3402.
101. Weston, J.E. and B.C.H. Steele, *Effects of inert fillers on the mechanical and electrochemical properties of lithium salt-poly(ethylene oxide) polymer electrolytes.* Solid State Ionics, 1982. 7(1): p. 75-79.
102. Du Pasquier, A., et al., *Plastic PVDF-HFP electrolyte laminates prepared by a phase-inversion process.* Solid State Ionics, 2000. 135(1–4): p. 249-257.
103. Prosini, P.P., P. Villano, and M. Carewska, *A novel intrinsically porous separator for self-standing lithium-ion batteries.* Electrochimica Acta, 2002. 48(3): p. 227-233.

104. Wang, M., et al., *Poly(vinylidene fluoride-hexafluoropropylene)/organo-montmorillonite clays nanocomposite lithium polymer electrolytes.* Electrochimica Acta, 2004. 49(21): p. 3595-3602.
105. Deka, M. and A. Kumar, *Electrical and electrochemical studies of poly(vinylidene fluoride)–clay nanocomposite gel polymer electrolytes for Li-ion batteries.* Journal of Power Sources, 2011. 196(3): p. 1358-1364.
106. Takemura, D., et al., *A powder particle size effect on ceramic powder based separator for lithium rechargeable battery.* Journal of Power Sources, 2005. 146(1–2): p. 779-783.
107. Jiang, Y.-X., et al., *A novel composite microporous polymer electrolyte prepared with molecule sieves for Li-ion batteries.* Journal of Power Sources, 2006. 160(2): p. 1320-1328.
108. Wachtler, M., et al., *A study on PVdF-based SiO2-containing composite gel-type polymer electrolytes for lithium batteries.* Electrochimica Acta, 2004. 50(2–3): p. 357-361.
109. Ciuffa, F., et al., *Lithium and proton conducting gel-type membranes.* Journal of Power Sources, 2004. 127(1–2): p. 53-57.
110. He, X., et al., *In situ composite of nano SiO2–P(VDF-HFP) porous polymer electrolytes for Li-ion batteries.* Electrochimica Acta, 2005. 51(6): p. 1069-1075.
111. Ollinger, M., et al., *Laser printing of nanocomposite solid-state electrolyte membranes for Li micro-batteries.* Applied Surface Science, 2006. 252(23): p. 8212-8216.
112. Stephan, A.M., et al., *Poly(vinylidene fluoride-hexafluoropropylene) (PVdF-HFP) based composite electrolytes for lithium batteries.* European Polymer Journal, 2006. 42(8): p. 1728-1734.
113. Wu, C.-G., et al., *PVdF-HFP/metal oxide nanocomposites: The matrices for high-conducting, low-leakage porous polymer electrolytes.* Journal of Power Sources, 2006. 159(1): p. 295-300.
114. Wang, M. and S. Dong, *Enhanced electrochemical properties of nanocomposite polymer electrolyte based on copolymer with exfoliated clays.* Journal of Power Sources, 2007. 170(2): p. 425-432.

115. Kalyana Sundaram, N.T. and A. Subramania, *Nano-size LiAlO2 ceramic filler incorporated porous PVDF-co-HFP electrolyte for lithium-ion battery applications.* Electrochimica Acta, 2007. 52(15): p. 4987-4993.
116. Subramania, A., et al., *Preparation of a novel composite micro-porous polymer electrolyte membrane for high performance Li-ion battery.* Journal of Membrane Science, 2007. 294(1–2): p. 8-15.
117. Li, Z.H., et al., *Effects of the porous structure on conductivity of nanocomposite polymer electrolyte for lithium ion batteries.* Journal of Membrane Science, 2008. 322(2): p. 416-422.
118. Wang, X.-L., et al., *Gel-based composite polymer electrolytes with novel hierarchical mesoporous silica network for lithium batteries.* Electrochimica Acta, 2008. 53(27): p. 8001-8007.
119. Saikia, D., et al., *Investigation of ionic conductivity of composite gel polymer electrolyte membranes based on P(VDF-HFP), LiClO4 and silica aerogel for lithium ion battery.* Desalination, 2008. 234(1–3): p. 24-32.
120. Li, Z.H., et al., *Macroporous nanocomposite polymer electrolyte for lithium-ion batteries.* Journal of Power Sources, 2008. 184(2): p. 562-565.
121. Pandey, G.P., R.C. Agrawal, and S.A. Hashmi, *Magnesium ion-conducting gel polymer electrolytes dispersed with nanosized magnesium oxide.* Journal of Power Sources, 2009. 190(2): p. 563-572.
122. Lalia, B., et al., *Physicochemical studies of PVdF–HFP-based polymer–ionic liquid composite electrolytes.* Applied Physics A: Materials Science & Processing, 2009. 96(3): p. 661-670.
123. Yang, C., et al., *Polyvinylidene fluoride membrane by novel electrospinning system for separator of Li-ion batteries.* Journal of Power Sources, 2009. 189(1): p. 716-720.
124. Vickraman, P. and V. Senthilkumar, *A study on the role of BaTiO₃ in lithum bis(perfluoroethanesulfonyl)imide-based PVDF-HFP nanocomposites.* Ionics, 2010. 16(8): p. 763-768.
125. Jeong, H.-S., et al., *Effect of phase inversion on microporous structure development of Al2O3/poly(vinylidene fluoride-hexafluoropropylene)-based ceramic composite separators for lithium-ion batteries.* Journal of Power Sources, 2010. 195(18): p. 6116-6121.

126. Zhang, P., et al., *Effects of preparation conditions on porous polymer membranes by microwave assisted effervescent disintegrable reaction and their electrochemical properties.* Journal of Membrane Science, 2010. 362(1–2): p. 113-118.
127. Zhang, D., et al., *Novel composite polymer electrolyte for lithium air batteries.* Journal of Power Sources, 2010. 195(4): p. 1202-1206.
128. Zhang, Y., et al., *Study on performance of composite polymer films doped with modified molecular sieve for lithium-ion batteries.* Electrochimica Acta, 2010. 55(20): p. 5793-5797.
129. Jeong, H.-S. and S.-Y. Lee, *Closely packed SiO2 nanoparticles/poly(vinylidene fluoride-hexafluoropropylene) layers-coated polyethylene separators for lithium-ion batteries.* Journal of Power Sources, 2011. 196(16): p. 6716-6722.
130. Valvo, M., et al., *Direct synthesis and coating of advanced nanocomposite negative electrodes for Li-ion batteries via electrospraying.* Journal of Power Sources, 2011. 196(23): p. 10191-10200.
131. Hwang, H.-Y., et al., *Effect of nanoclay on properties of porous PVdF membranes.* Transactions of Nonferrous Metals Society of China, 2011. 21, Supplement 1(0): p. s141-s147.
132. Mancini, M., et al., *High performance, environmentally friendly and low cost anodes for lithium-ion battery based on TiO2 anatase and water soluble binder carboxymethyl cellulose.* Journal of Power Sources, 2011. 196(22): p. 9665-9671.
133. Kumar, D., M. Suleman, and S.A. Hashmi, *Studies on poly(vinylidene fluoride-co-hexafluoropropylene) based gel electrolyte nanocomposite for sodium–sulfur batteries.* Solid State Ionics, 2011. 202(1): p. 45-53.
134. Huang, X., *Cellular porous polyvinylidene fluoride composite membranes for lithium-ion batteries.* Journal of Solid State Electrochemistry: p. 1-7.
135. Jeong, H.-S., et al., *Evaporation-induced, close-packed silica nanoparticle-embedded nonwoven composite separator membranes for high-voltage/high-rate lithium-ion batteries: Advantageous effect of highly percolated, electrolyte-philic microporous architecture.* Journal of Membrane Science, 2012. 415–416(0): p. 513-519.

136. Lalia, B., Y. Samad, and R. Hashaikeh, *Nanocrystalline cellulose-reinforced composite mats for lithium-ion batteries: electrochemical and thermomechanical performance.* Journal of Solid State Electrochemistry: p. 1-7.
137. Nunes-Pereira, J., et al., *Porous Membranes of Montmorillonite/Poly(vinylidene fluoride-trifluorethylene) for Li-Ion Battery Separators.* Electroanalysis, 2012. 24(11): p. 2147-2156.
138. Nunes-Pereira, J., et al., *Microporous membranes of NaY zeolite/poly(vinylidene fluoride-trifluorethylene) for Li-ion battery separators.* Journal of Electroanalytical Chemistry, 2013. 689: p. 223-232.
139. Nunes-Pereira, J., et al., *Li-ion battery separator membranes based on poly(vinylidene fluoride-trifluoroethylene)/carbon nanotube composites.* Solid State Ionics, 2013. 249–250(0): p. 63-71.
140. Nunes-Pereira, J., et al., *Li-ion battery separator membranes based on barium titanate and poly(vinylidene fluoride-co-trifluoroethylene): Filler size and concentration effects.* Electrochimica Acta, 2014. 117(0): p. 276-284.
141. Gentili, V., et al., *Composite gel-type polymer electrolytes for advanced, rechargeable lithium batteries.* Journal of Power Sources, 2007. 170(1): p. 185-190.
142. Croce, F., et al., *Physical and Chemical Properties of Nanocomposite Polymer Electrolytes.* The Journal of Physical Chemistry B, 1999. 103(48): p. 10632-10638.
143. Appetecchi, G.B. and S. Passerini, *PEO-carbon composite lithium polymer electrolyte.* Electrochimica Acta, 2000. 45(13): p. 2139-2145.
144. Kim, D.-W. and Y.-K. Sun, *Electrochemical characterization of gel polymer electrolytes prepared with porous membranes.* Journal of Power Sources, 2001. 102(1–2): p. 41-45.
145. Liu, X., H. Kusawake, and S. Kuwajima, *Preparation of a PVdF-HFP/polyethylene composite gel electrolyte with shutdown function for lithium-ion secondary battery.* Journal of Power Sources, 2001. 97–98(0): p. 661-663.
146. Rajendran, S., O. Mahendran, and R. Kannan, *Characterisation of [(1−x)PMMA–xPVdF] polymer blend electrolyte with Li+ ion.* Fuel, 2002. 81(8): p. 1077-1081.
147. Wang, Z.-l. and Z.-y. Tang, *A novel polymer electrolyte based on PMAML/PVDF-HFP blend.* Electrochimica Acta, 2004. 49(7): p. 1063-1068.

148. Michael, M.S. and S.R.S. Prabaharan, *Rechargeable lithium battery employing a new ambient temperature hybrid polymer electrolyte based on PVK+PVdF–HFP (copolymer).* Journal of Power Sources, 2004. 136(2): p. 408-415.
149. Lee, Y.M., et al., *Novel porous separator based on PVdF and PE non-woven matrix for rechargeable lithium batteries.* Journal of Power Sources, 2005. 139(1–2): p. 235-241.
150. Wang, Z. and Z. Tang, *Characterization of the polymer electrolyte based on the blend of poly(vinylidene fluoride-co-hexafluoropropylene) and poly(vinyl pyrrolidone) for lithium ion battery.* Materials Chemistry and Physics, 2003. 82(1): p. 16-20.
151. Kim, J.-U. and H.-B. Gu, *Electrochemical properties of VO–flyash composite for lithium polymer battery.* Journal of Power Sources, 2003. 119–121(0): p. 766-769.
152. Munch Elmer, A., et al., *Ion conductive electrolyte membranes based on co-continuous polymer blends.* Journal of Materials Chemistry, 2003. 13(9): p. 2168-2176.
153. Song, M.-K., et al., *Composite polymer electrolytes reinforced by non-woven fabrics.* Journal of Power Sources, 2004. 125(1): p. 10-16.
154. Cheng, C.L., C.C. Wan, and Y.Y. Wang, *Preparation of porous, chemically cross-linked, PVdF-based gel polymer electrolytes for rechargeable lithium batteries.* Journal of Power Sources, 2004. 134(2): p. 202-210.
155. Kum, K.-S., et al., *The effect of mixed salts in gel-coated polymer electrolyte for advanced lithium battery.* Electrochimica Acta, 2004. 50(2–3): p. 285-288.
156. Lee, Y.M., et al., *Electrochemical effect of coating layer on the separator based on PVdF and PE non-woven matrix.* Journal of Power Sources, 2005. 146(1–2): p. 431-435.
157. Sannier, L., et al., *Room temperature lithium metal batteries based on a new Gel Polymer Electrolyte membrane.* Journal of Power Sources, 2005. 144(1): p. 231-237.
158. Sannier, L., et al., *Evaluation of GPE performances in lithium metal battery technology by means of simple polarization tests.* Journal of Power Sources, 2006. 158(1): p. 564-570.

159. Xi, J., et al., *PVDF–PEO blends based microporous polymer electrolyte: Effect of PEO on pore configurations and ionic conductivity.* Journal of Power Sources, 2006. 157(1): p. 501-506.
160. Subramania, A., N.T.K. Sundaram, and G.V. Kumar, *Structural and electrochemical properties of micro-porous polymer blend electrolytes based on PVdF-co-HFP-PAN for Li-ion battery applications.* Journal of Power Sources, 2006. 153(1): p. 177-182.
161. Cao, J.-H., B.-K. Zhu, and Y.-Y. Xu, *Structure and ionic conductivity of porous polymer electrolytes based on PVDF-HFP copolymer membranes.* Journal of Membrane Science, 2006. 281(1–2): p. 446-453.
162. Jeon, J.-D. and S.-Y. Kwak, *Variable-Temperature 7Li Solid-State NMR Investigation of Li-Ion Mobility and Its Correlation with Conductivity in Pore-Filling Polymer Electrolytes for Secondary Batteries.* Macromolecules, 2006. 39(23): p. 8027-8034.
163. Zhang, H.P., et al., *A novel sandwiched membrane as polymer electrolyte for lithium ion battery.* Electrochemistry Communications, 2007. 9(7): p. 1700-1703.
164. Hwang, Y.J., et al., *Electrochemical studies on poly(vinylidene fluoride–hexafluoropropylene) membranes prepared by phase inversion method.* European Polymer Journal, 2007. 43(1): p. 65-71.
165. Reddy, C., et al., *Electrochemical studies on PVC/PVdF blend-based polymer electrolytes.* Journal of Solid State Electrochemistry, 2007. 11(4): p. 543-548.
166. Sundaram, N.T.K. and A. Subramania, *Microstructure of PVdF-co-HFP based electrolyte prepared by preferential polymer dissolution process.* Journal of Membrane Science, 2007. 289(1–2): p. 1-6.
167. Rajendran, S. and P. Sivakumar, *An investigation of PVdF/PVC-based blend electrolytes with EC/PC as plasticizers in lithium battery applications.* Physica B: Condensed Matter, 2008. 403(4): p. 509-516.
168. Bansal, D., B. Meyer, and M. Salomon, *Gelled membranes for Li and Li-ion batteries prepared by electrospinning.* Journal of Power Sources, 2008. 178(2): p. 848-851.
169. Sohn, J.-Y., et al., *Preparation and characterization of a PVDF-HFP/PEGDMA-coated PE separator for lithium-ion polymer battery by electron beam irradiation.* Radiation Physics and Chemistry, 2009. 78(7–8): p. 505-508.

170. Wang, Y.-J. and D. Kim, *The effect of F127 addition on the properties of PEGDA/PVdF cross-linked gel polymer electrolytes.* Journal of Membrane Science, 2008. 312(1–2): p. 76-83.
171. Xiao, Q., et al., *A novel sandwiched membrane as polymer electrolyte for application in lithium-ion battery.* Journal of Membrane Science, 2009. 326(2): p. 260-264.
172. Fan, L.-Z., X.-L. Wang, and F. Long, *All-solid-state polymer electrolyte with plastic crystal materials for rechargeable lithium-ion battery.* Journal of Power Sources, 2009. 189(1): p. 775-778.
173. Eo, S.-M., E. Cha, and D.-W. Kim, *Effect of an inorganic additive on the cycling performances of lithium-ion polymer cells assembled with polymer-coated separators.* Journal of Power Sources, 2009. 189(1): p. 766-770.
174. Ding, Y., et al., *The ionic conductivity and mechanical property of electrospun P(VdF-HFP)/PMMA membranes for lithium ion batteries.* Journal of Membrane Science, 2009. 329(1–2): p. 56-59.
175. Jeong, H.-S., J.H. Kim, and S.-Y. Lee, *A novel poly(vinylidene fluoride-hexafluoropropylene)/poly(ethylene terephthalate) composite nonwoven separator with phase inversion-controlled microporous structure for a lithium-ion battery.* Journal of Materials Chemistry, 2010. 20(41): p. 9180-9186.
176. Ulaganathan, M. and S. Rajendran, *Effect of different salts on PVAc/PVdF-co-HFP based polymer blend electrolytes.* Journal of Applied Polymer Science, 2010. 118(2): p. 646-651.
177. Li, H., et al., *Gel polymer electrolytes based on active PVDF separator for lithium ion battery. I: Preparation and property of PVDF/poly(dimethylsiloxane) blending membrane.* Journal of Membrane Science, 2011. 379(1–2): p. 397-402.
178. Saikia, D., et al., *Highly conductive and electrochemically stable plasticized blend polymer electrolytes based on PVdF-HFP and triblock copolymer PPG-PEG-PPG diamine for Li-ion batteries.* Journal of Power Sources, 2011. 196(5): p. 2826-2834.
179. Sohn, J.-Y., et al., *PVDF-HFP/PMMA-coated PE separator for lithium ion battery.* Journal of Solid State Electrochemistry, 2012. 16(2): p. 551-556.
180. Park, J.K., *Principles and Applications of Lithium Secondary Batteries*2012: Wiley.

181. Park, M., et al., *A review of conduction phenomena in Li-ion batteries.* Journal of Power Sources, 2010. 195(24): p. 7904-7929.

182. de las Casas, C. and W. Li, *A review of application of carbon nanotubes for lithium ion battery anode material.* Journal of Power Sources, 2012. 208(0): p. 74-85.

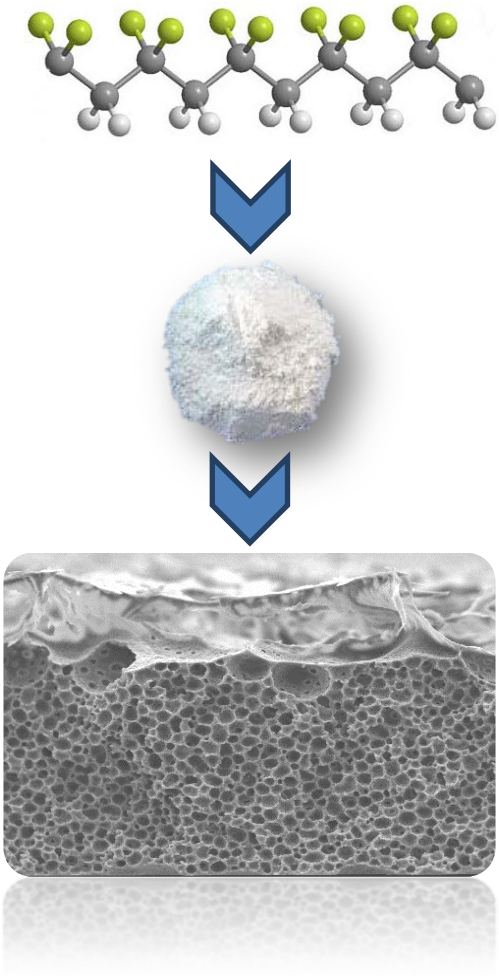

2. Materials and Methods

This chapter provides a description of the experimental procedures used in the preparation and characterization of the membranes, as well as for the battery tests.

2.1. Materials and sample preparation

2.1.1. P(VDF-TrFE) membranes

Poly(vinylidene fluoride-trifluoroethylene) (P(VDF-TrFE)) (70/30, M_w = 350000 g/mol) (*Solvay*, Brussels, Belgium) was dissolved in N,N-dimethyl formamide (DMF - *Merck*). The copolymer was dissolved in the solvent at room temperature with the help of a magnetic stirrer until a homogeneous solution was obtained. In order to prevent the formation of aggregates and help to dissolve the powder, was increased in 5ºC for 15 minutes the temperature of the solution. The solution was prepared using different P(VDF-TrFE)/DMF volume fractions: 5/95, 10/90 and 15/85, which allows tailoring porous dimensions and degree of porosity [1, 2]. For obtained non-porous membranes, solvent evaporation was achieved at 120 °C for 60 min and the sample was then melted at 210 °C and cooled at room temperature.

2.1.2. Composite membranes

Lithium perchlorate trihydrat ($LiClO_4.3H_2O$) was acquired from Merck.

The solid polymer electrolytes were identified by $P(VDF\text{-}TrFE)_nLiClO_4.3H_2O$, where n expresses the salt content as the number of ether oxygen atoms per Li^+ cation. Specific amounts of lithium perchlorate trihydrate were incorporated into P(VDF-TrFE) matrices, forming polymer electrolytes with compositions of $1.5 \leq n \leq 15$ [3].

The solution was prepared using a constant P(VDF-TrFE)/DMF volume fraction of 15/85. The lithium ions were added to DMF and dispersed with a magnetic stirrer. P(VDF-TrFE) powder were subsequently added to the solution and dissolved at room temperature. In order to obtain non porous samples, the solution was spread in a glass surface and the system was kept inside an over at 210 ºC during 10 minutes before cooling down at room temperature. Porous samples were obtained from the same solution but the solvent evaporation occurred at room temperature during 15 days [1].

2.1.3. Polymer blends

PEO (M_w = 10000 and M_w = 100000 g.mol^{-1}) were acquired from Polysciences.
P(VDF-TrFE)/PEO blends were prepared with compositions of 100/0, 80/20, 60/40, 40/60 and 0/100 weight ratio for the two molecular weights of PEO. Blends were prepared by dissolving the adequate amounts of both polymers in N,N-dimethylformamide (DMF) at a 15/85 w/v polymer/solvent ratio. The polymers were dissolved at 60 ºC during 4 hours with the help of a magnetic stirrer until a homogeneous and transparent solution was obtained. The solutions were poured in clean Petri dishes and the solvent was allowed to evaporate at 70 ºC for two hours. Finally, complete removal of the solvent was achieved in vacuum at 10^{-2} mm Hg and 70 ºC for another 3 hours. Membranes with a typical thickness of 30 μm were obtained.

2.1.4. P(VDF-HFP) membranes

Poly(vinylidene fluoride-co-hexafluoropropylene) (P(VDF-HFP), 88/12, M_w = 600,000 g mol^{-1}) were supplied from Solvay (Belgium). P(VDF-HFP)-based membrane was prepared by dissolving the polymer material in N,N-dimethylformamide (DMF, from Merck) at a 15/85 polymer/solvent weight ratio.
The copolymer was dissolved in the solvent (DMF) at room temperature with the help of a magnetic stirrer until a homogeneous and transparent solution was obtained. In order to prevent the formation of aggregates and help to dissolve the powders was increased in 5 ºC for 15 min the temperature of the solution.
After complete dissolution of the copolymer and then placed in a glass petri dish to evaporate DMF (15 days at room temperature in gas extraction chamber).

2.1.5. Composite electrodes

Composite electrodes were prepared by blending the active material ($LiFePO_4$ or Sn-C (Sn:C weight ratio equal to 3:7, [4-7]), the electronic conductor (Super-P carbon, MMM) and the binder (PVDF, Solvay) in *N*-methyl-pyrrolidone. The so-obtained slurry was cast onto aluminum ($LiFePO_4$) or copper (Sn) foil, allowing the solvent removal. Coin electrodes, having a 10 mm diameter and thickness ranging from 40 μm to 50 μm, were punched from the tapes. Finally, the electrodes were dried under vacuum at 110°C overnight and transferred in the glove box. The weight composition of electrodes

resulted 80:10:10 with an active material mass loading of 3.0 mg cm^{-2} (cathodes) and 4.6 mg cm^{-2} (anodes). Taking into account for a reversible specific capacity of 170 mA h g^{-1} ($LiFePO_4$) and 400 mA h g^{-1} (Sn-C), this corresponds to 0.5 mA h cm^{-2} ($LiFePO_4$) and 1.8 mA h cm^{-2} (Sn), respectively.

2.1.6. Cell preparation

All test cells were manufactured in the glove box. The ionic conductivity was investigated in 2032 coin-type cells with two stainless steel, blocking disk electrodes divided by a 400 μm PTFE circular spacer (having an internal area equal to 0.5 cm^2). The sample membrane (having a slightly higher thickness) was housed within the spacer. The Li/$LiFePO_4$ and Li/Sn-C half-cells were fabricated by housing in 2032 coin-type containers the sequence composed by a lithium disc anode (10 mm diameter), a swollen PVDF-based membrane (14 mm) and a $LiFePO_4$ (or Sn-C) electrode (10 mm).

2.2. Materials and sample characterization

The techniques used for the characterization of the different membranes covers different properties such as morphological, thermal, mechanical and electrochemical properties.

2.2.1. Porosity

The porosity of the samples was measured with a pycnometer by the following procedure: the weight of the pycnometer filled with ethanol, was measured and labeled as W_1; the sample, whose weight was W_s, was immersed in ethanol. After the sample was saturated by ethanol, additional ethanol was added to complete the volume of the pycnometer. Then, the pycnometer was weighted and labeled as W_2; the sample filled with ethanol was taken out of the pycnometer. The residual weight of the ethanol and the pycnometer was labeled W_3. The porosity of the membrane was calculated according to:

$$\varepsilon = \frac{W_2 - W_3 - W_s}{W_1 - W_3} \quad (1)$$

The mean porosity of each membrane was obtained as the average of the values determined in three samples.

2.2.2. Electrolyte solution and uptake

Propylene carbonate (PC), Lithium perchlorate trihydrat ($LiClO_4.3H_2O$) and 1M lithium hexafluorophosphate ($LiPF_6$) in ethylene carbonate/dimethyl carbonate (EC-DMC, 1/1 in weight (LP30)) were acquired from Merck. Lithium tetrafluoroborate ($LiBF_4$), Lithium Bis (Trifluoromethanesulfonyl) Imide (LiTFSI), Magnesium trifluoromethanesulfonate ($Mg(CF_3SO_3)_2$ and Sodium trifluoromethanesulfonate ($Na(CF_3SO_3)$ were purchased from Sigma Aldrich. The $LiClO_4$ powder was obtained by dehydration of $LiClO_4.3H_2O$ by thermal treatment [8]. The ionic liquid electrolyte was a mixture of the lithium bis(trifluoromethanesulfonyl)imide, LiTFSI (purchased from Solvionic) salt with the ionic liquid N-butyl-N-methylpyrrolidinium bis(trifluoromethanesulfonyl)imide, PYR14TFSI (Solvionic). The LiTFSI/PYR14TFSI (mole ratio fixed equal to 1/9) mixture, prepared by dissolving the lithium salt in the ionic liquid compound, was successively vacuum dried (the vapor pressure of ionic liquids is non-detectable) overnight at 120°C.

The membranes were immersed into 1M solution of $LiClO_4$, $LiClO_4 \cdot 3H_2O$, $LiBF_4$, LiTFSi, $Mg(CF_3SO_3)_2$ and $Na(CF_3SO_3)$ in PC for 24 h and the uptake was evaluated by equation 2:

$$\varepsilon = \left(\frac{M - M_0}{M_0} \right) * 100\% \quad , \quad (2)$$

where ε is the uptake of the electrolyte solution, M_0 is the mass of the membrane and M is the mass of the membrane after immersion in the electrolyte solution.

The liquid content (L_t) of the 1M $LiPF_6$-EC-DMC solution and the LiTFSI/PYR_{14}TFSI, achieved upon an immersion time equal to *t*, was evaluated by the following equation:

$$L_t = \left(1 - \left(\frac{M_0}{M_t} \right) \right) \times 100 \quad (3)$$

where M_0 is the mass of the pristine sample membrane and M_t is the mass of the swollen membrane after immersion in the electrolyte solution. This test was run until to achieve a time-stable liquid uptake within the separator membrane.

The electrolyte loss was determined by recording the weight variation of fully swollen sample membranes, exposed to the glove box atmosphere, as a function of the exposition time. The sample weight was normalized with respect to the initial one (e.g., fully swollen membrane). The test was not performed for the non-volatile ionic liquid electrolytes. The conductivity of the different electrolyte solution (1 M of $LiClO_4.3H_2O$, $LiBF_4$, LiTFSi, $Mg(CF_3SO_3)_2$ and $Na(CF_3SO_3)$ in PC) was measured in a Conductivity Meters (Crison-525).

2.2.3. Morphology and polymer phase

Samples were coated with gold using a sputter coating and their morphology was observed by scanning electron microscopy (SEM) (model JSM-6300, JEOL) with an accelerating voltage of 10 kV.

Polymer phase was determined through infrared measurements (FTIR) performed at room temperature in a Perkin-Elmer Spectrum 100 apparatus in ATR mode from 4000 to 650 cm^{-1}. FTIR spectra were collected with 32 scans and a resolution of 4 cm^{-1}.

2.2.4. Thermal properties

Thermogravimetric studies were performed in open platinum crucibles using a Rheometric Scientific TG 1000 thermobalance operating under a flowing argon atmosphere between 30ºC and 700ºC at a heating rate of 10 ºCmin^{-1}.

The activation energy of the degradation process was determined by the Broido method (Equation 4), assuming n = 1 and considering the specific heating rate $\beta = \partial T/\partial t$ [9]:

$$\ln\left[-\ln(1-\alpha)\right] = -\frac{E_a}{RT} + const \quad , \tag{4}$$

where α represents the degree of conversion of the sample under degradation, defined by: $\alpha = w_0 - w(t)/w_0 - w_\infty$, with w_0, $w_{(t)}$ and w_∞ being the weights of the sample before degradation, at time t and after complete degradation, respectively. E_a is the activation energy of the process, T is the temperature and R is the gas constant (8.314 J.mol^{-1}.K^{-1}).

Sections of the electrolytes for Differential Scanning Calorimetry (DSC) characterization were removed from films and subjected to thermal analysis under a flowing argon atmosphere between 25 and 200 ºC and at a heating rate of 10 ºC.min^{-1} using a Perking Elmer Diamond instrument.

The degree of crystallinity (ΔX_{cryst}) of the samples was calculated from the DSC scans using equation 5:

$$\Delta X_c = \frac{\Delta H_f}{\Delta H_{100}} \quad , \tag{5}$$

where ΔH_f is the melting enthalpy of the sample and ΔH_{100} is the melting enthalpy for a 100% crystalline sample, being 103.4 J g^{-1} for P(VDF-TrFE) [10] and 203 J g^{-1} for PEO [11].

2.2.5. Mechanical properties

The mechanical behaviour was characterized by dynamic mechanical analysis (DMA) performed in a DMA8000 apparatus from Perkin-Elmer or Seiko DMS210 apparatus using the tensile mode and a frequency scan from 0.01 to 20Hz at room temperature. Rectangular samples were used with typical dimensions of 10x4x0.030 mm.

Stress–strain mechanical measurements were carried out at room temperature with a TST350 tensile testing set up from Linkam Scientific Instruments at a strain rate of 15 μm/s. Rectangular samples of the membranes (~1 cm wide and 4 cm long) were cut from the original sheet.

2.2.6. Electrochemical impedance spectroscopy

Impedance spectroscopy was performed with an Autolab PGSTAT-12 (Eco Chemie) set up for frequencies between 500 mHz and 65 kHz, using a constant volume support equipped with gold blocking electrodes located within a Buchi TO 50 oven. The sample temperature variation ranged from 20 to 140 ^{o}C and was measured by means of a type K thermocouple placed close to the films. The ionic conductivity was measured during the heating cycles and the ionic conductivity was determined by

$$\sigma = \frac{t}{A \times R} \tag{6}$$

where t is the thickness, A is the area of the samples and R is the bulk resistance obtained from the intercept of the imaginary impedance (minimum value of Z'') with the slanted line in the real impedance (Z'). The tortuosity (τ), the ratio between the effective capillarity to thickness of the sample, was determined by [12]:

$$\sigma_{eff} = \sigma_0 \frac{\phi}{\tau^2} \tag{7}$$

where σ_0 is the conductivity of the liquid electrolyte, σ_{eff} is the conductivity of the membrane and the electrolyte set and ϕ is the porosity of the membrane.

The MacMullin number, N_M, describes the relative contribution of a separator to cell resistance and is defined by [13]:

$$N_M = \frac{\sigma_0}{\sigma_{eff}} \tag{8}$$

where σ_{eff} is the conductivity of the membrane and liquid electrolyte pair and σ_0 is the conductivity of the pure liquid electrolyte.

2.2.7. Cycle voltammetry

Evaluation of the electrochemical stability of the polymer electrolytes was carried out within a dry argon-filled glovebox using a two-electrode cell configuration with a gold microelectrode as working electrode. The preparation of the 25 μm diameter gold microelectrode surface by a conventional polishing routine was completed outside the glovebox. The microelectrode was then washed with Tetrahydrofuran (THF), dried with a hot-air blower and transferred into the glovebox. Cell assembly was initiated by locating a freshly-cleaned lithium disk counter electrode (10 mm diameter, 1mm thick, Aldrich, 99.9% purity) on a stainless steel current collector. A thin-film sample of the electrolyte was centered over the counter electrode and the cell assembly completed by placing a microelectrode in the centre of the sample disk. The assembly was held together firmly with a clamp and electrical contacts were made to an Autolab PGSTAT-12 (Eco Chemie) apparatus used to record voltammograms at a scan rate of 100 mVs^{-1}. Measurements were conducted at room temperature within a Faraday cage located inside the glovebox.

From the voltammograms, the diffusion coefficient of the electroactive species (D) was calculated according to the Randles-Sevcik equation [14]:

$$i_p = (2.69 \times 10^5)\, n^{3/2}\, A D^{1/2}\, v^{1/2}\, C_0 \qquad (9)$$

where i_p is the oxidative peak current, n is the number of ionic charges involved in the electrode reaction, A is the electrode area, v is the potential scan rate and C_0 is the concentration of the electroactive species.

2.2.8. Charge – discharge battery performance

The cycling performance of the $Li/LiFePO_4$ and Li/Sn-C half-cells was carried out using a multichannel Maccor 4000 battery tester at room temperature. The (galvanostatic) measurements were performed within the 2.0-4.0 V (cathode half-cells) and 0.01-2.0 V (anode half-cells) voltage range, respectively, at current rates from 0.1C through 2C.

2.3. References

1. California, A., et al., *Tailoring porous structure of ferroelectric poly(vinylidene fluoride-trifluoroethylene) by controlling solvent/polymer ratio and solvent evaporation rate.* European Polymer Journal, 2011. 47(12): p. 2442-2450.
2. Costa, C.M., et al., *Electroactive Poly(Vinylidene Fluoride-Trifluorethylene) (PVDF-TrFE) Microporous Membranes for Lithium-Ion Battery Applications.* Ferroelectrics, 2012. 430(1): p. 103-107.
3. Barbosa, P.C., et al., *Studies of solid-state electrochromic devices based on PEO/siliceous hybrids doped with lithium perchlorate.* Electrochimica Acta, 2007. 52(8): p. 2938-2943.
4. Brutti, S., et al., *A high power Sn–C/C–LiFePO4 lithium ion battery.* Journal of Power Sources, 2012. 217(0): p. 72-76.
5. Elia, G.A., et al., *Mechanically milled, nanostructured SnC composite anode for lithium ion battery.* Electrochimica Acta, 2013. 90(0): p. 690-694.
6. Hassoun, J., et al., *A lithium ion battery using nanostructured Sn–C anode, LiFePO4 cathode and polyethylene oxide-based electrolyte.* Solid State Ionics, 2011. 202(1): p. 36-39.
7. Scrosati, B., *Recent advances in lithium ion battery materials.* Electrochimica Acta, 2000. 45(15–16): p. 2461-2466.
8. Wickleder, M.S., *Crystal Structure of LiClO4.* Zeitschrift für anorganische und allgemeine Chemie, 2003. 629(9): p. 1466-1468.
9. Broido, A., *A simple, sensitive graphical method of treating thermogravimetric analysis data.* Journal of Polymer Science Part A-2: Polymer Physics, 1969. 7(10): p. 1761-1773.
10. Sencadas, V., S. Lanceros-Méndez, and J.F. Mano, *Characterization of poled and non-poled β-PVDF films using thermal analysis techniques.* Thermochimica Acta, 2004. 424(1–2): p. 201-207.
11. Porter, R.S., *Macromolecular physics, volume 3—crystal melting, Bernhard Wunderlich, Academic Press, New York, 1980, 363 pp. Price: $42.50.* Journal of Polymer Science: Polymer Letters Edition, 1980. 18(12): p. 824-824.
12. Karabelli, D., et al., *Poly(vinylidene fluoride)-based macroporous separators for supercapacitors.* Electrochimica Acta, 2011. 57(0): p. 98-103.

13. Patel, K.K., J.M. Paulsen, and J. Desilvestro, *Numerical simulation of porous networks in relation to battery electrodes and separators.* Journal of Power Sources, 2003. 122(2): p. 144-152.
14. Bard, A.J. and L.R. Faulkner, *Electrochemical Methods: Fundamentals and Applications*2000: Wiley.

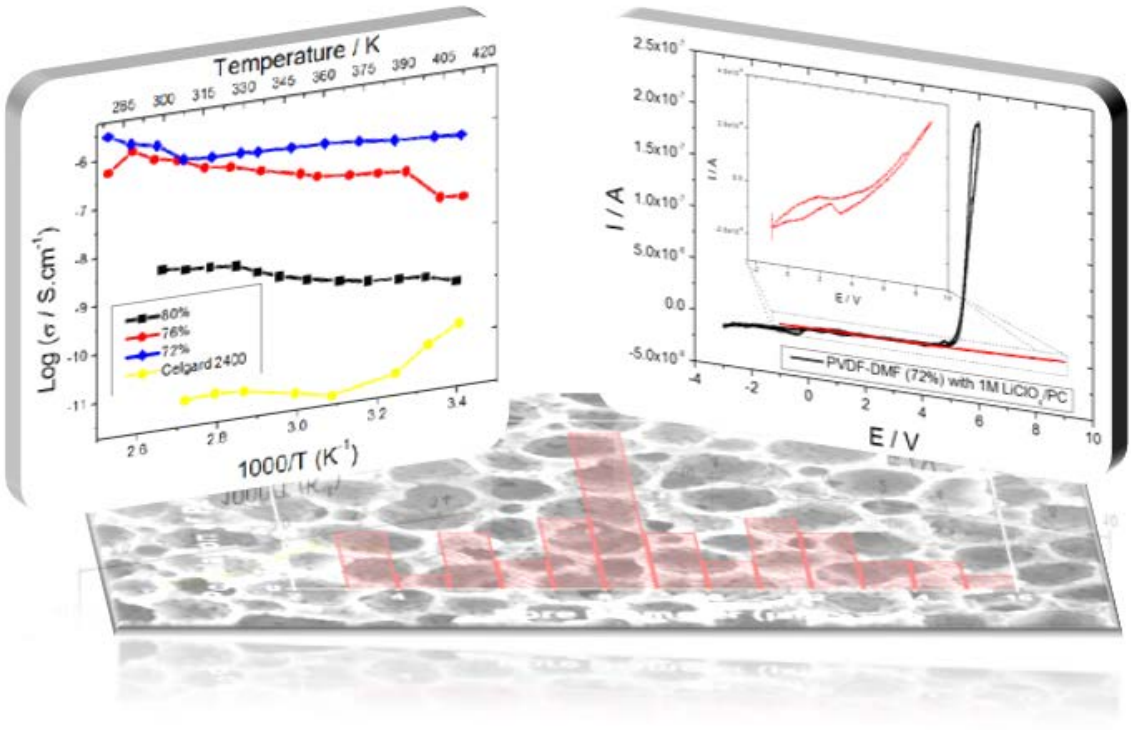

3. *Effect of the degree of porosity in the properties of P(VDF-TrFE) battery separators*

This chapter describes the effect of the porosity on the main characteristics of P(VDF–TrFE) membranes for Li-ion separators. The thermal, mechanical and electrical properties of the membranes are thus evaluated before and after liquid uptake of 1 M $LiClO_4$–PC

This chapter is based on the following publication:

"Effect of degree of porosity on the properties of poly(vinylidene fluoride-trifluoroethylene) for Li-ion battery separators", C. M. Costa, L. C. Rodrigues, V. Sencadas, M. M. Silva, J. G. Rocha, S. Lanceros-Méndez, Journal of Membrane Science 407-408 (2012) 193-201

3. Effect of the degree of porosity in the properties of P(VDF-TrFE) battery separators

3.1.Samples

The samples used in this chapter were prepared from P(VDF-TrFE)/DMF volume fractions of 5/95, 10/90 and 15/85 at room temperature following the experimental procedure described in the chapter 2. The samples P(VDF–TrFE)/DMF exhibit degrees of porosity of 80%, 76% and 72%, respectively. The electrolyte solution used is 1M $LiClO_4$ in PC.

3.2. Results and discussion

3.2.1. Polymer phase and microstructural characteristics

The porous membranes were prepared by the solvent-cast method at room temperature from a homogeneous solution in dimethyformamide with different relative polymer/solvent concentrations in order to produce different membranes morphologies [1, 2]. The effect of polymer – solvent interaction as a function of temperature and polymer concentration has been previously studied [1-3] and has been determined that polymer/solvent interactions (i.e, the evaporation of the solvent and the crystallization temperature) determine the final microstructure and properties of separators.

The membranes selected for the present investigation were prepared from P(VDF-TrFE)/DMF volume fractions of 5/95, 10/90 and 15/85 at room temperature. All samples show a thickness between 150 to 250 μm, mean pore size around 16±9μm and mean pore size around 9±3μm of membrane with higher and lower porosity, respectively (Figure 3.1) [4].

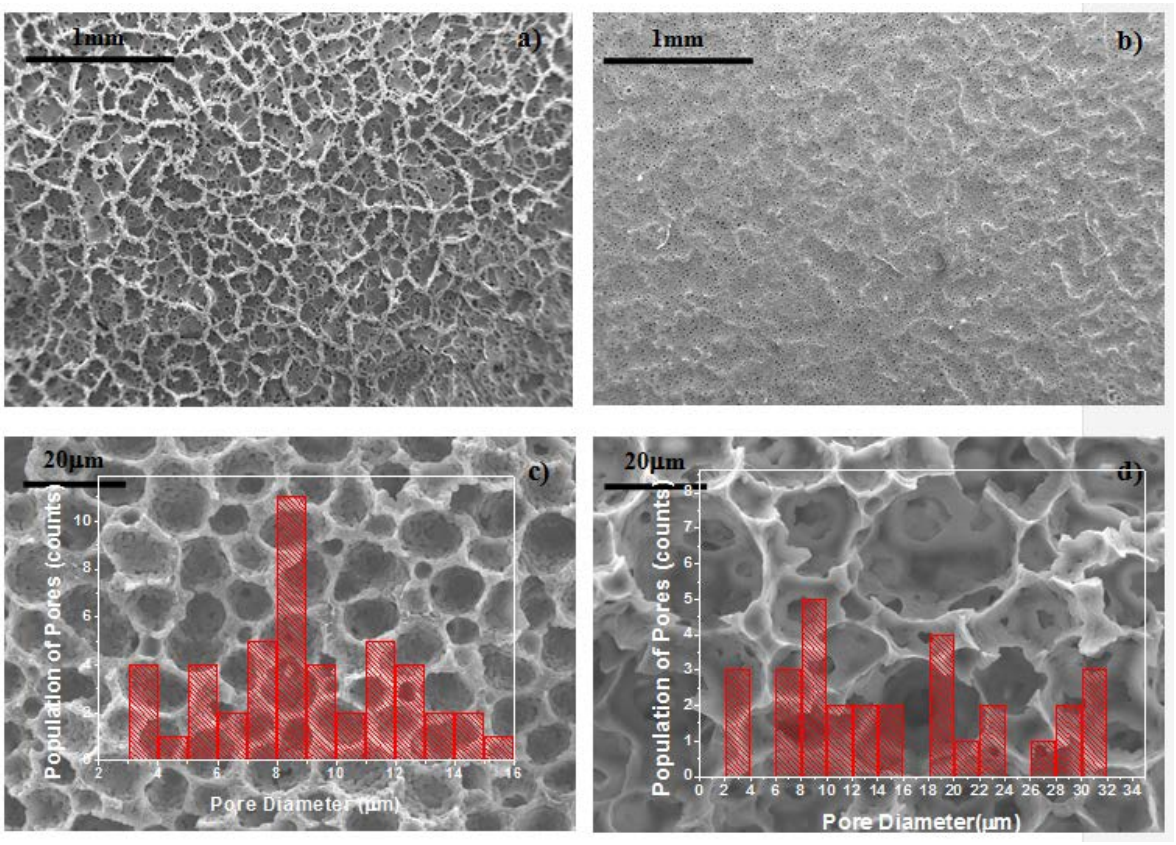

Figure 3.1 - Microstructure of the P(VDF-TrFE) membranes crystallized at room temperature. Surface characteristics of the samples with 72 % (a) and 80 % (b) porosity and cross-section details, respectively in (c) and (d). Insets in the figure (c) and (d) exhibits pore size distribution of the separators. The membranes were obtained from 15/85 and 5/95 polymer/solvent ratios, respectively.

The variation of the initial polymer concentration in the polymer/solvent solution allows obtaining porous membranes with same shape of pores but with different pore size and degree of porosity between 70 and 80%.

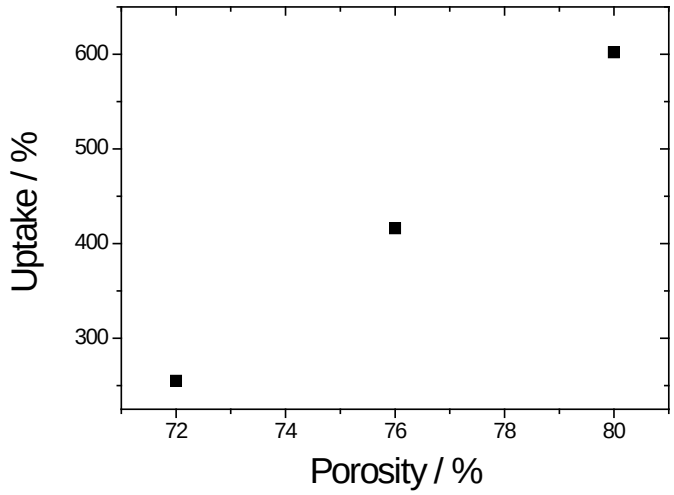

Figure 3.2 - Degree of porosity and 1M $LiClO_4$-PC solution uptake for membranes prepared from a solution with different initial polymer/solvent concentrations

Figure 3.2 shows the degree of porosity and corresponding uptake when the membrane is immersed for 24 h into a 1M $LiClO_4$-PC solution as a function of the relative polymer mass concentration in the solution. The increase of initial relative polymer mass concentration results in a decrease in the degree of porosity and therefore in the uptake of the 1M $LiClO_4$-PC solution, the uptake ranging from 250 to 600% from the samples with lower to higher degree of porosity. It is no notice the fact that as increase of about 10% in the degree of porosity induces a much larger increase in the uptake of about 350% (Figure 3.2). The reason is due the difference of the pore size distribution of the samples. The membrane with higher porosity present the pore size higher, i.e., has higher superficial area that results in the higher uptake of the electrolyte solution.

The membranes that were produced from P(VDF-TrFE)/DMF volume fractions of 5/95, 10/90 and 15/85 exhibit respectively 80%, 76% and 72% of porosity.

Explanation for this effect was investigated by the evaluation of the interaction between the polymer and lithium ions in the liquid electrolyte solution by FTIR (Table 1).

The characteristic infrared bands of $LiClO_4$, propylene carbonate (PC) and P(VDF-TrFE) and their assignment are given in Table 3.1.

Table 3.1 – Vibration modes characteristics of the different materials present during the uptake experiments [5, 6].

Wavenumber (cm^{-1})	Material	Vibrational mode
712	PC	symmetric ring deformation
777	PC	ring deformation
851	P(VDF-TrFE)	symmetric stretching (CF_2) or rocking (CF_2)
886	P(VDF-TrFE)	rocking (CF_2) or symmetric stretching (CF_2)
933	$LiClO_4$	Symmetric stretching mode, ion association in solution
944	$LiClO_4$	Contact ion pairs ($Li^+ClO_4^-$)
1120	PC	C_7-H wag + C_4-H bending
1291	P(VDF-TrFE)	symmetric stretching (CC)
1345	P(VDF-TrFE)	symmetric stretching (CC) in TG^+TG^- segment
1355	PC	C_7-H bending
1402	P(VDF-TrFE)	wagging (CH_2)
1428	P(VDF-TrFE)	bending (CH_2)
1453	P(VDF-TrFE)	bending (CH_2) in TG^+TG^- defect

The infrared spectra of the samples with different porosity both before and after immersion in the electrolyte solution are shown in figure 3.3.

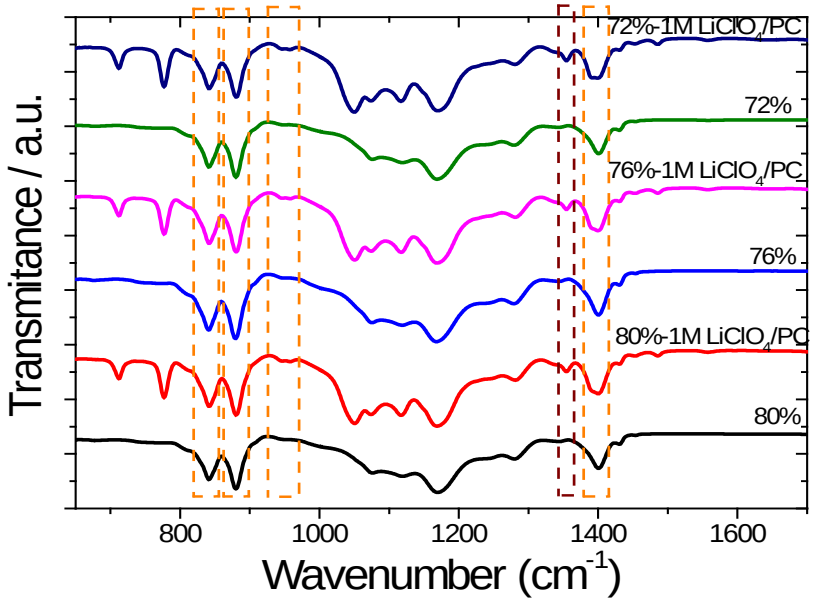

Figure 3.3 - Infrared Spectra for the porous P(VDF-TrFE) membranes with different initial polymer concentration before and after uptake from the electrolyte solution.

The characteristic vibration modes (851 cm^{-1}, 886 cm^{-1} and 1402 cm^{-1}) of the all-trans conformation of the polymer do not change for different porosity, indicating that the polymer crystallizes in the same phase [7]. Further, the presence of the electrolyte also does not modify the vibration modes characteristic of the polymer, i.e., no degradation or phase transformation occurs.

In the infrared spectra with electrolyte solution, the uptake is confirmed by the two strong bands related to the presence of propylene carbonate (712 cm^{-1} and 777 cm^{-1}), as well as the two vibration modes at 933 cm^{-1} and 1150 cm^{-1}, identified by symmetric stretching band and asymmetric bending band, respectively of ClO_4^- [8]. Finally, in the region between 900 cm^{-1} at 1200 cm^{-1}, it is observed the ion association of perchlorates, i.e, the propylene carbonate-ion interactions that depends of the salt concentration [5, 8].

3.2.2. Thermal and mechanical properties

The evaluation of the thermal and mechanical properties of the porous membranes is very important for the determination of the performance of the separator in the range of temperatures in which the battery must be stable.

The TGA results for the porous membranes and their corresponding degradation temperature, defined as the temperature associated to the initiation of sample main weight loss, as a function of porosity are shown in figure 3.4.

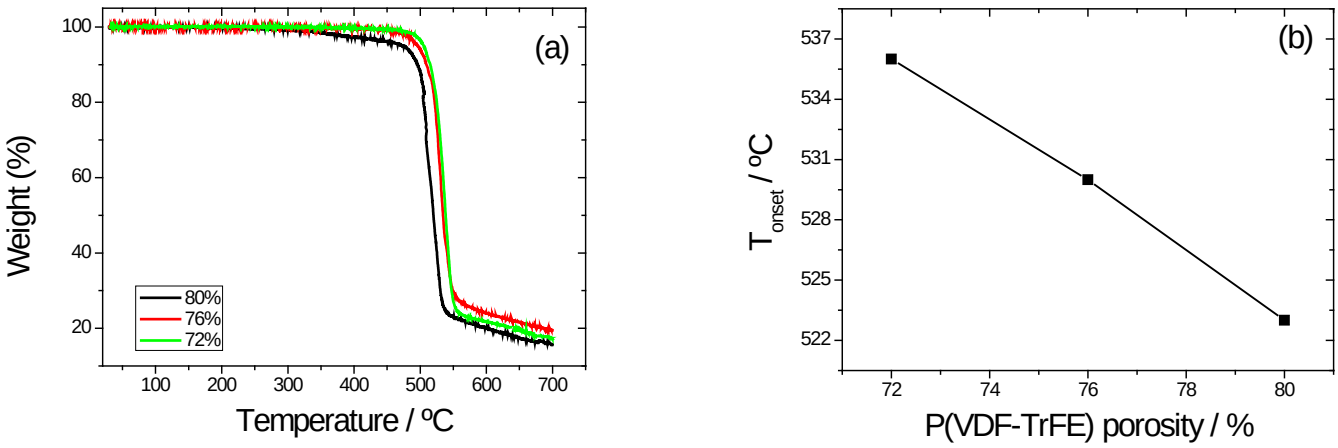

Figure 3.4 - (a): TGA curves for porous membranes with different initial polymer concentration and (b): degradation temperature as a function of initial polymer concentration

Figure 3.4 a show that all samples are characterized by an accentuated weight loss of almost 80%, above 500 ^{o}C due to the main degradation process of the polymer. The process occurs in one stage up to ~ 600 ^{o}C and slowly continues as the temperature is increased up to 700 ^{o}C. The remaining residue of ~20% in mass is retained for higher temperatures [9]. In the sample with higher porosity a small weight loss was found at temperatures of ~340 ^{o}C. This weight loss of ~4% has to be attributed to trapped solvent within the polymer structure, as it is not characteristic of the polymer phase [9].

Decreasing initial DMF solvent concentration stabilizes the polymer network as the thermal degradation shifts to higher temperatures, which is in agreement to the fact of the observation of the initial weight loss at lower temperatures of the samples with higher porosity and with previous results indicating that the degradation temperature of copolymers depends of the DMF concentration, due to the vaporization of DMF[10].

The activation process of the degradation process was calculated using the Broido method (equation 4, chapter 2), which is valid for first order reactions in dynamical thermogravimetric measurements [11].

A plot of ln(-ln(1-α)) vs 1/T (Figure 3.5) allows the evaluation of the activation energy of the process, E_a.

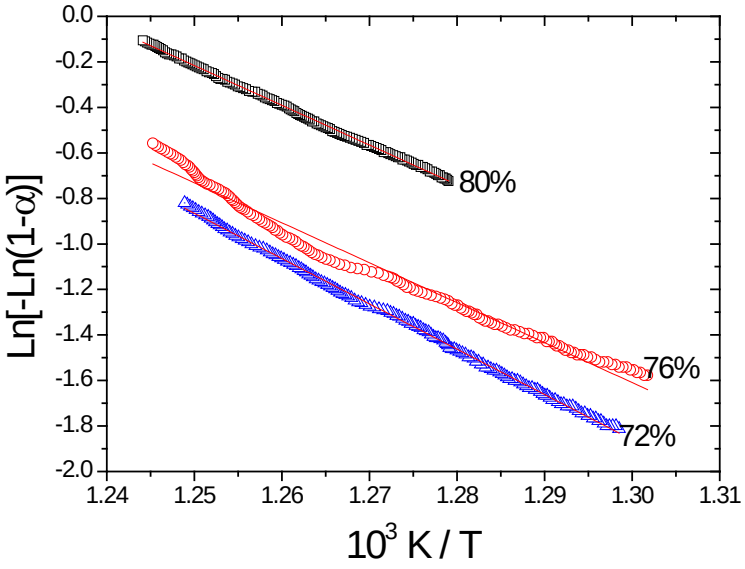

Figure 3.5 - Ln(-Ln(1-α)) vs 1000/T for porous membranes without electrolyte solution.

The obtained activation energy is represented in table 3.2 for each of the porous membranes.

Table 3.2 – Activation Energy for the obtained membranes

Samples	Ea(kJ/mol)
5/95	334.0
10/90	335.0
15/85	380.0

As expected, the initial polymer concentration in the polymer/solution fraction does not change strongly the activation energy for the degradation process, as the initial solvent concentration does not changes the degradation mechanism of the polymer, inducing just small variations on the activation energy for larger initial DMF concentrations [10].

Figure 3.6 shows the TGA curves for the porous membranes after electrolyte uptake from the solution. The derivative of the TGA curves (DTG) is also represented as an inset. Three degradation steps are identified defined by the three materials that compose the porous membranes with electrolyte solution.

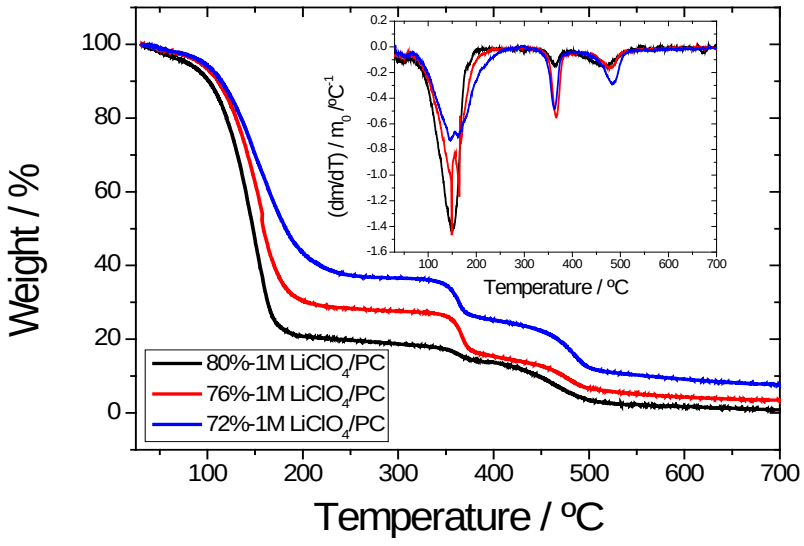

Figure 3.6 - TGA curves for the porous membranes with electrolyte solution. Insert: corresponding DTG curves.

The first step between 100ºC at 200ºC corresponds to the evaporation of the propylene carbonate (PC) [12], the second step between 300 ºC at 400 ºC is due to the

degradation of lithium ion ($LiClO_4$) [13] and the final step corresponds to the degradation of P(VDF-TrFE) [9].

The degradation temperature of the polymer after uptake of the electrolyte solution is the same as without electrolyte solution (Figures 3.5 and 3.6), i.e., the electrolyte solution does not affect the thermal stability of the polymer.

Figure 3.7 shows the DSC thermograms for the porous membranes without electrolyte solution. Two endothermic peaks are identified where the first peak corresponds to the ferroelectic-paraelectric phase transition, identified by T_{fp}, and the second peak represents the melting temperature, T_m [9].

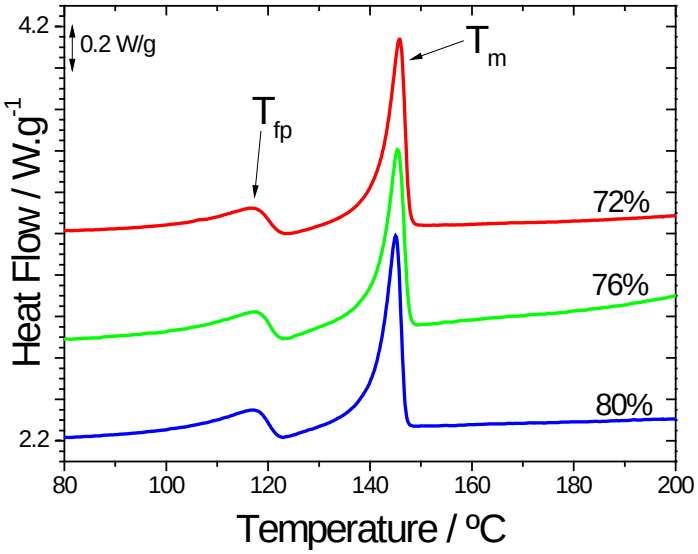

Figure 3.7 - DSC scans obtained for the porous membranes without electrolyte solution.

The degree of crystallinity (ΔX_{cryst}) was calculated applying equation 5, chapter 2. The ferroelectric-paraelectric transition temperature T_{fp} ~ 117 ºC; the melting temperature, T_m ~ 145 ºC and the degree of crystallinity, ΔX_{cryst} ~ 28%, calculated applying equation 5, chapter 2, are the same for the three membranes, being therefore independent of the initial polymer/solvent ratio.

The DSC results of the porous membranes after uptake of the electrolyte solution are represented in the figure 3.8.

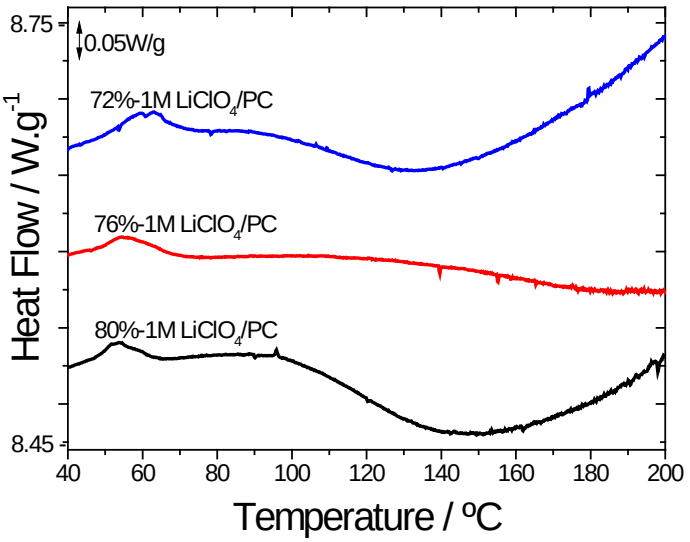

Figure 3.8 - DSC scans obtained for the porous membranes after uptake of the electrolyte solution.

In this case, the two endothermic peaks characteristics of the polymer are not observed. On the other hand, the DSC scan is characterized by a small endothermic peak around 50ºC and an exothermic peak around 140ºC.

The small endothermic peak has been previously related to the β'-relaxation of the amorphous phase of polymer and attributed to the fold-chain segment of polymer on the surface of crystalline phase [14, 15].

By adding electrolyte solution in the porous membranes, the effect of PC is mostly on the surface of the crystalline phase of the membranes, leading to the collapse of some crystallites of P(VDF-TrFE) and resulting in expansion of the surface area of the P(VDF-TrFE) crystalline phase [14]. Further, the Lithium ion has also a larger effect on the amorphous region of the polymer, resulting in interactions among PC, $LiClO_4$ and the amorphous region of P(VDF-TrFE) [14].

It is also observed that the exothermic peak of the DSC scans with electrolyte solution are dominated by the evaporation of the PC (figure 3.6, TGA result), which involves larger energies than any other effect at that temperature region.

The mechanical properties of the samples were obtained by dynamic mechanical analysis (DMA) through the measurement of the storage modulus E', related to the elastic properties of sample, and tan δ, related to the viscous properties, i.e. the ratio between lost and stored energy [16].

The storage modulus (E') and tan δ vs frequency for the porous membranes is shown in fig. 3.9 (a) and (b), respectively.

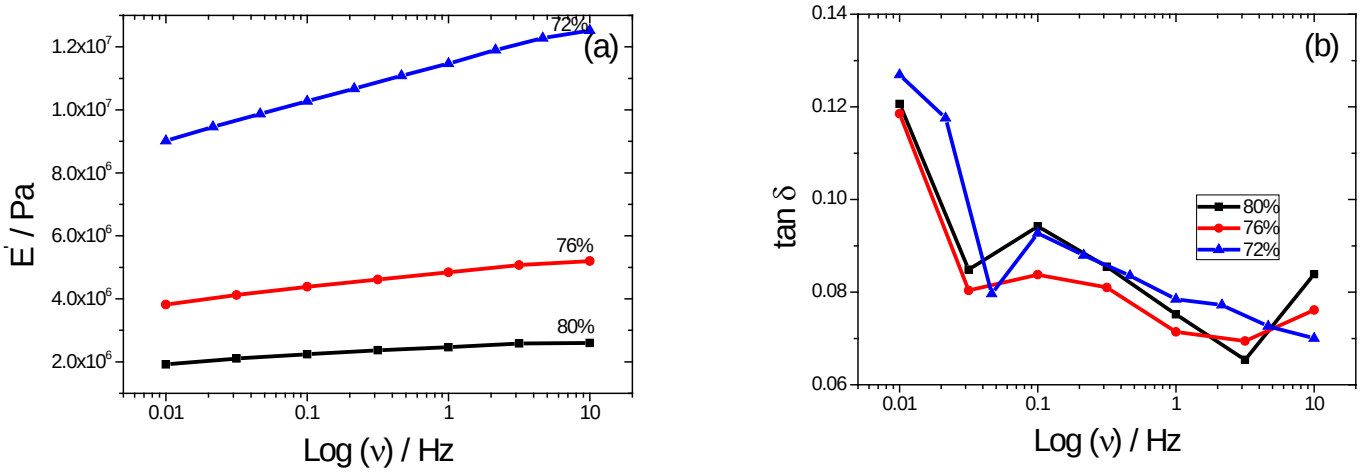

Figure 3.9 - DMA curves for (a): storage modulus, E' vs. log (ν) for porous membranes without electrolyte solution, (b): tan δ vs. log (ν) for porous membranes without electrolyte solution.

Fig. 3.9 (a) shows that increasing initial polymer concentration in the polymer/solvent ratio significantly increases the storage modulus of porous membranes in all frequency range. This behavior can be explained by the difference in the porosity of the membranes, as illustrated by the lower storage modulus of 5/95 (larger degree of porosity) as compared to 10/90 and 15/85. Tan δ does not show, on the other hand, significant variations as a function of the porosity. In all cases, E' increases and tan δ decreases as a function of frequency due the slow time response of the polymer [17].

The storage modulus, E' and tan δ as a function of porosity for membranes with and without electrolyte solution are represented in figure 3.10.

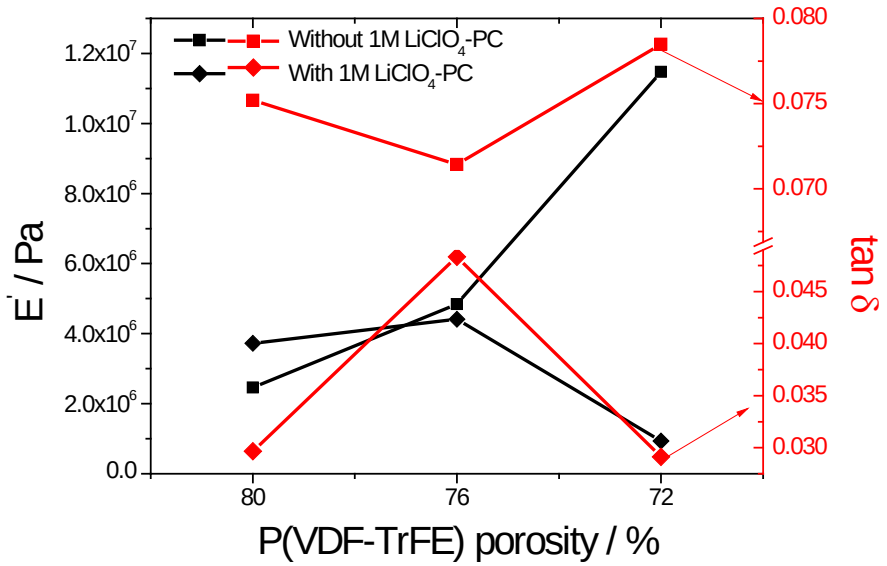

Figure 3.10 - Storage modulus, E' and tan δ in function of porosity for all membranes with and without electrolyte solution.

As a general trend, uptake of the electrolyte solution decreases both E' and tan δ values. The incorporation of the non-volatile electrolyte solution at room temperature within the membranes interacts with the polymer amorphous phase and increases the ratio of the amorphous phase through the incorporation of the PC [14] decreasing therefore the mechanical properties of porous membranes in comparison with porous membranes without electrolyte solution.

3.2.3. Electrical results

One of the main parameters of a porous membrane for battery separator applications is the ionic conductivity. The ionic conductivity was determined using impedance spectroscopy.

In figure 3.11 (a), the temperature dependence of the ionic conductivity of the porous membranes is shown and, by increasing initial polymer concentration in the solution, a decrease of the ionic conductivity of the polymer is observed.

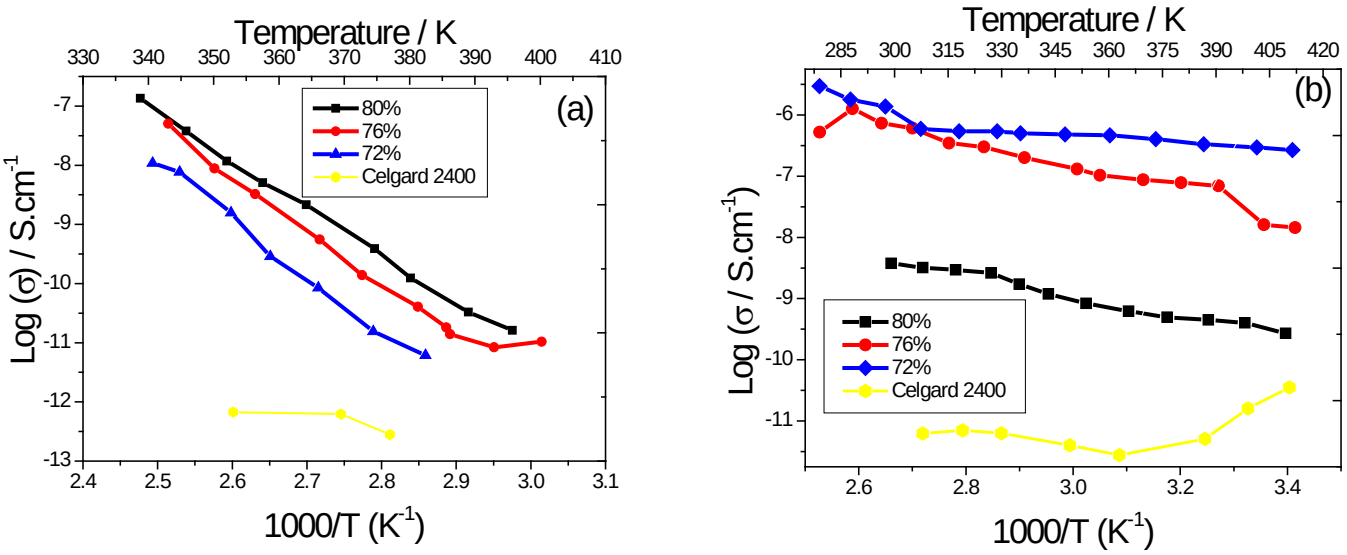

Figure 3.11 - Log (σ) vs 1000/T for all samples (a): without electrolyte solution, (b): with electrolyte solution

These variations have to be ascribed to interfacial effects [18] due to the different degree of porosity and, in particular, to the solvent trapped within the membranes which is higher for the membranes prepared from higher porosity, as observed by TGA (Figure 3.4).

The porosity of the separator and the uptake are the factors determining the final conductivity of the separators, the pores having to be completely filled by the electrolyte solution [19]. Without electrolyte solution, the ionic conductivity of the polymer is strongly affected by the temperature variation due to increased mobility of polymer charges [20]. The porosity and pore shape influencing also the ionic conductivity of the membranes [18]. The electrolyte solution strongly (figure 3.11 b) influences both the value of the ionic conductivity and its temperature dependence. Ionic conductivity increases as the electrolyte solution increases the mobility and the concentration of the ionic charge carriers [21]. The increase of the conductivity is larger for the samples with lower porosity and therefore lower uptake, indicative that the conductivity is along the polymer and not along the interconnected pores [22]. This fact supports previous results from [18, 22, 23], indicating that contributions to the conductivity are coming from the amorphous swollen polymer gel phase. Particularly relevant is the strong increase of the conductivity at lower temperatures, which allows to obtain polymer membranes with stable conductivity along the measured temperature range, in opposition to the strong

temperature dependence of the conductivity in the polymer membranes without electrolyte (figure 3.11)

As compared to the commercial Celgard 2400 membranes, the porous membranes produced in this work show higher ionic conductivity and thermal stability after uptake of the polymer electrolyte.

The apparent activation energy, E_a, for ions transport can be calculated from the Arrhenius equation in the measured temperature range:

$$\sigma = \sigma_0 \exp\left(\frac{-E_a}{RT}\right) \quad (1)$$

where σ is the ionic conductivity, σ_0, E_a, R and T are the pre-exponential factor, the apparent activation energy for ion transport, the gas constant (8.314 $J.mol^{-1}.K^{-1}$) and the temperature, respectively.

The apparent activation energy, E_a, is presented in table 3.3.

Table 3.3 – Activation energy for the porous membranes with and without electrolyte solution

Samples	Without Electrolyte Solution E_a(kJ/mol)	With Electrolyte Solution E_a(kJ/mol)
5/95	151.8	31.4
10/90	168.0	35.0
15/85	181.0	18.5

The activation energy for porous membranes without electrolyte solution is higher compared with electrolyte solution. The lithium ion and PC improve the mobility and ionic charge carriers and decreases the activation energy [24]. Whereas the activation energy for the polymer membranes before uptake increases with decreasing porosity, after uptake, it is lower for the sample with the lowest porosity, indicative of differences of the conduction process induced by the presence of the electrolyte [25-27].

The electrochemical stability of the membranes was measured by microelectrode cyclic voltammetry over the potential range –3.0V to 6.0V.

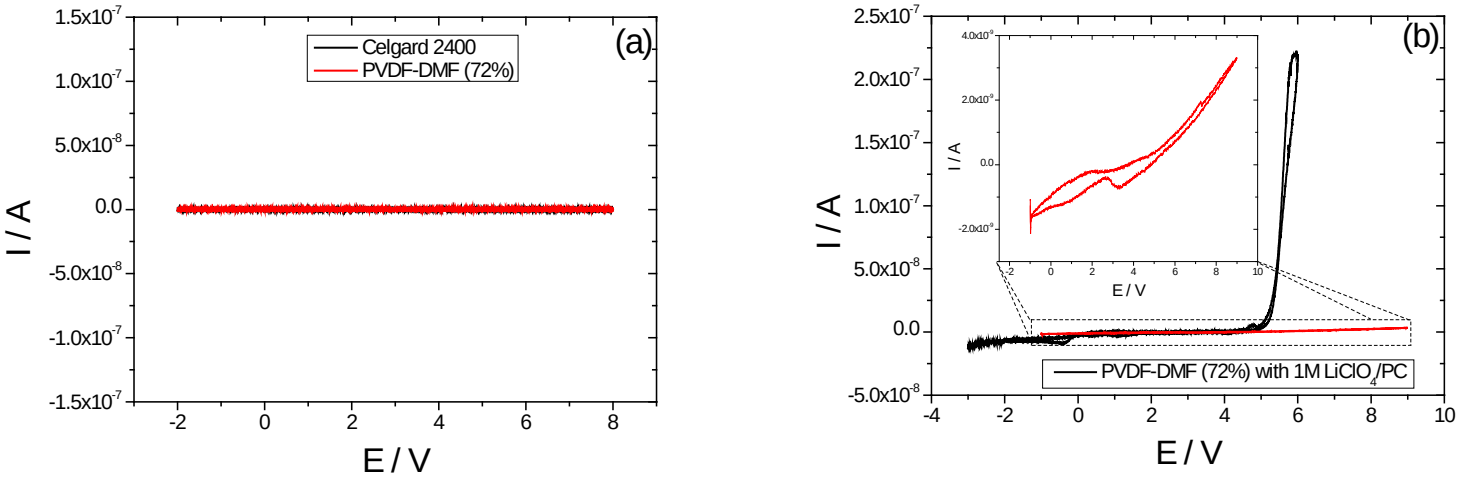

Figure 3.12 - Voltammogram of Celgard 2400 and 15/85 (a): without electrolyte solution, (b): with electrolyte solution.

The voltammogram for samples without electrolyte solution (figure 3.12 (a)) shows chemical stability, i.e. no reduction or oxidation peak is observed.With electrolyte solution (figure 3.12 (b)), the overall stability of porous membranes was excellent, with no electrochemical oxidation occurring at anodic potentials less than about 5V versus Li/Li+. The differences observed between the porous membranes and the commercial Celgard 2400 sample in the voltammogram is related to the different with ionic conductivity and pore distribution of the samples.

3.3. Conclusion

The P(VDF-TrFE) microporous membranes separators for lithium ion battery were prepared by the solvent-cast technique. The evaporation temperature of solvent and the polymer/solvent ratio determine the membrane structure. The porosity of membranes, ranging from 70 to 80%, determines the electrolyte solution uptake, being larger (250% vs 600%) for the samples with larger porosity. The membranes are thermally stable until 100ºC and show also a good mechanical stability both before and after electrolyte uptake. Uptake reduces, nevertheless, the storage modulus of the membranes.

The ionic conductivity of the membranes is larger for the samples with higher degree of porosity and shown a strong temperature dependence. After uptake, the larger conductivity is observed for the samples with lower porosity and therefore lower uptake. Further, the conductivity after uptake show stable values in the measured temperature range.

3.4. References

1. California, A., et al., *Tailoring porous structure of ferroelectric poly(vinylidene fluoride-trifluoroethylene) by controlling solvent/polymer ratio and solvent evaporation rate.* EPJ, 2011. Submited.
2. Ferreira, A., et al., *Poly[(vinylidene fluoride)-co-trifluoroethylene] Membranes Obtained by Isothermal Crystallization from Solution.* Macromolecular Materials and Engineering, 2010. 295(6): p. 523-528.
3. Magalhaes, R., et al., *The Role of Solvent Evaporation in the Microstructure of Electroactive -Poly(Vinylidene Fluoride) Membranes Obtained by Isothermal Crystallization.* Soft Materials, 2011. 9(1): p. 1-14.
4. Costa, C.M., et al., *Electroactive Poly(Vinylidene Fluoride-Trifluorethylene) (PVDF-TrFE) Microporous Membranes for Lithium-Ion Battery Applications.* Ferroelectrics, 2012. 430(1): p. 103-107.
5. Battisti, D., et al., *Vibrational studies of lithium perchlorate in propylene carbonate solutions.* The Journal of Physical Chemistry, 1993. 97(22): p. 5826-5830.
6. Faria, L.O. and R.L. Moreira, *Infrared spectroscopic investigation of chain conformations and interactions in P(VDF-TrFE)/PMMA blends.* Journal of Polymer Science Part B: Polymer Physics, 2000. 38(1): p. 34-40.
7. Prabu, A.A., et al., *Infrared spectroscopic studies on crystallization and Curie transition behavior of ultrathin films of P(VDF/TrFE) (72/28).* Vibrational Spectroscopy, 2006. 41(1): p. 1-13.
8. Chen, Y., Y.-H. Zhang, and L.-J. Zhao, *ATR-FTIR spectroscopic studies on aqueous LiClO4, NaClO4, and Mg(ClO4)2 solutions.* Physical Chemistry Chemical Physics, 2004. 6(3): p. 537-542.
9. Sencadas, V., S. Lanceros-Méndez, and J.F. Mano, *Thermal characterization of a vinylidene fluoride-trifluorethylene (75-25) (%mol) copolymer film.* Journal of Non-Crystalline Solids, 2006. 352(50-51): p. 5376-5381.
10. Kojima, T., M. Tsuchiya, and K. Tago, *Thermal analysis of polymer networks consisting of different homopolymers.* Journal of Thermal Analysis and Calorimetry, 1997. 49(1): p. 149-154.

11. Broido, A., *A simple, sensitive graphical method of treating thermogravimetric analysis data.* Journal of Polymer Science Part A-2: Polymer Physics, 1969. 7(10): p. 1761-1773.
12. Silva, L.B. and L.C.G. Freitas, *Structural and thermodynamic properties of liquid ethylene carbonate and propylene carbonate by Monte Carlo Simulations.* Journal of Molecular Structure: THEOCHEM, 2007. 806(1-3): p. 23-34.
13. Jian-he, H., et al., *Non-isothermal Decomposition Mechanism and Kinetics of LiClO4 in Nitrogen.* CHEM. RES. CHINESE UNIVERSITIES, 2010. 26(2): p. 4.
14. Tian, L.-y., X.-b. Huang, and X.-z. Tang, *Study on morphology behavior of PVDF-based electrolytes.* Journal of Applied Polymer Science, 2004. 92(6): p. 3839-3842.
15. El Mohajir, B.-E. and N. Heymans, *Changes in structural and mechanical behaviour of PVDF with processing and thermomechanical treatments. 1. Change in structure.* Polymer, 2001. 42(13): p. 5661-5667.
16. Swaminathan, G., K.N. Shivakumar, and L.C. Russell, *Anomalies, influencing factors, and guidelines for DMA testing of fiber reinforced composites.* Polymer Composites, 2009. 30(7): p. 962-969.
17. Paul, S.A., et al., *Dynamic mechanical analysis of novel composites from commingled polypropylene fiber and banana fiber.* Polymer Engineering & Science, 2010. 50(2): p. 384-395.
18. Djian, D., et al., *Macroporous poly(vinylidene fluoride) membrane as a separator for lithium-ion batteries with high charge rate capacity.* Journal of Power Sources, 2009. 187(2): p. 575-580.
19. Karabelli, D., et al., *Poly(vinylidene fluoride)-based macroporous separators for supercapacitors.* Electrochimica Acta, (0).
20. Sencadas, V., et al., *Poling of beta-poly(vinylidene fluoride): dielectric and IR spectroscopy studies.* e-Polymers, 2005. 2.
21. Ren, T., et al., *Synthesis and characterization of novel crosslinked polyurethane–acrylate electrolyte.* Journal of Applied Polymer Science, 2003. 89(2): p. 340-348.
22. Rajendran, S. and P. Sivakumar, *An investigation of PVdF/PVC-based blend electrolytes with EC/PC as plasticizers in lithium battery applications.* Physica B: Condensed Matter, 2008. 403(4): p. 509-516.

23. Quartarone, E., P. Mustarelli, and A. Magistris, *Transport Properties of Porous PVDF Membranes.* The Journal of Physical Chemistry B, 2002. 106(42): p. 10828-10833.

24. Every, H.A., et al., *Lithium ion mobility in poly(vinyl alcohol) based polymer electrolytes as determined by 7Li NMR spectroscopy.* Electrochimica Acta, 1998. 43(10-11): p. 1465-1469.

25. A, M.S., *Review on gel polymer electrolytes for lithium batteries.* European Polymer Journal, 2006. 42(1): p. 21-42.

26. Dampier, F.W., *Permselective membrane separators for organic electrolyte batteries.* Journal of Applied Electrochemistry, 1973. 3(3): p. 169-177.

27. Ulaganathan, M. and S. Rajendran, *Effect of different salts on PVAc/PVdF-co-HFP based polymer blend electrolytes.* Journal of Applied Polymer Science, 2010. 118(2): p. 646-651.

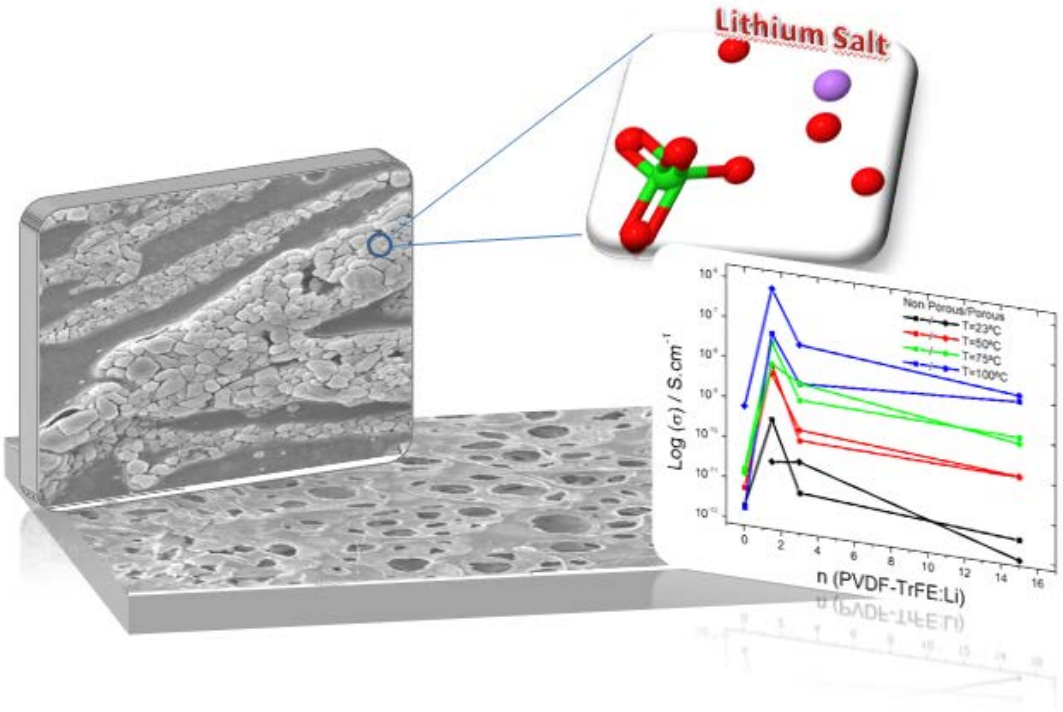

4. Processing and characterization of P(VDF-TrFE)$_n$LiClO$_4$.3H$_2$O composites membranes

This chapter describes the preparation and characterization of Poly[(vinylidene fluoride)-*co*-trifluoroethylene] membranes doped with different lithium perchlorate trihydrate contents. The samples were prepared by solvent evaporation at different temperatures in order to tailor membrane morphology. Infrared spectroscopies, thermal, mechanical and electrochemical measurements of the samples were performed.

This chapter is based on the following publication:

"Effect of the microsctructure and lithium-ion content in poly[(vinylidene fluoride)-co-trifluoroethylene]/lithium perchlorate trihydrate composite membranes for battery applications", C. M. Costa, L. C. Rodrigues, V. Sencadas, M. M. Silva, S. Lanceros-Méndez, Solid State Ionics 217 (2012) 19-26

4.1. Samples

Samples were identified by P(VDF-TrFE)$_n$LiClO$_4$.3H$_2$O, where n is $1.5 \leq n \leq 15$. The samples were prepared from solvent casting at two solvent evaporation temperatures: room temperature and 210 ºC.

4.2. Results and discussions

4.2.1. Separator membrane morphology

The morphology of the composite separators crystallized at different temperatures is presented in figure 4.1.

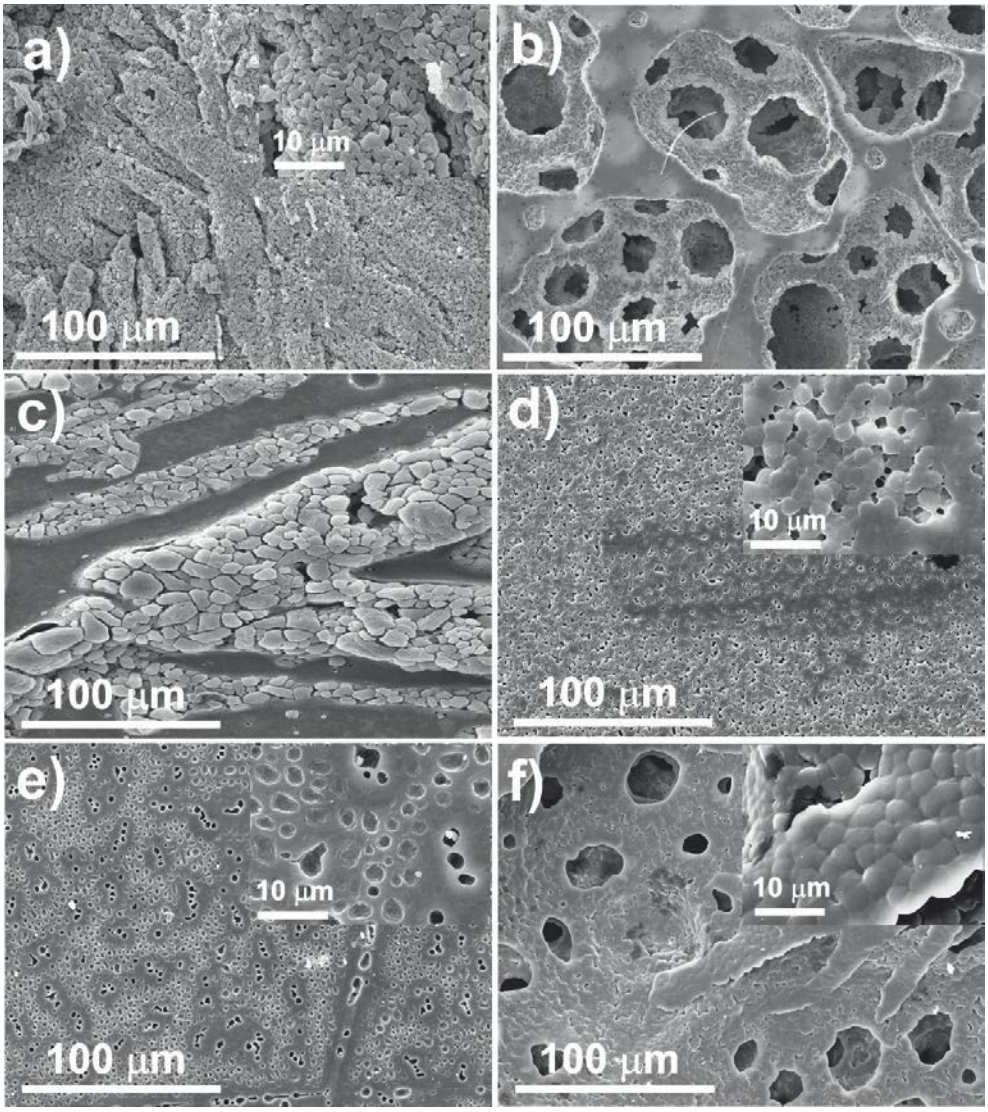

Figure 4.1 – Separator microstructure evolution for the different evaporation temperatures: a), c) and e) crystallized at 210ºC for n=1.5, n=3 and n=15, respectively and b), d) and f) crystallized at room temperature for n=1.5, n=3 and n=15, respectively.

It was found that even the composite samples where evaporation of the solvent occurred at 210 ºC present porosity, which is an uncommon behavior for the pure polymer membrane subject to same preparation process [1]. The inclusion of lithium ions into the polymeric matrix give origin to different composite patterns, depending of the filler amount present in the samples. For higher lithium ions present in the composite separator, the polymer crystallizes in the characteristic spherulite structure with the filler randomly dispersed into the polymeric matrix. It was observed a phase separation between the matrix and the filler for the P(VDF-TrFE)$_n$LiClO$_4$.3H$_2$O, with n=3 composite (Figure 4.1.c). The sample with lower amounts of lithium ions (n=1.5) presents small cavities non-interconnected between them and with some lithium ions inside. On the other hand, samples were solvent evaporation occurred at room temperature shows the characteristic porous structure, where spherical pores are shown with diameters around 100 μm, for the P(VDF-TrFE)$_n$LiClO$_4$.3H$_2$O separators with n =1.5 and 15 (figure 4.1b and f). It was also noted that pore wall are formed by adhered microspheres with diameter around 4 μm. The pores interconnectivity results from the spaces between the polymer microspheres that form the pore wall, while larger pore throats appear due to some defects in the structure [1-3]. For pure (PVDF-TrFE) the mechanism of polymer/solvent evaporation was explained has being a liquid/liquid spidonal decomposition followed by polymer crystallization [1-3].

P(VDF-TrFE)$_n$LiClO$_4$.3H$_2$O composite separator with n=3 showed porous around 1-2 μm and polymer microspheres of approximately same dimension. In this sample, the obtained microstructure is very similar to the one found for the pure homopolymer in the β-crystalline phase, obtained by solvent evaporation at room temperature [4]. In the case of porous structures, the lithium ions seem to have a randomly dispersion among the polymeric matrix, free of agglomerates or filler clusters, a very common result for the samples obtained by crystallization at 210ºC.

Different morphologies obtained for the polymer electrolyte (Figure 4.1) suggests that the microstructure of the P(VDF-TrFE)$_n$LiClO$_4$.3H$_2$O separators may be tailored by modulating experimental factors such as the polymer/solvent fraction in the solvent-cast, different amount of lithium ions and the crystallization temperature.

Porosity is one the most parameters for polymer electrolyte applications should be carefully monitored. The porosity present in each composite separator membrane was calculated according to the pycnometer method describe elsewhere [1]. In Figure 4.2 is

represented the evolution of the porosity for the separators obtained at different crystallization temperatures and with different lithium ions concentrations.

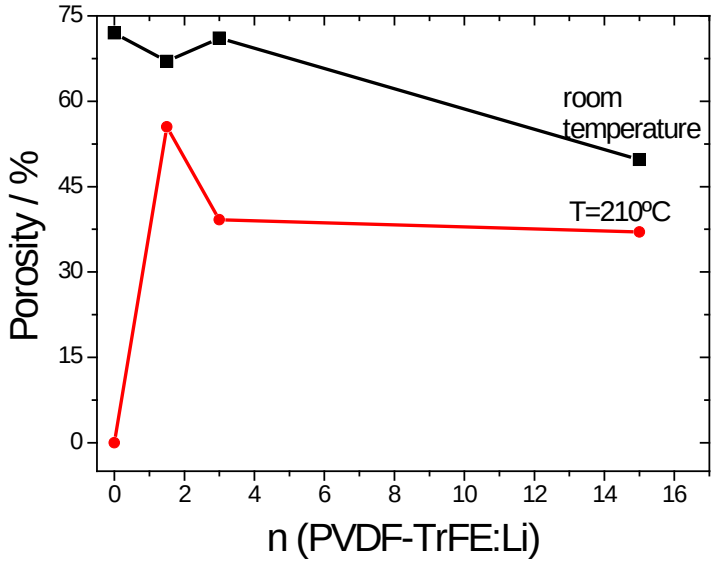

Figure 4.2 – Evolution of porosity in function of lithium ions amount for both crystallization temperatures.

The Figure 4.2 show, for the samples crystallized at room temperature that the porosity decreases with the decrease of the lithium ions present in the matrix from 72 % until a minimum of 50%. Moreover, for the samples crystallized at 210 ºC, the samples with no lithium ions has no porosity present in the membrane, but with the inclusion of the $LiClO_4.3H_2O$, a maximum of porosity was found around 55 % for the maximum amount of lithium ions present in the composite separator (n=1.5) and a decrease of porosity to approximately 39 % occur for the samples with n=3 and 15. The porosity of the prepared membranes by solvent evaporation at room temperature is quit higher than the porosity found for the commercial Celgard® 2400 that ranges between 30 and 40 %, but for the samples obtained by solvent evaporation at 210 ªC, the value of porosity is in the range of the Celgard® 2400 membranes, being the microstructure formed by dense porous similar to the commercial ones [5].

The obtained results suggests that the inclusion of $LiClO_4.3H_2O$ into the P(VDF-TrFE) matrix have influence in polymer matrix crystallization kinetics.

P(VDF-TrFE) copolymer is a semicrystalline polymer, and commonly crystallizes in the electroactive phase and such presence can be identified by infrared spectroscopy, mainly through the characteristic absorption band at 840 cm^{-1}.

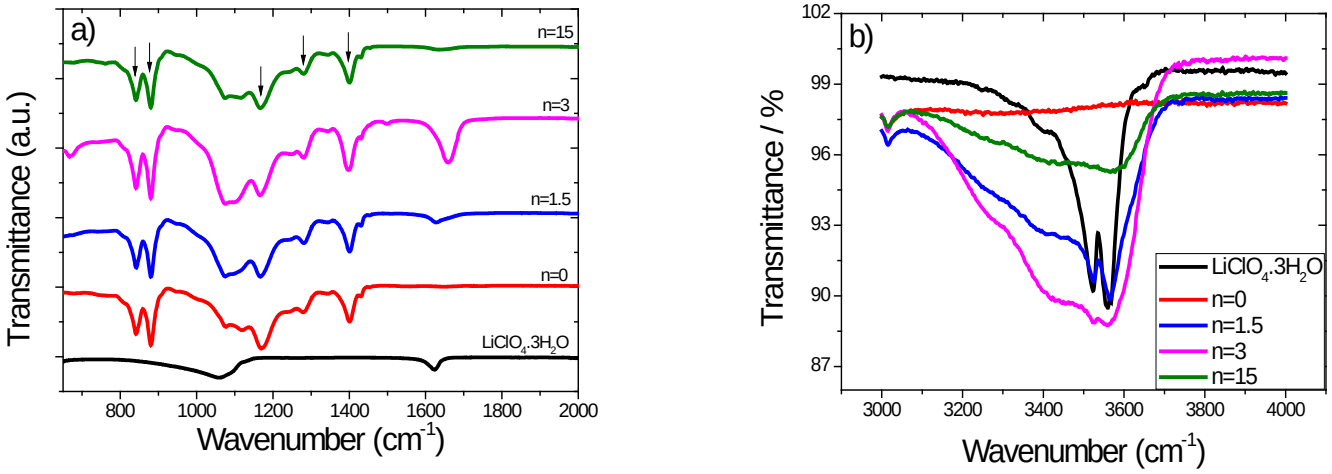

Figure 4.3 – Infrared Spectrum for samples with different lithium ions amount and crystallized at room temperature: a) Infrared Spectrum between 650 cm^{-1} and 2000 cm^{-1}; b) Infrared Spectrum between 3000 cm^{-1} and 4000 cm^{-1}.

In Figure 4.3 a is presented the infrared spectrum for the samples P(VDF-TrFE)$_n$$LiClO_4.3H_2O$ composite separators crystallized at different temperatures and with several amounts of lithium ions. It was detected the presence of vibrational modes at 840, 880, 1170, 1282 and 1402 cm^{-1} of P(VDF-TrFE), assigned to symmetric stretching or rocking modes of CF_2, asymmetric stretching mode of CF_2, symmetric stretching mode of CC and wagging CH_2, respectively [6, 7]. The obtained results show that the crystallization temperature and the inclusion of lithium ions into the polymer matrix do not have influence on the crystalline phase of P(VDF-TrFE) matrix.

In the infrared spectrum for the $LiClO_4.3H_2O$ two main vibrational modes are observed, one at 1060 cm^{-1} and the other at 1625 cm^{-1}, assigned to Cl-O asymmetric stretching band ($\nu_3(ClO_4^-)$) and O-H bending (H_2O), respectively [8]. Moreover, the characteristics absorption bands for the O-H stretching vibration modes are observed at 3527 cm^{-1} and 3568 cm^{-1} defined by [9], and their intensity are correlated to the amount of lithium ions present in the membrane separators (figure 4.3b). One big absorption band between 3200 and 3500 cm^{-1} attributed of O-H stretching is observed, and

generally is attributed to an ice-like component at 3230 cm^{-1} and an ice-like liquid component at 3420 cm^{-1} [8, 9].

The infrared spectrum for the samples in that solvent was evaporated at 210 ºC is the same that was obtained for the samples where the solvent evaporating was room temperature.

4.2.2. Thermal behavior

DSC thermographs for the P(VDF-TrFE)$_n$LiClO$_4$.3H$_2$O composite separators shows up to three endothermic peaks for the polymer electrolyte samples (Figure 4.4).

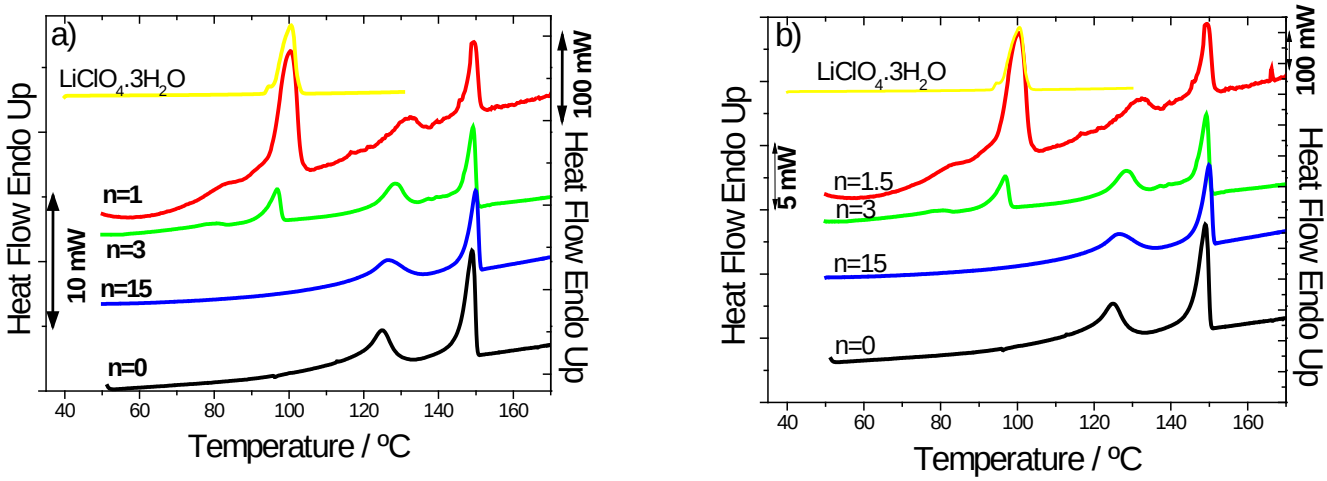

Figure 4.4 – DSC curves for samples with different lithium ions amount: a) samples crystallized at 210 ºC and b) room temperature.

Multiple DSC peak structures are typical in composite materials due to the interface effects and ill crystallized parts of the samples that melt at different temperatures than the main polymer body [10]. In the present composite samples, two peaks are observed for the polymeric matrix: the one that occurs at ~ 125 ºC, corresponds to the ferroelectric-paraelectric transition (FE-PE, Curie transition). The higher DSC endotherm corresponds to the melting of the paraelectric phase and it is located at ca.150 ºC. It can be observed that the solvent evaporation at 210 ºC and posterior crystallization at room temperature does not affect the melting behavior and thermal stability of the P(VDF-TrFE), but a slight increase of temperature was observed with

the decrease of lithium ions present in the P(VDF-TrFE)$_n$$LiClO_4.3H_2O$ separator composites (Figure 4.4a). A strong endothermic peak was observed for the lithium ions and is related to the water evaporation that is a constituent part of the $LiClO_4.3H_2O$, and occurs at ~100 ºC, and an enthalpy of 313 J/g was found. The H_2O evaporation was clearly observed for the samples with higher amounts of lithium ions, and decrease with the decrease of $LiClO_4.3H_2O$ present in the composite separators (Figure 4.4a).

For the samples where the solvent was removed at room temperature, same behavior was observed in terms of the thermal stability for the polymer matrix, being the melting temperature of the P(VDF-TrFE) practically unchanged with the inclusion of the lithium ions (Figure 4.4b). The FE-PE transition of the polymeric matrix occurs at ~117 ºC for all composite samples and pure polymer, which shows that the filler does not change the nature of the polymer Curie transition (Figure 4.4b). Moreover, the strong endothermic peak was observed for the lithium ions related to the water evaporation of the $LiClO_4.3H_2O$ that occurred at ~100 ºC, and an enthalpy of 313 J/g was calculated (Figure 4.4b).

The FE-PE transition does not depend on lithium ion content amount but is altered by the crystallization temperature. This fact can be related to a decrease in the gauche defect density in the molecular chains, i.e., a decrease in the number of gauche defects which have been introduced in all-trans chains on cooling from the hexagonal phase to the orthorhombic phase [11].

The degree of crystallinity of the samples determined by equation 5 (chapter 2), decreases with increasing lithium ions content independently of the crystallization temperature. For samples crystallized at room temperature, the degree of crystallinity is ~28% without lithium ion content but decreases to 14% with n=1.5 lithium-ion content. This occurrence shows that the lithium ions disturbs the structure packing of macromolecular chains, increasing its distance that resulting in an increase of amorphous region.

The interaction of the inorganic filler and the polymer can be explored by its effect in the polymer thermal degradation, which was measured by thermal-gravimetric analysis, TGA (Figure 4.5).

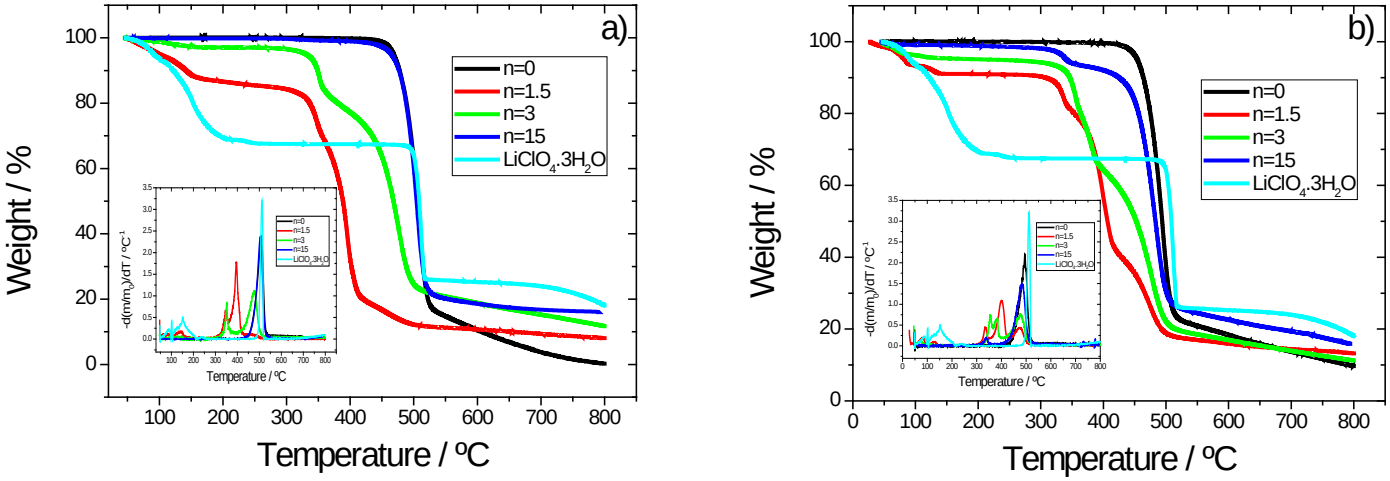

Figure 4.5 – TGA thermograms for the P(VDF-TrFE)$_n$LiClO$_4$.3H$_2$O composite separators: a) solvent evaporation at 210 ºC, b) solvent evaporation at room temperature.

P(VDF-TrFE) shows a single step degradation process with a T_{onset} at ~500 ºC. On the other hand, LiClO$_4$.3H$_2$O shows the water evaporation process that starts around 100 ºC and the degradation of the lithium salts occurs also at ~500 ºC (Figure 4.5). The incorporation of lithium salts promotes a decrease of stability on both set of samples. Up to three degradation processes were observed for the polymer electrolyte separators. The one at lower temperature is due to the water evaporation process, which is more visible for the samples with higher LiClO$_4$.3H$_2$O content with a mass reduction of ~30 %. The second process is due to the decomposition of the lithium ions, and it was observed that an increase of the filler in the polymer electrolyte corresponds to a decrease of the thermal stability of the separator. It was observed that the decomposition of the lithium ions decrease with the increase of the filler in the P(VDF-TrFE) membrane separator. Same behavior was observed for the polymeric matrix. The sample with lower LiClO$_4$.3H$_2$O content (n=15), shows a degradation pattern similar to the polymer matrix, which is related to the small amount of lithium ions compared to the polymer matrix (Figure 4.5).

The residual mass found for all composite samples are quite similar to the one observed for the polymer matrix at the end of the measurement (800 ºC) for the samples

where the solvent evaporated at room temperature, but for the samples where the solvent evaporation occurred at 210 ºC and posterior crystallization at room temperature, the residual mass at 800 ºC is higher for the samples with less lithium ions and a reduction of residual mass was observed with the increase of the filler content in the polymeric matrix.

4.2.3. Separators mechanical performance

The mechanical characteristics of polymer electrolyte will influence the material performance for membrane separators applications. Dynamical mechanical analysis (DMA) measurements were achieved at room temperature for all the P(VDF-TrFE)$_n$LiClO$_4$.3H$_2$O membrane separators (Figure 4.6).

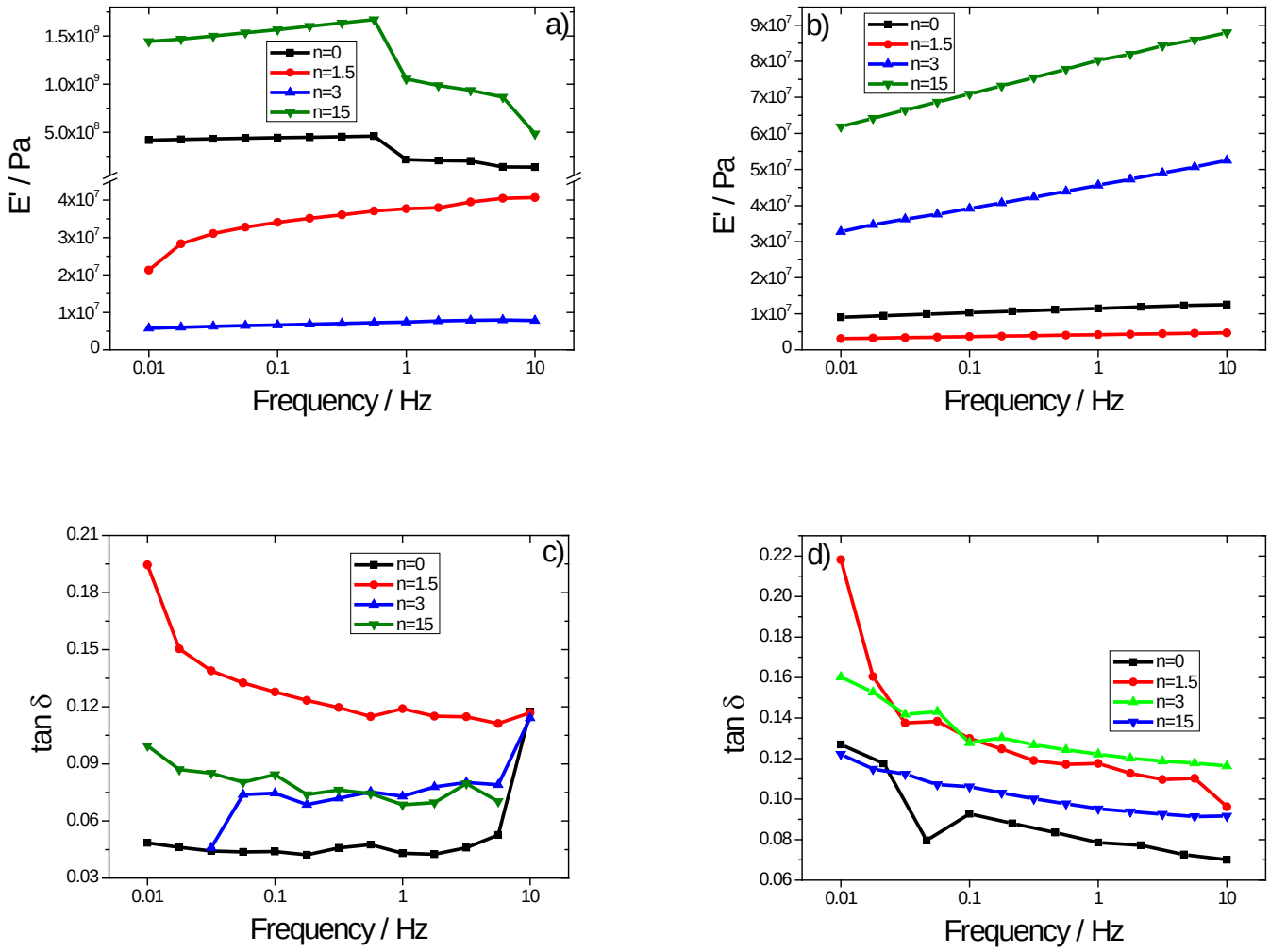

Figure 4.6 – Storage modulus for the E' P(VDF-TrFE)$_n$LiClO$_4$.3H$_2$O composite separators: a) solvent evaporation at 210 ºC, b) solvent evaporation at room temperature and tan δ for P(VDF-TrFE)$_n$LiClO$_4$.3H$_2$O composite separators: c) solvent evaporation at 210 ºC, d) solvent evaporation at room temperature.

For the samples were the solvent evaporation occurred at 210 ºC and posterior crystallization at room temperature, an increase of the storage modulus of the membrane separator was observed that for lower amounts of lithium ions present in the sample, which suggest that the lithium salts somehow influence the polymer crystallization, and is in good accordance to the results observed in Figure 4.1 and 4.2, was showed that the filler present in the sample change the polymer crystallization kinetics (figure 4.6a). Moreover, the increase of LiClO$_4$.3H$_2$O present in the sample gives origin to a reduction

of the storage modulus, when compared to the polymer matrix. The incorporation of lithium salts into the P(VDF-TrFE) gives origin to a porous structure with maximum for n=1.5, where the found porosity was 55 % (Figure 4.2) and a microstructure is composed by a random distribution of the filler among the polymeric matrix (Figure 4.1a). Although, the sample with n=3 present the lowest storage modulus. This effect is related to a competition between the porosity present in the material and the formation of lithium ions clusters (Figure 4.1c) among the polymeric matrix, hindering the crystal reorganization when a stress is applied. Further, due to the lower interaction strength between the cluster and the P(VDF-TrFE), some debonding and sliding of the lithium clusters probably occurs (Figure 4.6a).

The P(VDF-TrFE)$_n$$LiClO_4.3H_2O$ sample obtained from solvent evaporation at room temperature with n=1.5 present a decrease of the storage modulus when compared to the polymer matrix, which can be due to the high porosity (Figure 4.2) of sample membrane and to the lower interaction strength between the cluster and the P(VDF-TrFE) that promote some debonding and sliding of the lithium clusters (Figure 4.2).

The storage modulus increase with the decrease of the $LiClO_4.3H_2O$ content present in polymeric electrolyte which can be due to the decrease of the porosity, giving origin to stiffer samples (Figure 4.6b).

4.2.4. Ionic conductivity and cycle performance of batteries

One of the main parameters of a porous membrane for battery separator applications is the ionic conductivity. The ionic conductivity was determined using impedance spectroscopy.

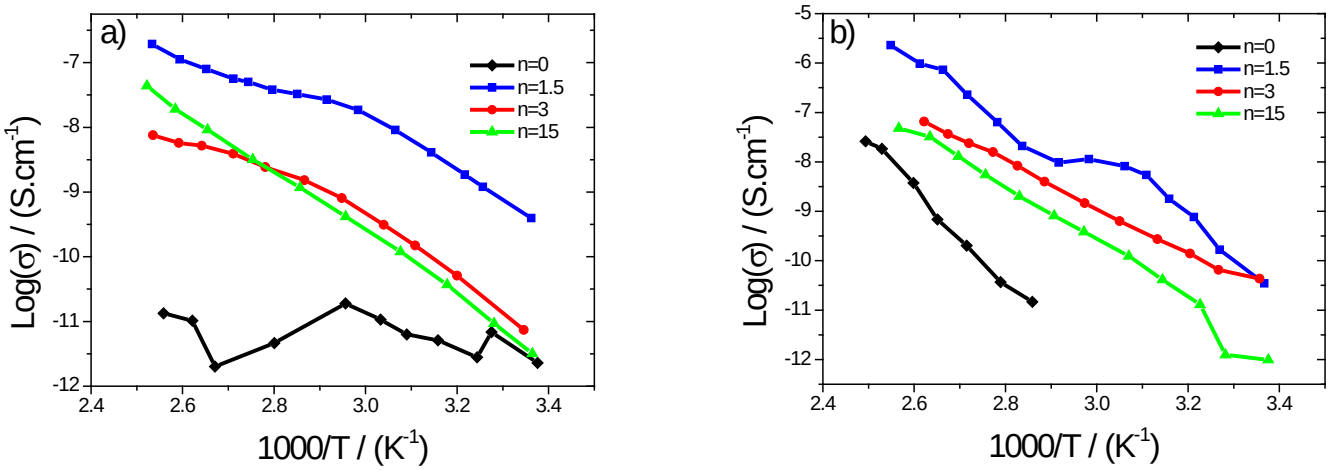

Figure 4.7 – Log (σ) vs 1000/T in function for all sample: a) solvent evaporation at 210 ºC, and b) solvent evaporation at room temperature.

In Figure 4.7, the temperature dependence of the ionic conductivity of the porous membranes is shown and, by increasing the $LiClO_4.3H_2O$ concentration in the polymer electrolyte, an increase of the ionic conductivity is observed. These variations have to be ascribed to interfacial effects [12] due to the different degree of porosity and, in particular amount of lithium ions trapped within the separators membranes which is higher for the P(VDF-TrFE)$_n$$LiClO_4.3H_2O$ membranes prepared with n=1.5.

The porosity of the separator and the amount of $LiClO_4.3H_2O$ are the factors determining the final conductivity of the separators. Without lithium ions, the ionic conductivity of the polymer is strongly affected by temperature variation due to increased mobility of polymer ions [13]. Further, the porosity and pore shape also influence the ionic conductivity of the membranes [12].

The $LiClO_4.3H_2O$ salts (Figure 4.7) strongly influences both the value of the ionic conductivity and its temperature dependence. Ionic conductivity increases as the electrolyte increases the mobility and the concentration of the ionic charge carriers [14]. The increase of the conductivity is greater for the samples with higher $LiClO_4.3H_2O$ electrolyte and is higher for the P(VDF-TrFE)$_n$$LiClO_4.3H_2O$ sample obtained by solvent evaporation at room temperature with n=1.5 which indicates that along the polymer plays an important role in the connectivity along with the sample morphology and lithium ions distribution observed through by SEM images (Figure 4.1). This observations supports previous results from [12, 15, 16], indicating that contributions to

the conductivity are coming from the amorphous swollen polymer gel phase. Particularly relevant is the strong increase of the conductivity at lower temperatures, which allows obtaining polymer membranes with stable conductivity along the measured temperature range, in opposition to the strong temperature dependence of the conductivity in the polymer membranes without electrolyte (Figure 4.8). The dependence of ionic conductivity in the temperature and the lithium ions content can be rationalized by the free volume model [17]. As the mechanism of ionic transport is depends on the flexibility of the polymer chain, components that increase free volume may be expected to have a beneficial influence on conductivity.

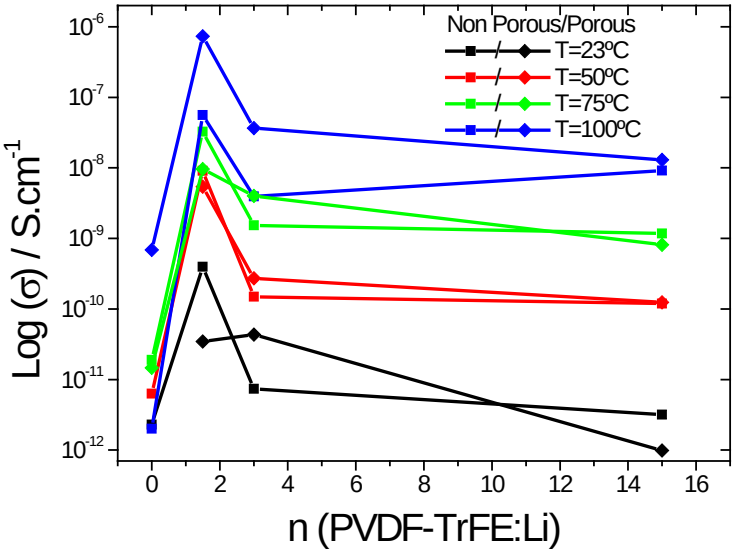

Figure 4.8 – Log (Ionic conductivity) in function of lithium ion for various temperatures.

As shown in Figure 4.8, independently of the evaporation temperature, for higher lithium ion content, the diffusion of ions results in a rapid decrease in resistance as it provides sufficient ion-conducting phase to enhance electrical conductivity. The temperature and lithium ions content leads to an increase in ion mobility and polymer segmental mobility that will support ion transport in the electrolytes [18].

The apparent activation energy, Ea, for ions transport has been calculated from the Arrhenius equation (eq. 1, chapter 3) and is summarized in Table 4.1.

Table 4.1 – Activation energy determined through the equation 3 for all samples.

Solvent Evaporation Temperature	**E_a**	**Solvent Evaporation Temperature**	**E_a**
210 ºC	**kJ/mol**	Room Temperature	**kJ/mol**
n=0	143.0	n=0	181.0
n=1.5	57.4	n=1.5	102.0
n=3	68.6	n=3	87.0
n=15	91.0	n=15	105.0

The activation energy for porous membranes without $LiClO_4.3H_2O$ electrolyte solution is higher compared with electrolyte solution. The lithium ion contents promote the number and mobility of ionic charge carriers and decreases the activation energy [15]. Whereas the activation energy for the polymer decreases with increasing $LiClO_4.3H_2O$ electrolyte present in the membranes separators, it was observed that the solvent evaporation temperature also influences the activation energy behavior. Higher values of the citation energy were found for the samples with the same $LiClO_4.3H_2O$ electrolyte concentration obtained by solvent evaporation at room temperature, i.e. when the degree of porosity is lower.

The electrochemical stability of the membranes was measured by microelectrode cyclic voltammetry over the potential range –3.0V to 6.0V.

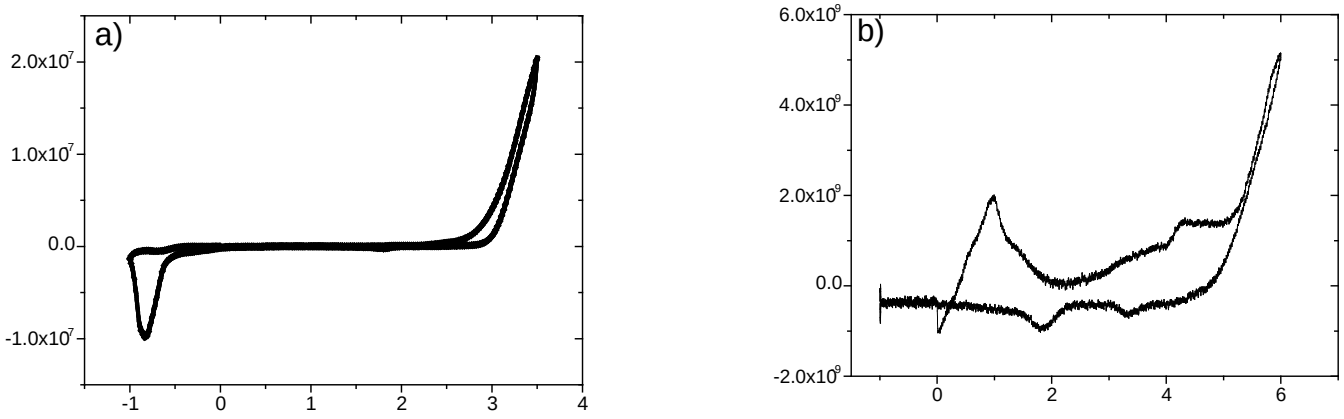

Figure 4.9 – Cycle Voltammogram of $P(VDF\text{-}TrFE)_nLiClO_4.3H_2O$ composite separators with n=1: a) solvent evaporation at 210 ºC, and b) solvent evaporation at room temperature.

The voltammogram for samples where the solvent evaporation occurred at 210 ºC and posterior crystallization at room temperature (figure 4.9a) shows good electrochemical stability, with an electrochemical oxidation peak around at -0.8 V and for anodic potentials higher than 5.0V versus Li/Li+ (Figure 4.9b). Further, for the samples, where the solvent evaporation occurred at room temperature, several electrochemical oxidation peaks can be observed (Figure 4.9b) between 0.0 and 5.0V versus Li/Li+, which can be correlated to the decomposition of the ions inside the porous sample.

4.3. Conclusion

Composites membranes based P(VDF-TrFE) with Lithium perchlorate trihydrat ($LiClO_4.3H_2O$) has been produced by solvent-cast techniques at different evaporation temperatures. The evaporation temperature not changes the polymer phase but affects the porosity and pore size of membranes.

The results of the conductivity measurements have shown that the P(VDF-TrFE)$_n$$LiClO_4.3H_2O$ electrolytes may be viable alternatives to others electrolytes. The obtained results revealed that the lithium salt concentration influences the ionic conductivity of electrolytes and the best values of 2.3×10^{-6} S/cm at 120ºC were obtained for P(VDF-TrFE)$_{1.5}$$LiClO_4.3H_2O$ sample obtained by solvent evaporation at room temperature (E_a = 57.4 KJ.mol^{-1}). In addition, the thermal and electrochemical stability of the P(VDF-TrFE)$_n$$LiClO_4.3H_2O$ are sufficient to justify further studies to develop attractive electrolyte components. The overall stability of the electrolyte is good with no electrochemical oxidation occurring at potentials less than 3.0 V. This result confirms that the electrolyte system has adequate electrochemical stability for application in practical primary and secondary cells. The results of DSC and TGA analysis are consistent with a minimum thermal stability of about 100 ºC for the P(VDF-TrFE)$_{1.5}$$LiClO_4.3H_2O$ electrolyte composition, a value considered acceptable for applications under normal operating conditions. The results show a clear decrease in thermal stability with increasing salt concentration, confirming that the salt has a destabilizing influence on the matrix host.

4.4. References

1. California, A., et al., *Tailoring porous structure of ferroelectric poly(vinylidene fluoride-trifluoroethylene) by controlling solvent/polymer ratio and solvent evaporation rate.* European Polymer Journal, 2011. 47(12): p. 2442-2450.
2. Ferreira, A., et al., *Poly(vinylidene fluoride-trifluoroethylene) (72/28) interconnected porous membranes obtained by crystallization from solution.* MRS Online Proceedings Library, 2011. 1312: p. null-null.
3. Ferreira, A., et al., *Poly[(vinylidene fluoride)-co-trifluoroethylene] Membranes Obtained by Isothermal Crystallization from Solution.* Macromolecular Materials and Engineering, 2010. 295(6): p. 523-528.
4. Bar-Cohen, Y., *Electroactive Polymer (EAP) Actuators as Artificial Muscles: Reality, Potential, and Challenges, Second Edition*2004: SPIE Publications. 816.
5. Celgard. *Monolayer Polypropylene (PP).* 2011; Available from: http://www.celgard.com/monolayer-pp.aspx.
6. Faria, L.O. and R.L. Moreira, *Infrared spectroscopic investigation of chain conformations and interactions in P(VDF-TrFE)/PMMA blends.* Journal of Polymer Science Part B: Polymer Physics, 2000. 38(1): p. 34-40.
7. Kobayashi, M., K. Tashiro, and H. Tadokoro, *Molecular Vibrations of Three Crystal Forms of Poly(vinylidene fluoride).* Macromolecules, 1975. 8(2): p. 158-171.
8. Chen, Y., Y.-H. Zhang, and L.-J. Zhao, *ATR-FTIR spectroscopic studies on aqueous LiClO4, NaClO4, and Mg(ClO4)2 solutions.* Physical Chemistry Chemical Physics, 2004. 6(3): p. 537-542.
9. Zhang, Y.-H. and C.K. Chan, *Observations of Water Monomers in Supersaturated NaClO4, LiClO4, and Mg(ClO4)2 Droplets Using Raman Spectroscopy.* The Journal of Physical Chemistry A, 2003. 107(31): p. 5956-5962.
10. Kap Jin, K. and K. Gwan Bum, *Curie transition, ferroelectric crystal structure and ferroelectricity of a VDF/TrFE (7525) copolymer: 2. The effect of poling on Curie transition and ferroelectric crystal structure.* Polymer, 1997. 38(19): p. 4881-4889.

11. Barique, M.A. and H. Ohigashi, *Annealing effects on the Curie transition temperature and melting temperature of poly(vinylidene fluoride/trifluoroethylene) single crystalline films.* Polymer, 2001. 42(11): p. 4981-4987.
12. Djian, D., et al., *Macroporous poly(vinylidene fluoride) membrane as a separator for lithium-ion batteries with high charge rate capacity.* Journal of Power Sources, 2009. 187(2): p. 575-580.
13. Karabelli, D., et al., *Poly(vinylidene fluoride)-based macroporous separators for supercapacitors.* Electrochimica Acta, (0).
14. Barbosa, P.C., et al., *Studies of solid-state electrochromic devices based on PEO/siliceous hybrids doped with lithium perchlorate.* Electrochimica Acta, 2007. 52(8): p. 2938-2943.
15. Every, H.A., et al., *Lithium ion mobility in poly(vinyl alcohol) based polymer electrolytes as determined by 7Li NMR spectroscopy.* Electrochimica Acta, 1998. 43(10-11): p. 1465-1469.
16. Quartarone, E., P. Mustarelli, and A. Magistris, *Transport Properties of Porous PVDF Membranes.* The Journal of Physical Chemistry B, 2002. 106(42): p. 10828-10833.
17. Miyamoto, T. and K. Shibayama, *Free-volume model for ionic conductivity in polymers.* Journal of Applied Physics, 1973. 44(12).
18. Ulaganathan, M. and S. Rajendran, *Effect of different salts on PVAc/PVdF-co-HFP based polymer blend electrolytes.* Journal of Applied Polymer Science, 2010. 118(2): p. 646-651.

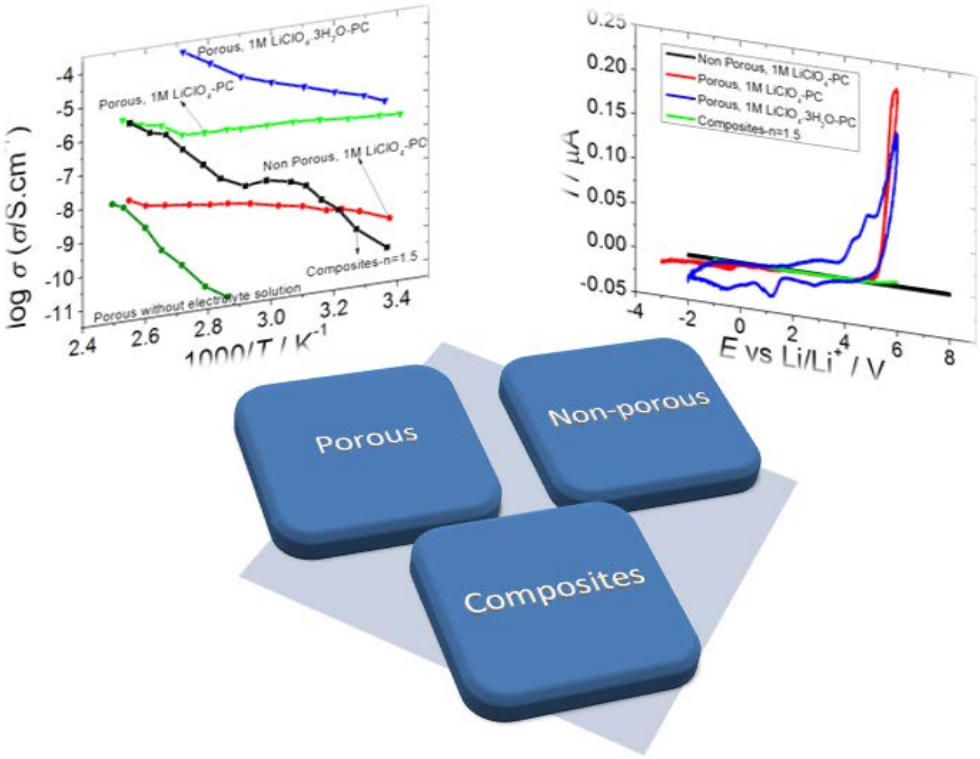

5. *Main processing parameters influencing the performance of P(VDF-TrFE) as battery separators*

This chapter describes the main parameters affecting P(VDF-TrFE) membrane separator performance such as porosity, dehydration of lithium ions and processing technique (Li-ion uptake versus composite preparation) .

This chapter is based on the following publication:

"Evaluation of the main processing parameters influencing the performance of poly(vinylidene fluoride-trifluoroethylene) lithium-ion battery separators", C. M. Costa, V. Sencadas, J. G. Rocha, M. M. Silva, S. Lanceros-Méndez, J. Solid State Electrochem 17 (2013) 861-870

5.1. Samples

Table 5.1 shows the different membranes produced and the value of the porosity and uptake for each sample.

Table 5.1 - Microstructure, electrolyte solution, porosity and lithium ions uptake for the P(VDF -TrFE) membranes.

Sample	Microstructure Type	Electrolyte Solution	Porosity (%)	Uptake (%)
P(VDF-TrFE)	Porous	1 M $LiClO_4$	72	255
P(VDF-TrFE)	Non Porous	1 M $LiClO_4$	0	0
P(VDF-TrFE)	Porous	1 M $LiClO_4.3H_2O$	72	223
$P(VDF\text{-}TrFE)_{1.5}$ $LiClO_4.3H_2O$	Porous	-------	67	--------

5.2. Results

The microstructure of the samples produced after solvent evaporation at room temperature with or without Li-ions reveals a porous structure (Figure 5.1 a and b). A small variation of the degree of porosity has been found depending on the lithium incorporation. The degree of porosity for the samples without lithium ions is 72% and for the $P(VDF\text{-}TrFE)_{1.5}LiClO_4.3H_2O$ composite samples 67%, indicating that the presence of the Li-ions does not influences significantly the crystallization characteristics of the polymer. The samples prepared after solvent evaporation at 210 °C shows no porosity, figure 5.1-c).

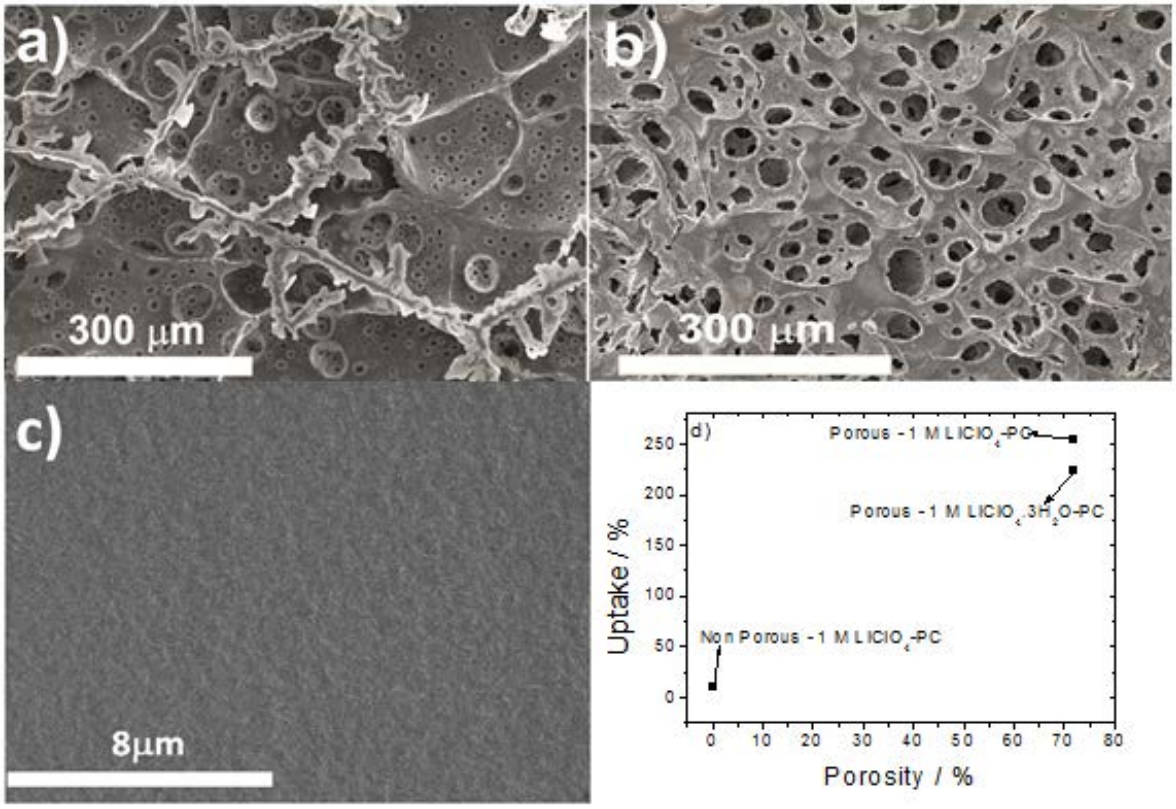

Figure 5.1 - Separator microstructure for the samples prepared after the different processing techniques: a) sample without lithium ions crystallized at room temperature, b) microstructure of the membrane for lithium ions (*n*=1.5) crystallized at room temperature, c) microstructure of sample crystallized at 210 °C without lithium ions and d)Uptake for porous and non-porous samples for the different electrolyte solution.

In this way, the porosity of the membranes can be controlled evaporating the solvent at different temperatures (figure 5.1) [1]. The cross-section images for the uptake samples are illustrated in the [2] and for the composites samples in [3] where are observed the homogeneous distribution of the pore size. The pore size medium is 9 ±3 μm and the tortuosity value is 115 for the uptake samples that indicate the pores are not well connected. Porous and non-porous pure polymer samples were immersed in 1 M $LiClO_4$-PC or 1 M $LiClO_4.3H_2O$-PC solutions and their initial and final weight was measured after 24 h immersion.

Figure 5.1 d) shows the degree of porosity versus uptake for the different samples. The uptake for the non-porous samples is ~10% due to the absorption of the lithium ions in the polymer surface (figure 5.1 d)). The porous P(VDF-TrFE) membranes show a maximum uptake of ~ 255% for the sample with 72% porosity (figure 5.1 a).

Increasing porosity is associated to an increase of the specific surface area and consequently higher adsorption of lithium ions leading to an increase of the uptake [2].

P(VDF-TrFE) is a semicrystalline polymer that crystallizes in the electroactive phase that can be identified by infrared spectroscopy through specific absorption bands [4, 5]. Figure 5.2 shows the infrared spectrum for the samples (porous and non-porous) before and after lithium ions uptake as well as for the $P(VDF\text{-}TrFE)_{1.5}LiClO_4.3H_2O$ composite.

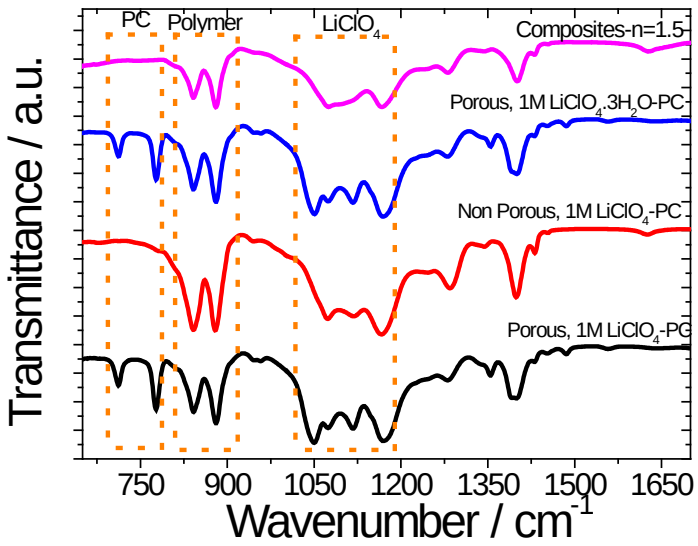

Figure 5.2 - Infrared spectrum for the different samples

All samples show the characteristic vibrational bands **at** 840, 880, 1170, 1282 and 1402 cm^{-1} of P(VDF-TrFE), assigned to symmetric stretching or rocking modes of CF_2, asymmetric stretching mode of CF_2, symmetric stretching mode of CC and wagging CH_2, respectively [6], indicating that the polymer crystalline phase is not affect by the incorporation of the Li-ions by uptake or by the preparation of the composites: no polymer degradation or phase transformation was detected.

The samples with electrolyte solution, the FTIR spectra also shows the presence of two strong bands related to the presence of propylene carbonate at 712 cm^{-1} and 777 cm^{-1} [7].

By comparison of the FTIR spectra of the samples with the two different lithium ions, in both cases it is possible observe the four vibration modes at 933 cm^{-1}, 1060 cm^{-1}, 1150 cm^{-1} and 1625 cm^{-1}, identifying the O-H stretching band, assigned to Cl-O

asymmetric stretching band ($\nu_3(ClO_4$-), asymmetric bending band of ClO_4, and O-H bending (H_2O), respectively [8].

Figure 5.2 also shows strong differences between the two processing techniques (uptake vs. composite formation) in the region between 900 cm^{-1} at 1200 cm^{-1}, in the ion association of perchlorates. In the aqueous solutions, the interaction between cations and perchlorate ions appears, resulting in the symmetry decrease of perchlorate ions. This dependence is higher for the uptake technique due to the propylene carbonate-ion interactions which is salt concentration dependent [7, 8]. The dimensional stability of the different samples was determined through the dynamical mechanical analysis in previous work that shown good mechanical properties in function of the uptake by electrolyte solution [2] and in the composite material [3].

One of the key parameters of a membrane for battery separators is its ionic conductivity. Figure 5.3 a-c) shows the Nyquist plot for different samples produced before and after soaking in different electrolytes solutions and for the composite sample and figure 5.3 d) present the Nyquist plot for non-porous membrane soaked with 1 M $LiClO_4$-PC as a function of temperature.

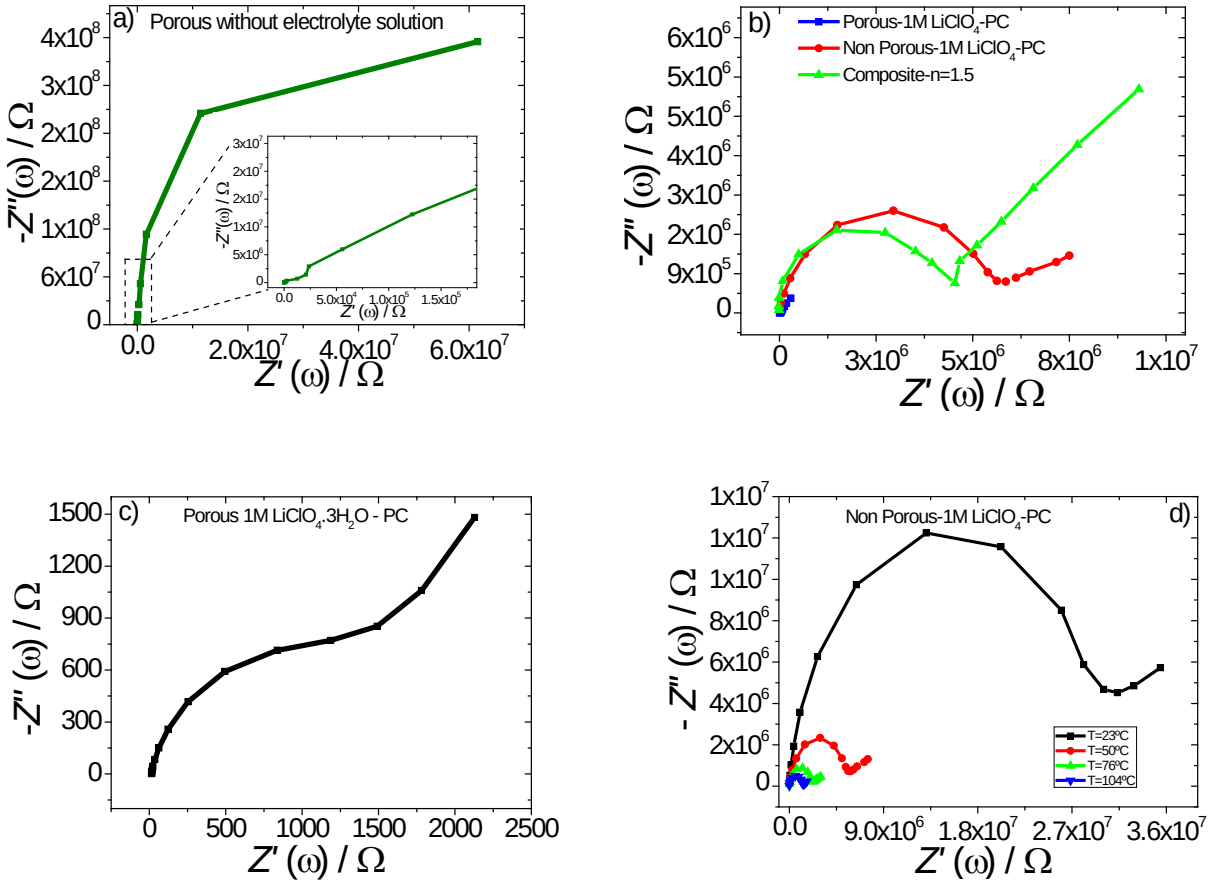

Figure 5.3 - Nyquist plot for: a-c) P(VDF-TrFE) samples at 50 °C and d) non porous membrane with 1 M $LiClO_4$-PC.

In the Nyquist plot represented in figure 5.3 a-c), three characteristic parts can be identified in all cases except for the porous membrane before introducing the electrolyte solution: a semicircle located in the high-frequency range that corresponds to the charge transfer process (bulk material properties), a transition controlled by the diffusion of counter ions inside the electrode, and straight line for lower frequency that is related to the diffusion process, i.e. the membrane/electrode interface (figure 5.3) [9, 10].

The impedance decreases for all membrane with different electrolyte solutions and independently of the microstructure and the processing technique in comparison to the porous membrane without lithium ions due the increase of the ionic conductivity of the membranes ascribed to the presence of the Li ions. The Figures 5.3 a-c) shows this impedance behavior of all membranes.

Despite the samples immersed in both electrolyte solutions showing similar trends, Figure 5.3 b) shows that the nature of the lithium ions present in the polymer electrolyte membrane influences the diffusion process of the ions in the polymeric matrix, being the diffusion coefficient of the 1 M $LiClO_4.3H_2O$-PC smaller when compared to the 1 M $LiClO_4$-PC, figure 5.3 b). The water molecules present in $LiClO_4.3H_2O$-PC improve the charge transfer, especially at higher frequencies (figure 5.3 c).

The porous samples with different electrolyte solutions (figure 5.3 b and 5.3 c) after uptake show the semi-circle at higher frequencies and the samples behavior is controlled by the capacitive response at a broader frequency range which shows that the diffusion process of lithium ions in these samples controls the material electrochemical response.

The difference of the impedance behavior between samples prepared after uptake and composite samples is related to the charge transfer process due the solvent used in the electrolyte solution that improves the mobility of lithium ions in the amorphous phase of the polymer [11] confirmed in the diffusion process presents in the figure 5.3 b).

These results show that the polymer microstructure influences the main electrochemical mechanism of the lithium cell and that the solvent used in the electrolyte solution improves the ions diffusion through the porous membrane.

The impedance behavior in function of temperature was studied for all samples. It is observed that the conductivity increases when increases the temperature. In the figure 5.3 d) is represented the impedance behavior in function of temperature for non-porous membrane with 1 M $LiClO_4$-PC.

Analyzing of figure 5.3 d), observed that with increase of temperature the semi-circle moves to the left by decreasing its value. This behavior was observed for all samples.

For example, in the non-porous sample with uptake for different temperatures (figure 5.3 d), the semi-circle is observed in a broader frequency range, especially at lower temperatures, which demonstrates that the charge transfer through polymer is the most relevant factor issue in the electrochemical response of samples after uptake.

The Bode diagram was obtained for all samples at different frequencies and same temperature of 50 °C (figure 5.4).

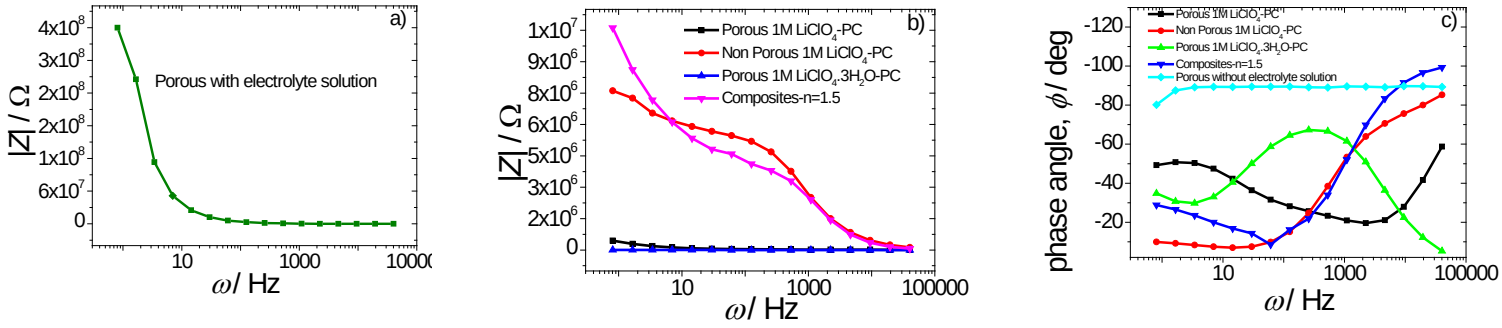

Figure 5.4 - a and b) Impedance modulus and c) Phase angle for all samples at 50 °C

It is observed a different frequency dependence for the different samples, which proves the influence of the microstructure, the different lithium ions type and the processing techniques (uptake vs. composites) on the impedance modulus (figure 5.4). All polymer electrolyte separators show a decrease of the impedance modulus with increasing frequency figure 5.4a and b).

For all membranes, the impedance depends on the frequency for lower frequencies, but for frequencies above 1 kHz the impedance modulus strongly decreases (figure 5.4a and b).

For membrane with same electrolyte solution, it is possible observe the dependence of the frequency domain in the different microstructure. For non-porous microstructure observed the major dependence in the high frequency domain.

In all polymer electrolyte porous separators soaked with the different electrolyte solution, the decrease in the modulus of the impedance is due to the lithium ions diffusion process, whose motion can be free or eventually restricted by the barriers of the cavities and by the polymer swollen regions [12, 13].

Uptake porous membrane with electrolyte solution has a quite lower value of the $|Z|$ modulus when compared to the composite ones with same lithium ions, which reveals that the ion diffusion and mobility is easier for the uptake samples, due of the porosity of the membranes.

Figure 5.4 c) shows that the phase angle depends on microstructure, lithium ions type, processing techniques (uptake and composites) and frequency.

The phase angle for 104 °C reaches a value close to 60º, indicating capacitive behavior between the membrane and electrode interface [14]. This behavior is similar for porous and non-porous polymer electrolyte separator with 1 M $LiClO_4$-PC

Bode plot presents for porous membranes with 1 M $LiClO_4$-PC, a phase angle with maximum at -70 °C. For an ideal capacitor, the maximum phase angle should be around -90º, but for the samples with 1 M $LiClO_4.3H_2O$-PC, a maximum of -70º was reached for at temperatures ≤ 50 °C for frequencies below 1 kHz.

By comparing to the uptake samples with same lithium solution, the composite polymeric electrolyte membranes show a behavior very close to an "ideal" capacitor and resistor polymeric separator, with the phase angle near -90º at 50 °C temperature and 1 kHz.

5.3. Discussion

The porous microstructure of the separator membranes is determined, as in the pure co-polymer, by the solvent evaporation temperature and does not depend on the lithium ions placed in the solution [1, 3]. The microstructure of the membrane will have influence in the mechanical and electrochemical properties of the separator membranes (figure 5.1) [2].

The porosity, adsorption of the different electrolyte solutions and the introduction of the salts within the polymer matrix in the preparation of the composite samples do not change the crystalline phase of the polymer, as identified by the characteristic absorption bands of the polymer at 840 cm^{-1}, indicative of the chain conformations corresponding to the polar phase [2, 4] (figure 5.2).

The electrochemical impedance spectroscopy was analyzed in terms of an equivalent electrical circuit. The commonly used equivalent electrical circuit is the Randles circuit [15] consisting in electrolyte resistance between working and reference electrodes (R_1), the double-layer capacitance (C_2) and the faradaic impedance: the charge-transfer resistance (R_2) in parallel of Warburg impedance (Z_w) [16] (Figure 5.5).

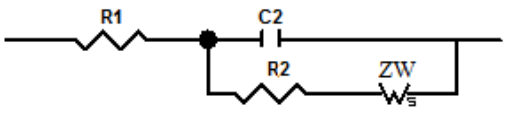

Figure 5.5 - Illustration of Randles circuit

The charge-transfer resistance (R_2) in parallel of Warburg impedance (Z_w) reflects the influence of the mass transport of electroactive species on the total impedance of the electrochemical cell [15].

The double-layer capacitance (C_2) is used to accommodate the non-ideal behavior of the capacitance [17]. The capacitance (C_2) is defined by the following equation:

$$C_2 = C^{1/n} \times R^{1-n/n} \quad (1)$$

where the parameter n represent the nonideal behavior having a value of zero for pure resistive behavior and the value of one for capacitive behavior.

Figure 5.6 shows the simulated Nyquist plot by EIS Spectrum Analyser [18] for Randles circuit (figure 5.5) where the charge transfer and diffusion processes are observed. The parameters used in the simulation are: R_1 = 1x10^4 Ω, R_2 = 4x10^4 Ω, C_2 = 5 nF, n=1 and Z_w = 5000 Ω•s$^{-0.5}$.

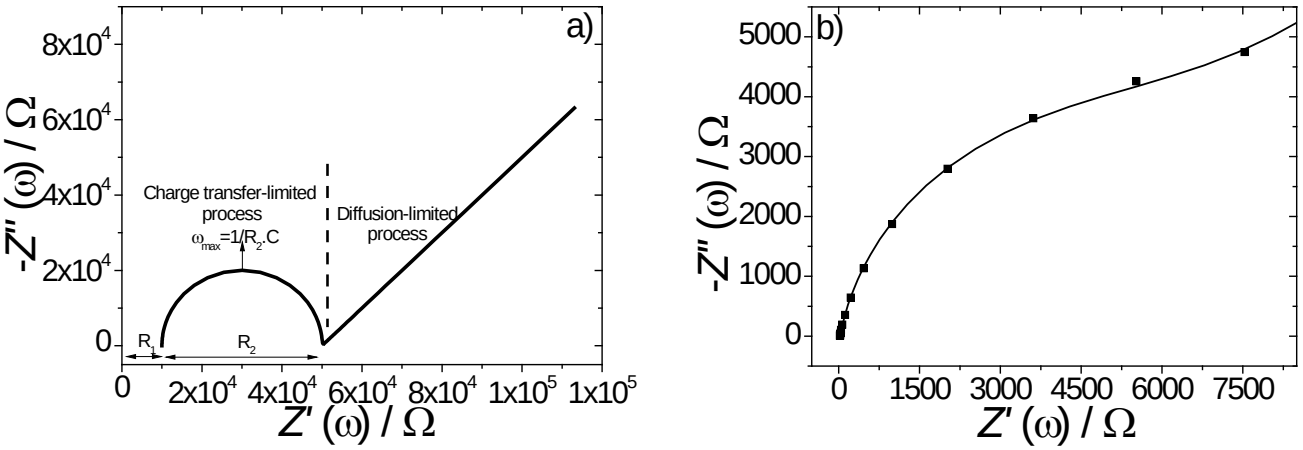

Figure 5.6 - a) Nyquist plot simulated through the Randles circuit. The identification of processes was adapted by [15] and b) shows the Nyquist plot for porous membrane with 1 M $LiClO_4.3H_2O$-PC at room temperature (squares) and the line represent the fitting with Randles circuit.

From the intercept of the imaginary impedance (minimum value of Z'') with the slanted line in the real impedance (Z') (figure 5.3) is obtained the bulk resistance, R_2 through of Randles circuit. Then, the ionic conductivity can be determined by $\sigma = t/A \times R_2$ where t is the thickness and A is the area of the membranes.

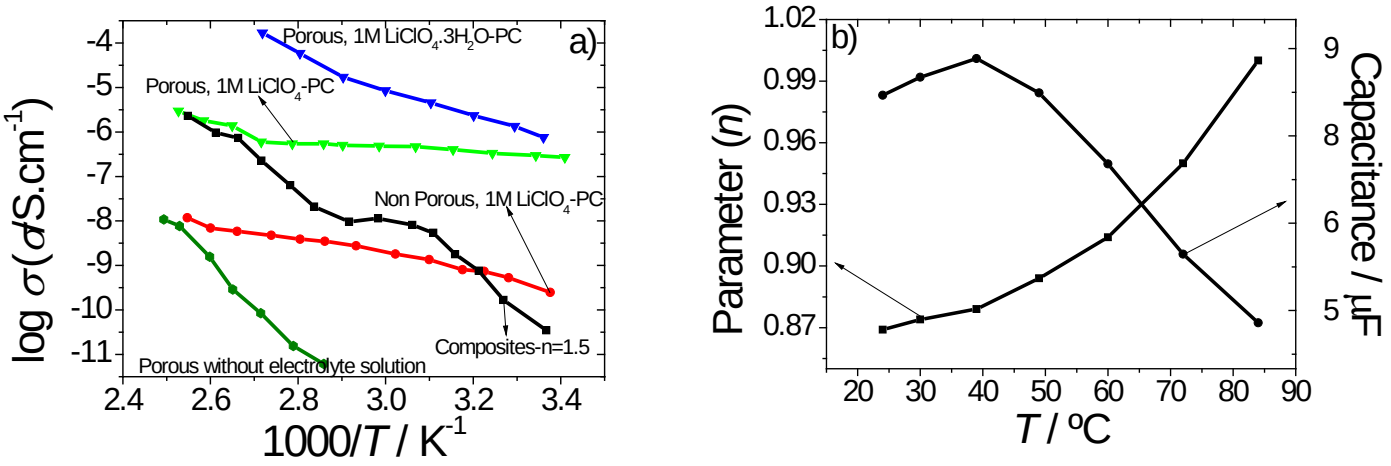

Figure 5.7 - a) Ionic conductivity as a function of temperature all membrane samples and b) parameter n and capacitance for porous membrane with 1 M $LiClO_4.3H_2O$-PC.

Figure 5.7 a) shows the ionic conductivity as a function of temperature for all membranes and figure 5.7 b) shows the parameter n and capacitance simulated by the Randles circuit as a function of temperature for the membrane with the highest ionic conductivity: Porous membrane with 1 M $LiClO_4.3H_2O$-PC uptake.

Without lithium ions, the ionic conductivity of the polymer porous membrane is strongly affected by temperature variation due to increased mobility of polymer ionic charges [19]. Further, the porosity and pore shape also influence the ionic conductivity of the membranes [20] due to its influence in the specific surface available for lithium ions adsorption and trapping.

With the inclusion of the lithium ions in the polymeric matrix of all membranes, the ionic conductivity increases and also increases with increasing temperature for both types of separators. The membrane with higher ionic conductivity is the porous membrane with 1 M $LiClO_4.3H_2O$-PC.

This observations supports previous results from [20-22], indicating that contributions to the conductivity are coming from the amorphous swollen polymer gel phase.

The incorporation of 1 M $LiClO_4$-PC salts by uptake strongly influences the behavior of the polymer electrolyte membranes. For the samples dip coated in $LiClO_4.3H_2O$ a strong dependence of the ionic conductivity was observed when compared to the 1 M $LiClO_4$-PC ions. Molar mass for both electrolyte lithium solutions

are the same, but it seems that the addition of $3H_2O$ results in an enhancement of the conductivity [23], and consequently the performance of the polymer electrolyte separator.

The temperature dependence of the ionic conductivity for the composite polymeric electrolyte membrane is shown in figure 5.7 a) and, as expected, the conductivity of the lithium ions in such samples is lower when compared to the uptake ones, due to the lower concentration and reduced mobility of the lithium ions that are trapped by surrounding polymeric phase and the interaction between organic solvent (PC) and the polymeric matrix.

Figure 5.7 b) show that slight variations in the parameter *n* and *C* for the membrane with higher ionic conductivity in the room temperature at 100 °C range. The parameter *n* increases with increasing temperature and present a high value, very close to 1 for all temperatures, indicating a capacitive behavior [24].

A decrease in the capacitance (figure 5.7 b) with increasing temperature in the polymeric matrix may be due to the release of trapped ionic charges followed by the accumulation of these charges in the polymeric matrix or mobility of the polymer chain.

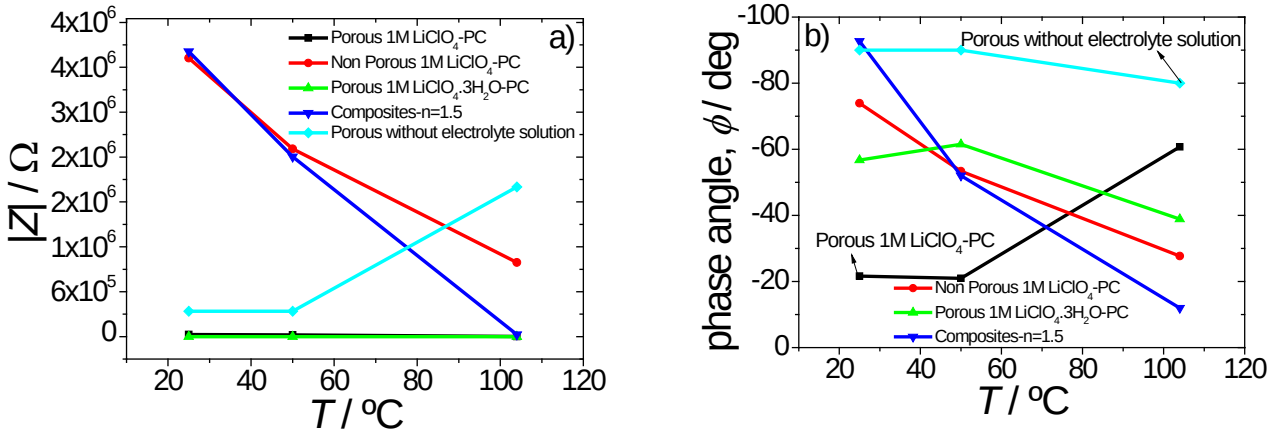

Figure 5.8 - For all samples a) Impedance modulus of |*Z*| as a function of temperature at 1 kHz and b) phase angle as a function of temperature at 1 kHz.

Figure 5.8 shows the impedance modulus and phase angle, respectively as a function of temperature for 1 kHz.

For different polymer microstructures but same electrolyte solution, it is possible to observe a major dependence of the temperature for porous membrane due to the porosity present in the sample which results in increased absorption of the lithium ions.

The temperature increases the mobility of lithium ions for both microstructures. This fact is observed for all membranes except for membrane without electrolyte solution.

Additionally, for porous samples, an increase in temperature is accompanied by an increase in the capacitive behavior for porous microstructure verified by displacement in the frequency domain for different temperatures (figure 5.8 a and b). Moreover, such capacitive behavior was not demonstrated by the non-porous membranes due the lower value of uptake lithium ions.

By comparing the uptake samples with composite membranes, it is revealed that the ion diffusion and mobility is easier for the uptake samples, due to the larger amount of ions present in the sample when compared to the composite membranes (figure 5.8). Moreover, for the composite polymeric electrolyte membranes, the lithium ions forms clusters that are trapped by the surrounding polymer, which promotes and increase of the impedance modulus. For correlate the electric results obtained for all membranes samples, was determined the electrochemical stability of the all membranes through of the microelectrode cyclic voltammetry over the potential range -2.0 V to 6.0 V. The cyclic voltammogram for all samples are shows in the figure 5.9.

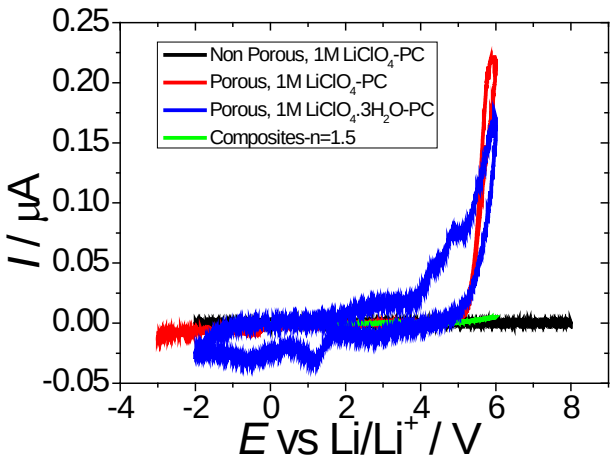

Figure 5.9 - Cycle Voltammogram of all membrane samples

It is observed that membranes with electrolyte solution, exhibit excellent stability in the chemical stability and with no electrochemical oxidation occurring at anodic potentials less than about 5 V vs. Li/Li^+.

5.4. Conclusion

Poly(vinylidene fluoride – trifluoroethylene) membranes have been investigated in order to evaluate the effect of porosity, dehydration of lithium ions and different experimental Li-ion loading techniques for Li-ion battery separator applications.

The impedance properties are represented through the Nyquist and Bode plots and the ionic conductivity was determined by Nyquist plot. The electric behavior observed for all samples was interpreted by the Randles circuit. The porosity, dehydration of lithium ions and the experimental processing technique does not modify the vibration peaks characteristics of polymer present in the membrane. The electrical behavior of the membrane is influenced by all parameters studied in this work. As a conclusion, the parameters that more influence the membrane for battery applications are porosity and Li-ion loading technique. For the lithium ion applications, the best membrane must have porosity, the lithium ions preferably without dehydration and loaded by the uptake technique. The result of cyclic voltammetry confirms that the porous membrane based of P(VDF-TrFE) has adequate electrochemical stability for lithium-ion battery applications.

5.5. References

1. California, A., et al., *Tailoring porous structure of ferroelectric poly(vinylidene fluoride-trifluoroethylene) by controlling solvent/polymer ratio and solvent evaporation rate.* European Polymer Journal, 2011. 47(12): p. 2442-2450.
2. Costa, C.M., et al., *Effect of degree of porosity on the properties of poly(vinylidene fluoride-trifluorethylene) for Li-ion battery separators.* Journal of Membrane Science, 2012. 407-408(0): p. 8.
3. Costa, C.M., et al., *Effect of the microsctructure and lithium-ion content in poly[(vinylidene fluoride)-co-trifluoroethylene]/lithium perchlorate trihydrate composite membranes for battery applications.* Solid State Ionics, 2012. 217(0): p. 19-26.
4. Faria, L.O. and R.L. Moreira, *Infrared spectroscopic investigation of chain conformations and interactions in P(VDF-TrFE)/PMMA blends.* Journal of Polymer Science Part B: Polymer Physics, 2000. 38(1): p. 34-40.
5. Prabu, A.A., et al., *Infrared spectroscopic studies on crystallization and Curie transition behavior of ultrathin films of P(VDF/TrFE) (72/28).* Vibrational Spectroscopy, 2006. 41(1): p. 1-13.
6. Kobayashi, M., K. Tashiro, and H. Tadokoro, *Molecular Vibrations of Three Crystal Forms of Poly(vinylidene fluoride).* Macromolecules, 1975. 8(2): p. 158-171.
7. Battisti, D., et al., *Vibrational studies of lithium perchlorate in propylene carbonate solutions.* The Journal of Physical Chemistry, 1993. 97(22): p. 5826-5830.
8. Chen, Y., Y.-H. Zhang, and L.-J. Zhao, *ATR-FTIR spectroscopic studies on aqueous LiClO4, NaClO4, and Mg(ClO4)2 solutions.* Physical Chemistry Chemical Physics, 2004. 6(3): p. 537-542.
9. Chang, B.-Y. and S.-M. Park, *Electrochemical Impedance Spectroscopy.* Annual Review of Analytical Chemistry, 2010. 3(1): p. 207-229.
10. Park, S.-M. and J.-S. Yoo, *Electrochemical Impedance Spectroscopy for better electrochemical measurements.* Analytical Chemistry, 2003. 75(21): p. 445 A-461 A.

11. Kufian, M. and S. Majid, *Performance of lithium-ion cells using 1 M $LiPF_6$ in EC/DEC (v/v= 1/2) electrolyte with ethyl propionate additive.* Ionics, 2010. 16(5): p. 409-416.
12. Binder, K., et al., *Polymer + Solvent Systems: Phase Diagrams, Interface Free Energies, and Nucleation Advanced Computer Simulation*, C. Dr. Holm and K. Prof. Dr. Kremer, Editors. 2005, Springer Berlin / Heidelberg. p. 130-130.
13. Eikerling, M., A. Kornyshev, and E. Spohr, *Proton-Conducting Polymer Electrolyte Membranes: Water and Structure in Charge Fuel Cells I*, G. Scherer, Editor 2008, Springer Berlin / Heidelberg. p. 15-54.
14. Sivaraman, P., et al., *All-solid secondary polyaniline-zinc battery.* Journal of Applied Electrochemistry, 2008. 38(2): p. 189-195.
15. Fernández-Sánchez, C., C.J. McNeil, and K. Rawson, *Electrochemical impedance spectroscopy studies of polymer degradation: application to biosensor development.* TrAC Trends in Analytical Chemistry, 2005. 24(1): p. 37-48.
16. Lasia, A., *Electrochemical Impedance Spectroscopy and its Applications Modern Aspects of Electrochemistry*, B.E. Conway, J.O.M. Bockris, and R.E. White, Editors. 2002, Springer US. p. 143-248.
17. Barsoukov, E.M., James Ross, *Impedance spectroscopy: theory, experiment, and applications*2005, Hoboken: John Wiley & Sons.
18. homepage, P. http://www.abc.chemistry.bsu.by/vi/; Available from: http://www.abc.chemistry.bsu.by/vi/.
19. Karabelli, D., et al., *Poly(vinylidene fluoride)-based macroporous separators for supercapacitors.* Electrochimica Acta, 2011. 57(0): p. 5.
20. Djian, D., et al., *Macroporous poly(vinylidene fluoride) membrane as a separator for lithium-ion batteries with high charge rate capacity.* Journal of Power Sources, 2009. 187(2): p. 575-580.
21. Quartarone, E., P. Mustarelli, and A. Magistris, *Transport Properties of Porous PVDF Membranes.* The Journal of Physical Chemistry B, 2002. 106(42): p. 10828-10833.
22. Every, H.A., et al., *Lithium ion mobility in poly(vinyl alcohol) based polymer electrolytes as determined by 7Li NMR spectroscopy.* Electrochimica Acta, 1998. 43(10-11): p. 1465-1469.

23. Bohnke, O., et al., *Fast ion transport in new lithium electrolytes gelled with PMMA. 2. Influence of lithium salt concentration.* Solid State Ionics, 1993. 66(1-2): p. 105-112.

24. Younas, M., et al., *Metal-semiconductor transition in $NiFe_2O_4$ nanoparticles due to reverse cationic distribution by impedance spectroscopy.* Journal of Applied Physics, 2011. 109(9): p. 093704.

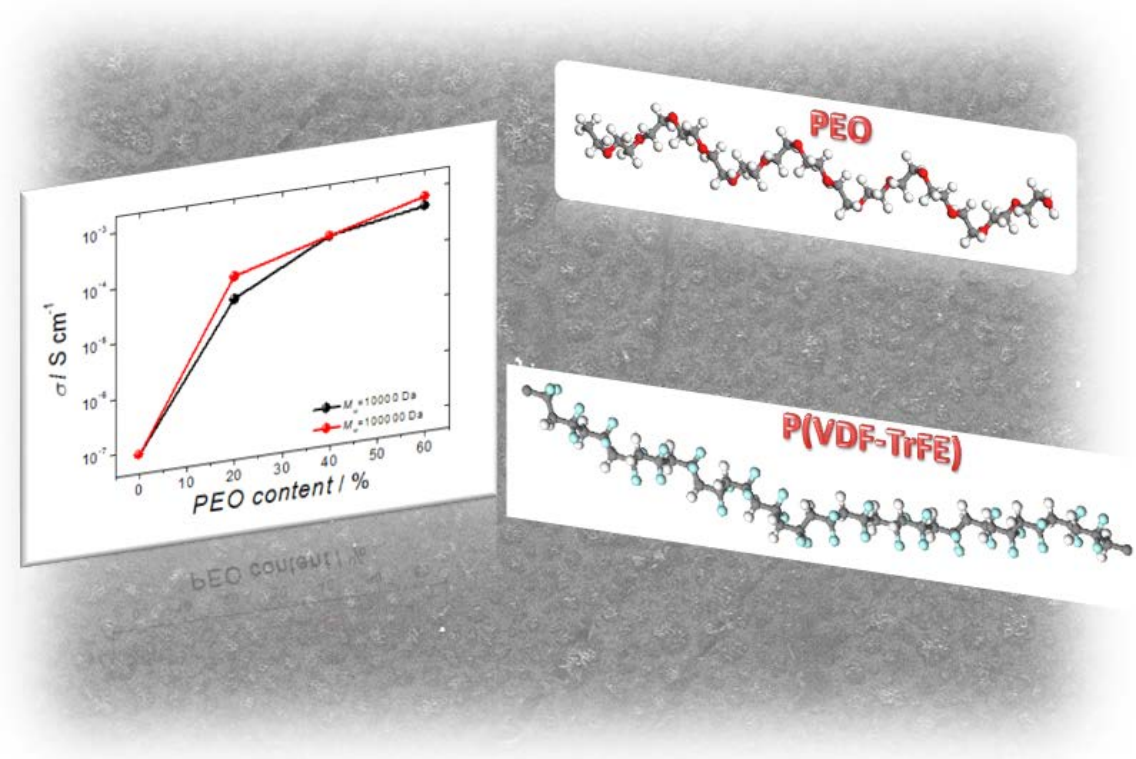

6. *Polymer Blends of P(VDF-TrFE)/PEO*

This chapter describes the properties of polymer blends based on poly(vinylidene fluoride-trifluoroethylene)/poly(ethylene oxide), P(VDF-TrFE)/PEO, with different PEO content and molecular weight for their use as Li-ion battery separator membranes.

This chapter is based on the following publication:

"Influence of poly(ethylene oxide) molecular weight in the characteristics of poly(vinylidene fluoride – trifluoroethylene) / poly(ethylene oxide) blend membranes for lithium ion battery applications", C. M. Costa, J. Nunes-Pereira, M. M. Silva, J. L. Gomez Ribelles, S. Lanceros-Méndez, submitted

6.1. Samples

The P(VDF-TrFE)/PEO polymer blend samples studied in this chapter have compositions of 100/0, 80/20, 60/40, 40/60 and 0/100 weight ratio for the two molecular weights of PEO. PEO with M_w = 10000 Da and with M_w = 100000 Da will be called hereafter PEO-10k and PEO-100k respectively. The electrolyte solution used is 1M $LiClO_4.3H_2O$ in PC.

6.2. Results and discussion

6.2.1. Microstructure, polymer phase and thermal properties

Blends of P(VDF-TrFE) and PEO with up to 60% by weight PEO have been evaluated for lithium ion battery separator membranes. Larger PEO contents in the blend leads to very fragile membranes, in particular for PEO-10k. The microstructure of P(VDF-TrFE)/PEO blends is determined by the crystallization process during membrane formation as both polymers are semicrytalline. The micrographs of the polymer membrane cross-section for P(VDF-TrFE)/PEO-10k is shown in Figure 6.1.

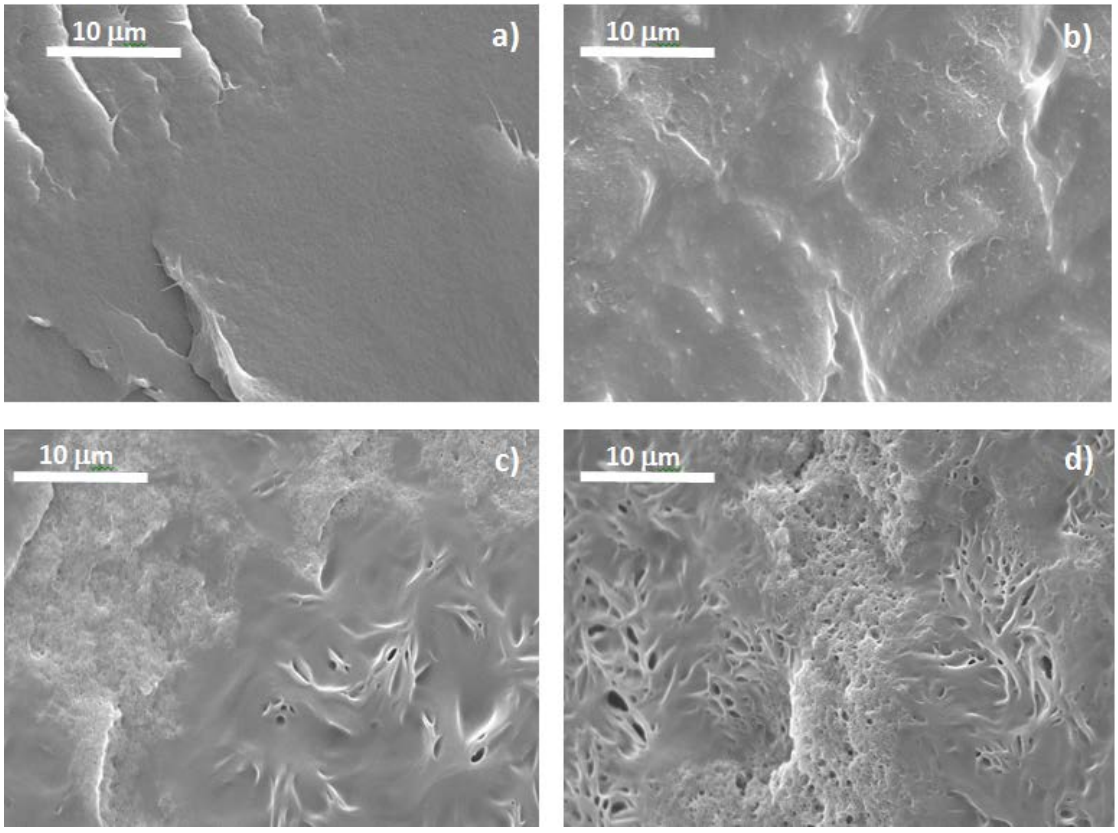

Figure 6.1 - Cross-section SEM images of P(VDF-TrFE)/PEO blend for PEO (M_w=10 kDa): a) 100/0, b) 80/20, c) 60/40, d) 40/60

The morphology for these polymer blends is very similar to that reported for blends containing PEO-100k in reference [1]. Figure 6.1a shows a uniform, dense and homogeneous cryogenic fracture in P(VDF-TrFE) that do not reveal crystallites morphology at this magnification. For low PEO contents (Figure 6.1b), the roughness of fracture surface indicates the presence of the two polymers leading to a heterogeneous microstructure. For PEO contents above 20% wt (Figures 6.1c and 6.1d) the presence of PEO crystals is observed and the samples show some degree of porosity that was also shown by the blends with high molecular weight PEO [2]. The presence of microporosity in the membrane observed the cross-section SEM images (Figures 6.1a-d) may facilitate lithium ion conduction along the interface [3]. Microporosity can appear during crystallization of P(VDF-TrFE) at 70 ºC from the solution in DMF in presence of molten PEO, in fact it has been previously shown [4] that a porous structure is produced by liquid-liquid or solid-liquid spinodal decomposition during solvent evaporation in the crystallization of pure P(VDF-TrFE) from the DMF solution. Although the presence of PEO diluted in the solution in DMF will obviously modify the phase diagram of P(VDF-TrFE) polymer, the appearance of voids during crystal growth cannot be discarded. On the other hand, PEO crystals grow during cooling from 70 ºC to room temperature in the dry blend. The contraction of the PEO phase during crystallization can also produce voids since it takes place in a volume confined by the semycrystalline P(VDF-TrFE) phase.

Fourier transform infrared spectroscopy (FTIR) allows characterizing the polymer phase of the polymers and to evaluate the possible interaction between the two components of the polymer blends [5]. The spectra of the polymer blends prepared with PEO-10k are similar to those determined in the blend with PEO-100k [1] and are not shown in this work. It was concluded that the presence of P(VDF-TrFE) has influence in the chain conformation of PEO leading to a transformation from zigzag into helix conformation this fact being independent of the PEO molecular weight.

The thermal properties of the polymer blend membranes were evaluated by DSC in heating scans. The DSC thermograms for the pristine P(VDF-TrFE) polymer and the P(VDF-TrFE)/PEO, 60/40 blends with both molecular weights are shown in Figure 6.2.

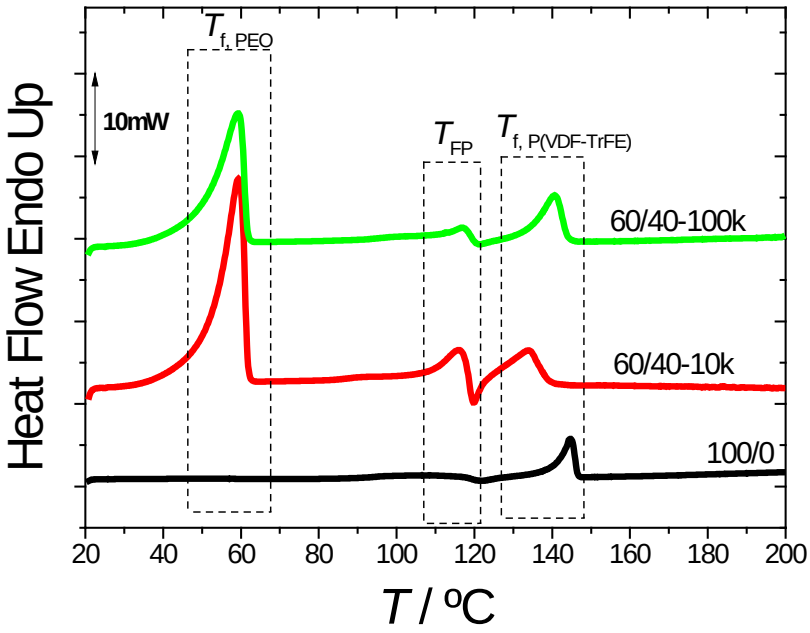

Figure 6.2 - DSC thermograms of the blend membrane, 60/40 for both molecular weight in the heating scan

Three peaks are observed for the polymer blend membranes independently of the molecular weight of PEO. The lower temperature peak corresponds to the melting temperature of PEO, around 55 ºC - 68 ºC [6] depending on PEO content, and the higher temperature ones correspond to P(VDF-TrFE): the one at ~117 ºC corresponds to the ferroelectric-paraelectric transition (FE-PE, Curie transition) and the one around 145 ºC corresponds to the melting of the paraelectric phase [7].

Melting temperatures and crystalline fraction of the each component within the blends were calculated with equation 5, chapter 2 (Table 6.1).

Table 6.1 – Degree of crystallinity and melting temperature of each polymer as a function of the polymer blend composition for both molecular weight.

	P(VDF-TrFE)/PEO-100k				**P(VDF-TrFE)/PEO-10k**			
	P(VDF-TrFE)		**PEO**		**P(VDF-TrFE)**		**PEO**	
P(VDF-TrFE)/PEO	T_f (ºC)	χ (%)	T_f (ºC)	χ (%)	T_f (ºC)	χ (%)	T_f (ºC)	χ (%)
100/0	145	28	---	---	145	28	---	---
80/20	146	22.5	55	10	135	25	55	35
60/40	141	16.7	59	27.5	134	20	59	35
40/60	141	10	62	62.5	142	12.5	63	70

Table 6.1 shows that the melting temperature and degree of crystallinity of PEO increases with increasing PEO content in the polymer blends independently of the molecular weights of PEO. Increasing PEO content increases of the nucleation density of PEO from the melt that result in the PEO crystals embedded in the P(VDF-TrFE) polymer [1]. The degree of crystallinity of PEO is higher for the lower molecular weight as shown in Table 6.1 what can be explained by the higher mobility of the molten low molecular weight PEO chains.

The Curie transition temperature of P(VDF-TrFE), on the other hand, is independent of blend composition and PEO molecular weight. The crystallization of P(VDF-TrFE) from the solution in DMF is nevertheless influenced by the presence of PEO as indicated by the modification of the melting temperature of P(VDF-TrFE) and of the degree of crystallinity. This fact is dependent of blend composition but independent of the molecular weight of PEO. Increasing dilution of P(VDF-TrFE) copolymer chains hinders crystal growth. Thus, in the blend containing 40% P(VDF-TrFE), the blend film is nearly amorphous, consisting presumably in a homogeneous mixture of both components, although a small fraction of P(VDF-TrFE) crystals is dispersed in this medium. Then, on cooling, PEO crystals grow forming a continuous semicrystalline PEO phase.

6.2.2. Mechanical properties of the blend membranes

The dynamic-mechanical properties of the polymer blends are influenced by molecular weight and have an important role in the material performance for membrane separators applications [8]. The *E'* vs log*f* plots corresponding to blends with PEO-10k and PEO-100k are parallel to each other. The dependence of *E'* measured at 1 Hz with blend composition and molecular weight is shown in Figure 6.3.

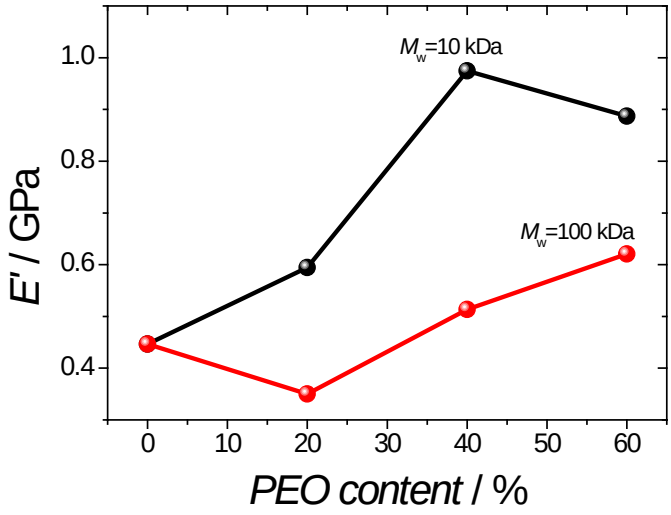

Figure 6.3 - Storage modulus, *E'*, measured at 1 Hz and 25 ºC, as a function of PEO content for the polymer blend membranes for the two PEO molecular weight.

The storage modulus, *E'*, decreases with increasing PEO molecular weight for all polymeric blend compositions. This fact was previously reported in [8, 9] and was ascribed to the fact that the lower molecular weight fractions can act as diluents and retard the crystallization of the polymer with respect to the higher molecular weight fractions and the differences observed in the degree of crystallinity [8] which plays a major role in the mechanical properties of the material. Independently of the molecular weight of PEO, the storage modulus, *E'*, increases with increasing PEO content in the blend due to an increase of the degree of crystallinity as shown in Figure 6.3 and Table 6.1 at room temperature.

The differences in the storage modulus, *E'*, for both molecular weight are attributed to the interphase region between the ordered crystalline regions and the isotropic conformational disordered amorphous regions [8, 10]. For same PEO content, independently of molecular weight, is verified that with the higher molecular weight

(M_w=100k Da) or the longer polymer chain, present more difficulty of molecular reorganization from the entanglements when requested in frequency and too of the differences in the degree of crystallinity (Figure 6.3).

6.2.3. Uptake and electrical properties

As discussed above, some porosity remains in the dry blend samples. The specific surface area and micro-porosity affects $LiClO_4.3H_2O$ solution uptake as presented in Table 6.2.

Table 6.2 – Uptake, effective conductivity and MacMullin number of the separator membranes. Electrolyte: 1M $LiClO_4.3H_2O$; σ_0 (S/cm)=9.8 mS cm^{-1} at 25 ºC.

Sample	Uptake / (%)	σ_{eff} (S cm^{-1})	N_M
80/20, M_w=100 kDa	49	8×10^{-5}	124
60/40, M_w=100 kDa	92	3×10^{-4}	33
40/60, M_w=100 kDa	49	7×10^{-4}	14
80/20, M_w=10 kDa	28	3×10^{-5}	329
60/40, M_w=10 kDa	43	2×10^{-4}	49
40/60, M_w=10 kDa	29	5×10^{-4}	20

The differences observed in the uptake value do not vary monotonously with PEO content in the blend neither in PEO-10k nor in PEO-100k, the maximum corresponds to a PEO content of 40%. This behavior can be due to the opposite effects of PEO content increasing solution sorption and PEO crystallinity decreasing it. Nevertheless, the main effect seems to be PEO molecular weight which determines the variations in the degree of crystallinity and are correlated of the different morphology but more with the PEO dissolution and capacity for swelling [11].

PEO is a water soluble polymer and in this polymer blend, the uptake is governed by the confinement produced by P(VDF-TrFE) whose shape is only slightly changed by swelling since electrolyte absorption in pure P(VDF-TrFE) is quite modest.

The important parameter is the MacMullin number, N_M, that describes the relative contribution of a separator to cell resistance and is therefore related to the effective conduction process (chapter 2, equation8).

The MacMullin numbers, N_M, are listed in Table 6.2, showing a dependence on the amount and molecular weight of PEO. Independently of the molecular weight of PEO, the N_M decreases with increasing PEO content in the polymeric due to the increase of

ionic conductivity. N_M is correlated to the morphology, tortuosity value and the affinity between polymeric blend and electrolyte solution [12].

The complex impedance plots (Nyquist plot, i.e., imaginary impedance $Z^{''}$ against real impedance $Z^{'}$) for the P(VDF-TrFE)/PEO blend membranes with a PEO molecular weight of M_w=100 kDa without electrolyte solution are presented in Figure 6.4, the results corresponding to blends with PEO-10k are similar and are not shown.

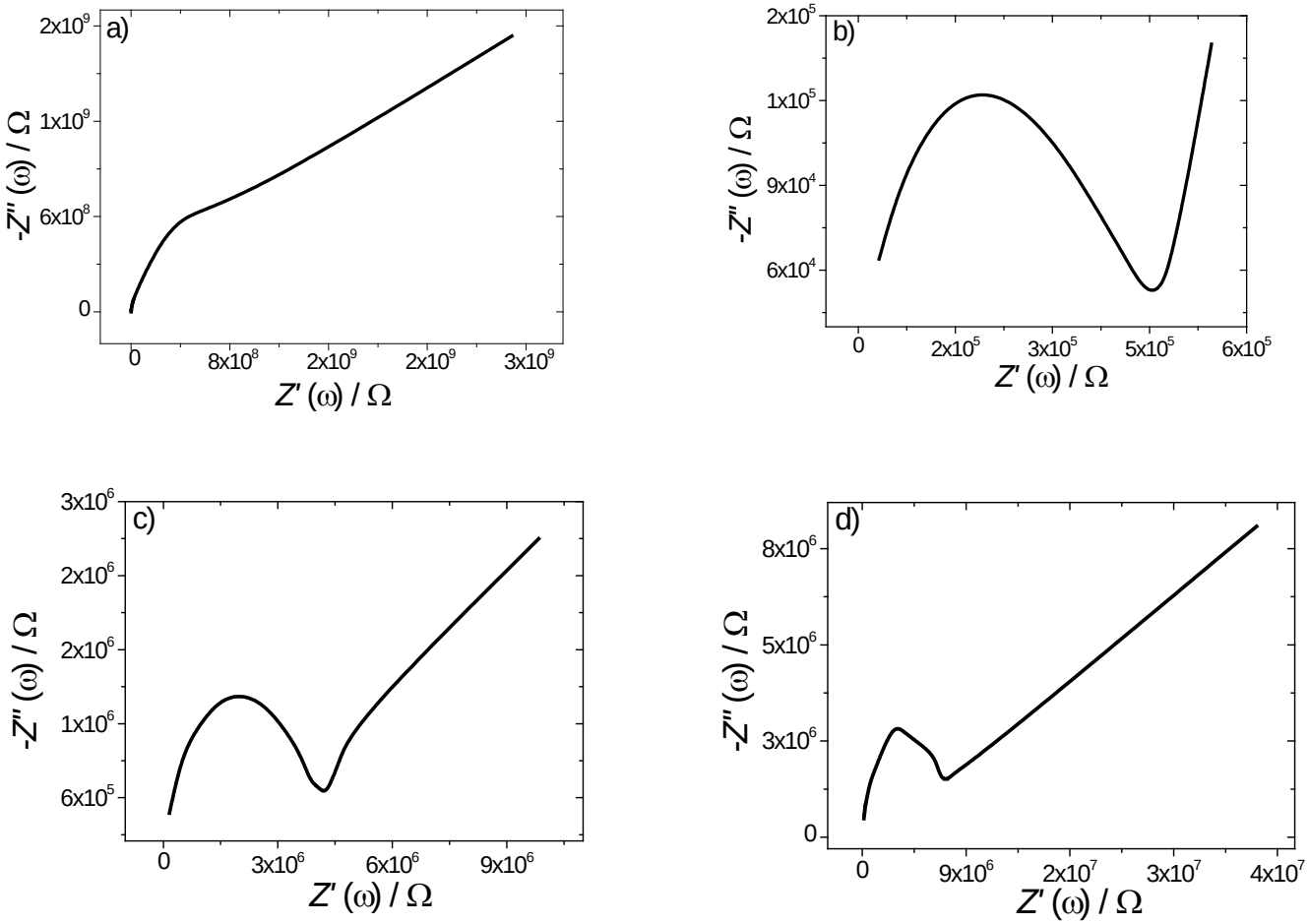

Figure 6.4 - Nyquist plot of PVDF-TrFE)/PEO-100k blends measured without electrolyte solution at room temperature for: a) 100/0, b) 80/20, c) 60/40 and d) 40/60 blends.

Three distinct regions can be identified in Nyquist plot: a semicircle located at the high-frequency range that corresponds to the charge transfer process, a straight line for the lowest frequencies that is related to the diffusion process and the transition between these processes as shown in Figure 6.4 [13]. The width of the semicircle in the charge transfer process represents the bulk resistance of the polymer blend and it decreases

with increasing PEO content in the P(VDF-TrFE)/PEO blend due to the higher *d.c.* conductivity contribution and the dipole-orientation relaxation process of PEO [14].

Figure 6.4 shows that PEO content influences the diffusion process at low frequency, the straight line in this frequency range increasing with increasing PEO content due to the migration of charges and the surface in-homogeneity of the electrodes [15]. The ionic conductivity at room temperature determined by equation 6 (chapter 2) from the data presented in Figure 6.4 is represented in Figure 6.6a as a function of PEO content for the two molecular weights showing that the ionic conductivity increases with increasing PEO content in the blend.

After electrolyte solution uptake, the Nyquist plots for P(VDF-TrFE)/PEO-100k blend membrane shows the disappearance of the semicircle in the Nyquist plots for the membranes with PEO due to the fact that the total conductivity is mainly the result of ion conduction [16] (Figure 6.5).

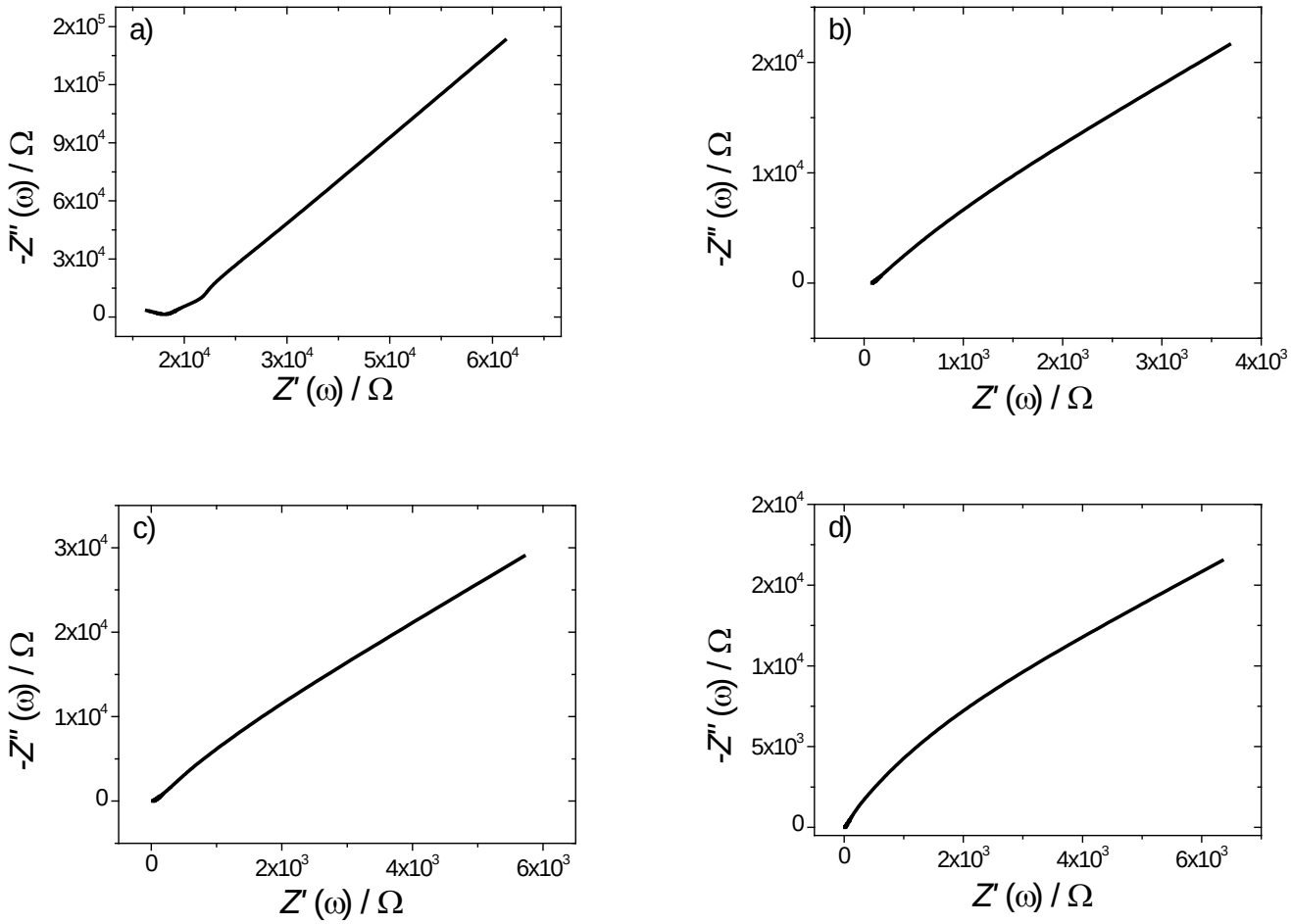

Figure 6.5 - Nyquist plot of P(VDF-TrFE)/PEO-100k membrane with electrolyte solution for: a) 100/0, b) 80/20, c) 60/40 and d) 40/60 blends.

The reason for this behavior is the diffusion of the polymer chain with ions coordinated and the liquid uptake of polymeric blend membrane that benefits the ions migration where result one low impedance. Ionic conductivity at room temperature was determined by equation 6 (chapter 2) and the data of Figures 6.4 and 6.5 without and with electrolyte solution, respectively (Figure 6.6). Ion transport in the blend membranes depends on PEO molecular weight for samples without and with electrolyte solution as shown in Figure 6.6.

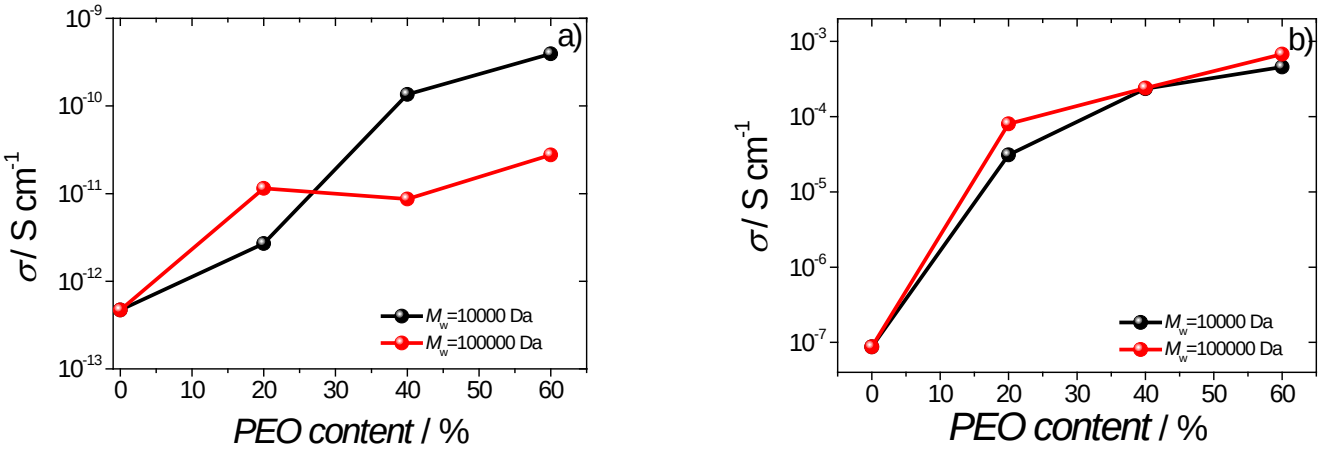

Figure 6.6 - Ionic conductivity as a function of PEO content for P(VDF-TrFE)/PEO blend without electrolyte (a) and with electrolyte solution uptake (b).

Figure 6.6a shows that PEO content increases ionic conductivity in three orders of magnitude independently of PEO molecular weight. Without electrolyte uptake, the conductivity is larger for the blend samples with higher PEO contents due to the dispersion of ill-crystallized PEO within the P(VDF-TrFE) matrix.

The electrolyte solution (Figure 6.6b) strongly influences the value of the ionic conductivity of the P(VDF-TrFE)/PEO blend membrane in comparison with Figure 6.6a resulted from the segmental motion of the chains surrounding salt ions, creating a liquid-like environmental around the ions and the presence of the lithium salts in the polymer blend [17].

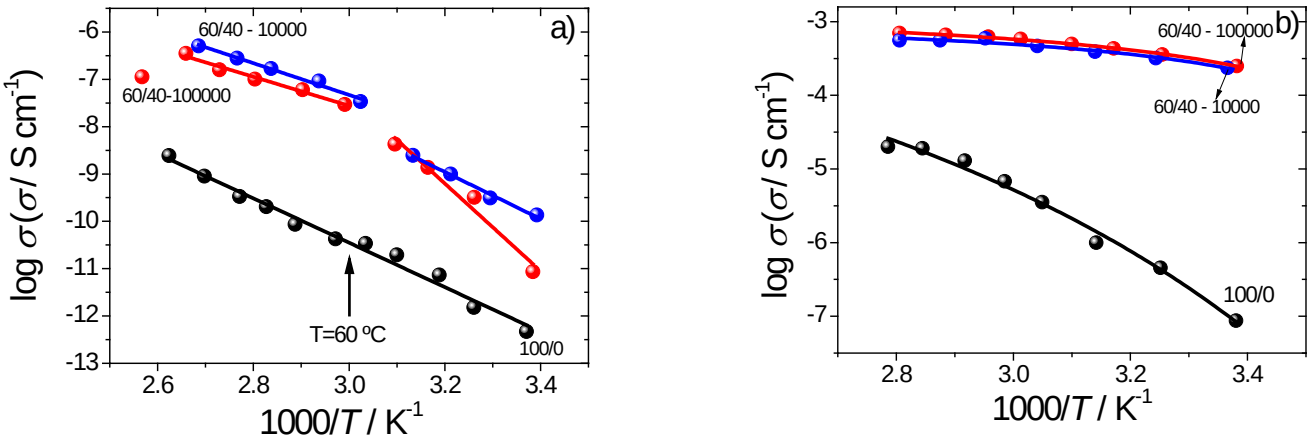

Figure 6.7 - Logarithm of conductivity, σ, as function of reciprocal temperature, 1000/T for P(VDF-TrFE)/PEO blend without electrolyte (a) and with electrolyte solution uptake (b) for both molecular weight.

Figure 6.7 shows the temperature dependence of the ionic conductivity for pristine polymer, P(VDF-TrFE) and the polymer blend membrane, 60/40 for both molecular weights without and with electrolyte solution. The behavior of the ionic conductivity as a function of the temperature for other polymer blends is very similar to that shown in Figure 6.7.

Increasing temperature increases free volume and polymers segmental mobility and charge mobility, increasing therefore ionic conductivity [18].

Around 60 ºC ($1/T$=0.003 K^{-1}) the conductivity versus reciprocal temperature plot show a clear change of slope due to melting of PEO crystals (Figure 6.7a), but interestingly enough at temperatures above melting the conductivity of the blends containing 40% or more PEO is still one order of magnitude lower than in the 80/20 blend independently of molecular weight of PEO. Above 60 ºC, the polymer blend membrane molten PEO mix in some extent with amorphous P(VDF-TrFE) chains producing a continuous conductive phase thus improving ion conductivity of the blend.

After electrolyte uptake (Figure 6.7 b) polymer blends exhibit high conductivity higher than 10^{-4} S cm^{-1} at room temperature for PEO contents above 20% and practically independent of blend composition, within experimental error. Ionic conductivity of the membrane depends strongly on the inclusion of PEO polymer in the P(VDF-TrFE)/PEO blends but not so much on the PEO content itself and its molecular weight.

Ionic conductivity of the blends after electrolyte solution uptake (figure 6.7b) increases in comparison to the samples without electrolyte solution (figure 6.7a) in three orders of magnitude as verified in Figure 6.6 at room temperature. This is due to the larger concentration of ionic charge carriers and their mobility [19]. Inclusion of PEO also increases thermal stability of the ionic conductivity of the samples with respect to the PVDF-TrFE (Figure 6.7) and again thermal stability is independent of the content and molecular weight of PEO.

Temperature dependence of electrical conductivity of blends without electrolyte solution can be fitted to Arrhenius equation (equation 1, chapter3)

Values of E_a, calculated for the temperature intervals below and above 60 ºC are listed in Table 6.3.

Table 6.3 – Activation Energy for the blend membranes without electrolyte solution

	Before 60 ºC	**After 60 ºC**
Sample	E_a **/ (eV)**	
100/0	0.93	
80/20, M_w=100 kDa	0.82	0.56
60/40, M_w=100 kDa	1.72	0.61
40/60, M_w=100 kDa	1.5	0.55
80/20, M_w=10 kDa	1.61	0.76
60/40, M_w=10 kDa	1.23	0.66
40/60, M_w=10 kDa	1.15	0.44

The activation energy above 60 ºC decreases with increasing PEO content due the transition between semi-crystalline region and completely amorphous region for PEO polymer. This fact is verified for the two molecular weights of PEO. Below 60 ºC, the activation energy is higher due of the semi-crystalline states for the two polymers present in the P(VDF-TrFE)/PEO blend membranes.

Temperature dependence of ionic conductivity in blends with electrolyte solution does not obey Arrhenius behavior. The curvature evident in Figure 6.7b is better described by Vogel-Tamman-Fulcher (VTF) equation [18, 20]:

$$\sigma(T) = AT^{-1/2} \exp\left(\frac{B}{R(T - T_0)}\right) \quad (1)$$

A is a parameter indicative of the number of charge carriers, B is related to the segmental motion of the polymer chains for ion transport and T_0 is a parameter correlated to the glass temperature, i.e, reference temperature at which the

configurational entropy of the polymer became zero. Equation 1 describes the coupling between lithium ions and polymer chains dynamics and properly describes the behavior of the electrolyte solution and the blends in the entire temperature range.

Table 6.4 represents the VTF parameters obtained from the fittings of the data of Figure 6.7 b for all polymeric blends membranes with electrolyte solution.

Table 6.4 – Fitting parameters obtained by VTF equation for all P(VDF-TrFE)/PEO membranes with electrolyte solution

Sample	A / S^{-1} cm^{-1} $K^{-1/2}$	B / (eV)	T_0 / (K)
100/0	5	0.19	182
80/20, M_w=100 kDa	4	0.007	256
60/40, M_w=100 kDa	3	0.008	249
40/60, M_w=100 kDa	2	0.012	230
80/20, M_w=10 kDa	6	0.005	263
60/40, M_w=10 kDa	4	0.007	251
40/60, M_w=10 kDa	4	0.0008	265

It is evident a low value of B which is close to those of the liquid electrolyte solution independently of amount and molecular weight of PEO and is indicative of an easy ion transport in the P(VDF-TrFE)/PEO blend. The differences in the A and B parameters for all polymer blends membranes is related with microstructure, porosity and uptake values. The variations of the pre-exponencial factor A, related to the number of effective charge carriers are independents of the molecular weight of PEO but decrease with increasing of the PEO content in the polymer blend membrane.

In the B parameter of Table 6.4 is verified that the electrolyte solution improves the mobility and ionic charge carriers present in the all polymeric blends membranes [21]. As verified without electrolyte solution, the mobility of ionic charge carriers depends of PEO presence but not depend of content and molecular weight of PEO.

The differences observed for the T_0 in all polymeric blend membranes are related of the variations of the amorphous phase content of the each polymer and its miscibility. The magnitude of T_0 decreased with increasing of PEO amount and suggested enhanced segmental motion of the polymer chain except for 60% weight ratio of PEO with M_w=10 kDa. This fact is independent of the molecular weight of PEO.

The working voltage range, i.e., electrochemical windows for polymer electrolytes is a critical parameter from their applications in battery and electrochromic devices. The electrochemical stability (voltammograms) of the polymeric blend membranes and the

diffusion coefficients (equation 9, chapter 2) were determined through cyclic voltammetry over the potential range -2.0 V to 8.0 V (figure 6.8).

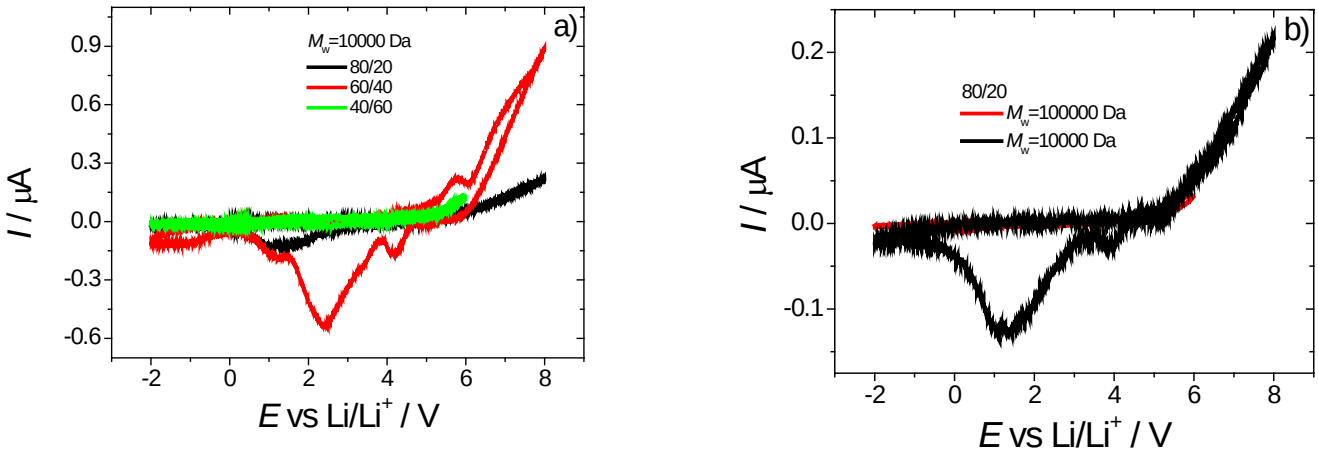

Figure 6.8 - a) Voltammogram of P(VDF-TrFE)/PEO for M_w=10 kDa for all polymer blends membranes at 1 V/s and b) Voltammogram of P(VDF-TrFE)/PEO for 80/20 with two molecular weights of PEO (M_w=10 kDa and M_w=100 kDa) at 1V/s.

The both cathodic and anodic current peaks are present in the voltammograms of Li cells as illustrated in Figure 6.8.

The voltammogram of the polymer blend membranes with M_w=10 kDa at room temperature is represented in Figure 6.8 a). The voltammogram is independent of the scanning rate. This membrane exhibits good electrochemical stability with anodic potentials higher than 5.0 V versus Li/Li^+ and oxidation peak around at 2.0 V. The anodic current onset may be associated with the decomposition of the polymer electrolyte and the excellent affinity to the carbonate based liquid electrolyte solution which can partially swell the polymers. The anodic current depends on the PEO content as shown in Figure 6.8a due of the interaction between PEO polymer and lithium ions. Increasing potential sweeping rate shifts the cathodic peak potential in the negative direction. Figure 6.8a shows a small peak around 2.0 V in the electrolytes films which has been previously ascribed to reduction of low level of water presented in PEO or oxygen impurities [22]. The cathodic and anodic peak potentials are separated, which may be expected for a two electron-transfer reaction.

An anodic potential higher than 5 V was found for same scanning rate (1 V/s) and PEO content (20%) for both PEO molecular weights. The oxidation peak around of 1 V demonstrated that electrochemical stability depends of the molecular weight of PEO. The variations observed in the voltammogram (Figure 6.8b) of P(VDF-TrFE)/PEO blend membranes are related to the porosity and the tortuosity value present in the membranes. From these data, the diffusion coefficients of the polymer blend membranes, calculated by equation 9 (chapter 2), are in the order of 2×10^{-5} cm^2 s^{-1} for 80/20 with M_w=10 kDa and 3×10^{-5} cm^2 s^{-1} for same composition but with different molecular weight of PEO. The diffusion coefficient depends on PEO content and its value is between 2×10^{-5} cm^2 s^{-1} at 1×10^{-4} cm^2 s^{-1} for PEO contents of 20% for 60% wt.

6.3. Conclusions

Polymer blends based on poly(vinylidene fluoride-trifluoroethylene)/poly(ethylene oxide) have been developed and investigated as a function of amount and molecular weight of PEO for Li-ion battery separator applications. The polymer blend membranes were prepared by solvent casting at 70 ºC due that this temperature is higher than the melting point of PEO. At this evaporation temperature, P(VDF-TrFE) crystallizes from the solution and the melted PEO is confined by P(VDF-TrFE) semicrystalline phase. The microstructure is dependent of the phase separation between P(VDF-TrFE) and PEO that produces interconnected micropores. The IR vibration modes characteristic of P(VDF-TrFE) are not influenced by the presence of PEO in the polymer blend. The capacity of the blend film to absorb the lithium salt solution is highly dependent on film porosity, PEO crystallinity and confinement. The mechanical and electrical properties are dependent of the amount and molecular weight of PEO and correlates with the degree of crystalinity. Without electrolyte solution the charge transfer process is dominant and follows the Arrhenius behavior. Electrical properties of the polymer blend membranes with electrolyte solution are dominated by diffusion and the ionic conductivity as a function of temperature and follows the VTF behavior. Ionic conductivity has a maximum in the membrane containing 60% PEO for M_w=100 kDa, reaching a value of 0.7 mS cm^{-1} at room temperature. Blend membranes with absorbed electrolyte show low dependence of conductivity with temperature, i.e., a high thermal stability. The molecular weight affects working voltage range determined by cyclic voltammetry. The result of cyclic voltammetry confirms that the polymeric blends also have adequate electrochemical stability for lithium-ion battery applications.

6.4. References

1. Costa, C.M., et al., *Composition-dependent physical properties of poly[(vinylidene fluoride)-co-trifluoroethylene]–poly(ethylene oxide) blends.* Journal of Materials Science, 2013. 48(9): p. 3494-3504.
2. Costa, C.M., et al., *Novel poly(vinylidene fluoride-trifluoroethylene)/poly(ethylene oxide) blends for battery separators in lithium-ion applications.* Electrochimica Acta, 2013. 88(0): p. 473-476.
3. Saikia, D. and A. Kumar, *Ionic transport in P(VDF-HFP)–PMMA–LiCF3SO3–(PC+DEC)–SiO2 composite gel polymer electrolyte.* European Polymer Journal, 2005. 41(3): p. 563-568.
4. California, A., et al., *Tailoring porous structure of ferroelectric poly(vinylidene fluoride-trifluoroethylene) by controlling solvent/polymer ratio and solvent evaporation rate.* European Polymer Journal, 2011. 47(12): p. 2442-2450.
5. Wilhelm, P., *Modern Polymer Spectroscopy*2009: Wiley.
6. Afifi-Effat, A.M. and J.N. Hay, *Enthalpy and entropy of fusion and the equilibrium melting point of polyethylene oxide.* Journal of the Chemical Society, Faraday Transactions 2: Molecular and Chemical Physics, 1972. 68: p. 656-661.
7. Li, W., et al., *Crystalline morphologies of P(VDF-TrFE) (70/30) copolymer films above melting point.* Applied Surface Science, 2008. 254(22): p. 7321-7325.
8. Cai, J., et al., *Effects of molecular weight on poly(ω-pentadecalactone) mechanical and thermal properties.* Polymer, 2010. 51(5): p. 1088-1099.
9. Ward, I.M. and J. Sweeney, *An Introduction to the Mechanical Properties of Solid Polymers*2005: Wiley.
10. Flory, P.J. and D.Y. Yoon, *Molecular morphology in semicrystalline polymers.* Nature, 1978. 272(5650): p. 226-229.
11. Appetecchi, G.B., Y. Aihara, and B. Scrosati, *Investigation of swelling phenomena in PEO-based polymer electrolytes: II. Chemical and electrochemical characterization.* Solid State Ionics, 2004. 170(1–2): p. 63-72.
12. Djian, D., et al., *Macroporous poly(vinylidene fluoride) membrane as a separator for lithium-ion batteries with high charge rate capacity.* Journal of Power Sources, 2009. 187(2): p. 575-580.

13. Chang, B.-Y. and S.-M. Park, *Electrochemical Impedance Spectroscopy.* Annual Review of Analytical Chemistry, 2010. 3(1): p. 207-229.
14. Money, B.K., K. Hariharan, and J. Swenson, *Glass Transition and Relaxation Processes of Nanocomposite Polymer Electrolytes.* The Journal of Physical Chemistry B, 2012.
15. Marcinek, M., et al., *Effect of Filler Surface Group on Ionic Interactions in PEG−LiClO4−Al2O3 Composite Polyether Electrolytes.* The Journal of Physical Chemistry B, 2000. 104(47): p. 11088-11093.
16. Jacob, M.M.E., S.R.S. Prabaharan, and S. Radhakrishna, *Effect of PEO addition on the electrolytic and thermal properties of PVDF-LiClO4 polymer electrolytes.* Solid State Ionics, 1997. 104(3–4): p. 267-276.
17. Teran, A.A., et al., *Effect of molecular weight on conductivity of polymer electrolytes.* Solid State Ionics, 2011. 203(1): p. 18-21.
18. Gray, F.M., *Solid Polymer Electrolytes: Fundamentals and Technological Applications*1991: John Wiley & Sons.
19. Ren, T., et al., *Synthesis and characterization of novel crosslinked polyurethane–acrylate electrolyte.* Journal of Applied Polymer Science, 2003. 89(2): p. 340-348.
20. Croce, F., et al., *A safe, high-rate and high-energy polymer lithium-ion battery based on gelled membranes prepared by electrospinning.* Energy & Environmental Science, 2011. 4(3): p. 921-927.
21. Every, H.A., et al., *Lithium ion mobility in poly(vinyl alcohol) based polymer electrolytes as determined by 7Li NMR spectroscopy.* Electrochimica Acta, 1998. 43(10–11): p. 1465-1469.
22. Aurbach, D., et al., *The electrochemistry of noble metal electrodes in aprotic organic solvents containing lithium salts.* Journal of Electroanalytical Chemistry and Interfacial Electrochemistry, 1991. 297(1): p. 225-244.

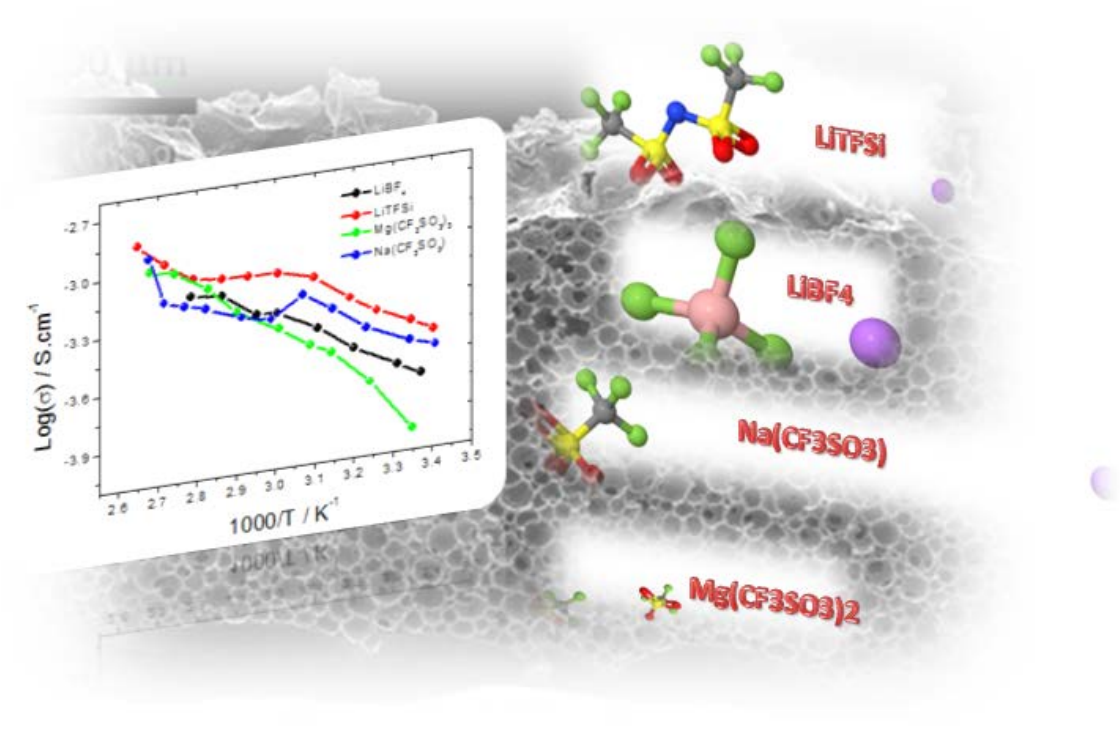

7. *Effect of different salts in the electrolyte solution of P(VDF-TrFE) battery separator membranes*

This chapter describes the effect of different salts in the electrolyte solution of P(VDF-TrFE) membranes. Poly(vinylidene fluoride-co-trifluoroethylene), P(VDF-TrFE) solid polymer electrolytes were prepared using porous membranes soaked in lithium tetrafluoroborate ($LiBF_4$), lithium bis(trifluoromethanesulfonyl)imide (LiTFSI), magnesium triflate ($Mg(CF_3SO_3)_2$) and sodium triflate ($Na(CF_3SO_3)$) electrolyte solutions. The polymer electrolytes based on P(VDF-TrFE) porous membranes show adequate properties for lithium, magnesium and sodium-ion batteries.

This chapter is based on the following publication:

"Approach of different salts in electrolyte solution of poly(vinylidene fluoride-co-trifluoroethylene) battery separator membranes for batteries applications", C. M. Costa, R. Leones, M. M. Silva, S. Lanceros-Méndez, submitted

7.1. Samples

P(VDF-TrFE) porous membrane soaked in different electrolyte (1 M solution of $LiBF_4$, LiTFSi, $Mg(CF_3SO_3)_2$ and $Na(CF_3SO_3)$ in PC) solution will be called hereafter by the salt name: $LiBF_4$, LiTFSi, $Mg(CF_3SO_3)_2$ and $Na(CF_3SO_3)$.

7.2. Results and discussion

7.2.1. Morphology, uptake, polymer phase and molecular interactions

The porous microstructure morphology of the membranes is illustrated through the SEM images shown in figure 7.1a (surface) and 7.1b (cross-section).

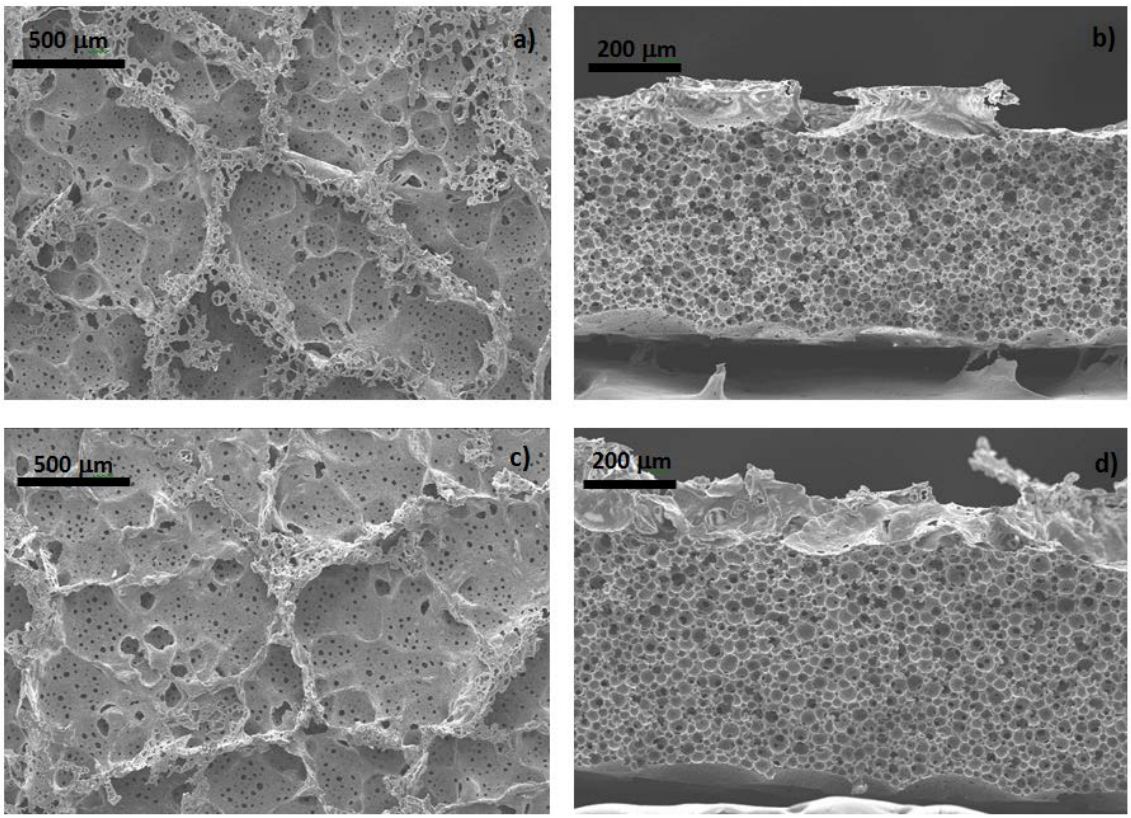

Figure 7.1 – SEM images showing the microstructure of the P(VDF–TrFE) membranes prepared by solvent evaporation at room temperature a) surface; b) cross section of the samples before electrolyte uptake. c) Surface and d) cross section of the samples after 1M LiTFSI in PC electrolyte uptake.

The porous microstructure is characteristics of the P(VDF-TrFE)/DMF systems when samples are prepared from room temperature solvent evaporation [1, 2] and depends on

the specific place of the polymer/solvent phase diagram in which the isothermal crystallization begins [2]. The cross-section images (figure 7.1 b) reveal a homogeneous pore distribution with average pore size of 9±3 μm.

The addition of the electrolyte solution does not affect the porous microstructure of the samples as shown in figures 7.1 c) and d) after 1M LiTFSI in PC electrolyte uptake. This fact is verified for all other electrolyte solutions studied in this work.

SEM images containing electrolyte solution (figure 7.1c) and d)) do not show phase separation of the electrolyte solution and membrane indicating the good compatibilization between polymer and organic solvent.

Comparing the cross-section images (figure 7.1 b, without electrolyte solution and figure 1 d, 1M LiTFSI in PC) is observed the increase of the thickness of the membrane with electrolyte solution due of the uptake effect illustrated in the figure 7.2a). The increase of the thickness of the membrane is verified in all electrolyte solution used in this work. This fact is independently of the different ions type and organic solvent.

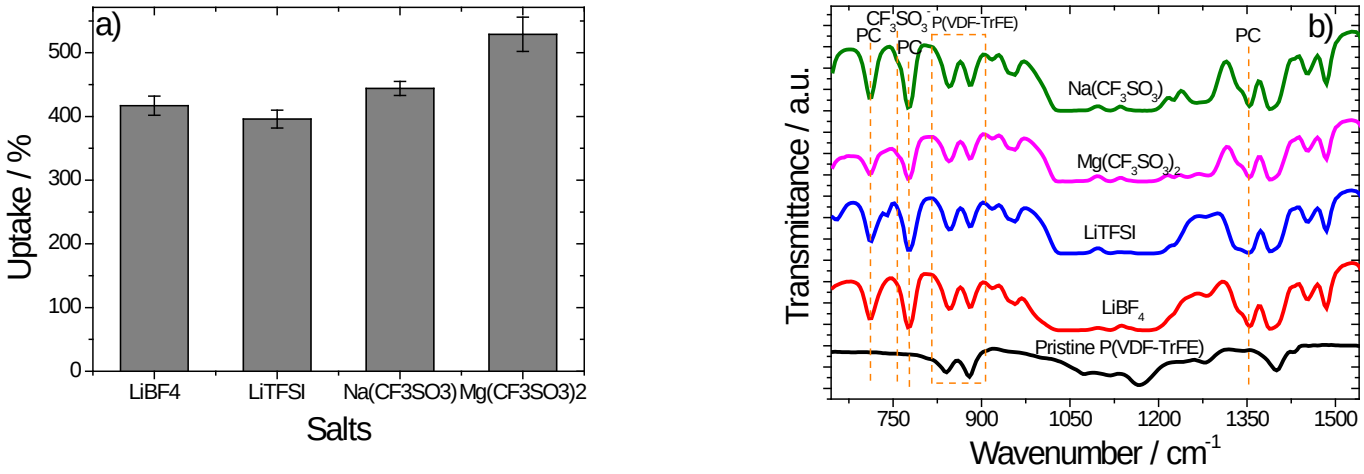

Figure 7.2 –a) Uptake value of the P(VDF–TrFE) immersed in the different electrolyte solution and b) Infrared spectroscopy after uptake of the different electrolyte solution.

Figure 7.2 a) shows the uptake for the membrane immersed in the different electrolyte solution. The uptake value ranged from 396% for the LiTFSI salt to 529% for the $Mg(CF_3SO_3)_2$ depending basically on salt type as the degree of porosity is the same in all samples.

The degree of porosity of the membrane is 72% [3], leading to a high degree of uptake independently of the electrolyte solution. The differences observed between the uptake values can explain by the interaction between the polymer and the electrolyte solution and also by the different viscosity of the electrolyte solution.

The information/investigation of the characteristics bands of the polymer, ion-solvating ability and interaction between ions of polymer is provided by infrared spectroscopy as shown in figure 7.2 b).

Figure 7.2b) shows the vibration modes at 851 cm^{-1}, 886 cm^{-1} and 1402 cm^{-1}, characteristic of the P(VDF-TrFE) polymer in the all-trans conformation and indicates that the presence of the different electrolyte solutions do not affect the crystalline phase of the polymer [3].

Also is observed in the FTIR spectra (figure 7.2b) of the membranes with electrolyte solution the existence of the two strong bands at 712 cm^{-1} and 777 cm^{-1} that is related to the presence of propylene carbonate (PC) in the samples.

The vibration spectrum of the electrolyte solution with $LiBF_4$ salt doesn't show the vibration mode of free BF_4^- anions, the band corresponding to the ion pairs of BF_4^- appearing at 770 cm^{-1} in which confirms the existence of ion pairs in this salt [4].

It is detected at 768 cm^{-1}, one vibration band that is attributed to the free triflate anion ($CF_3SO_3^-$) in the vibration spectrum of the following salts: $Mg(CF_3SO_3)_2$, $Na(CF_3SO_3)$. LiTFSI salt do not has the $CF_3SO_3^-$ anion as show the structure in the table1, but its vibration modes ($CF_3SO_2^-$) are very similar to free triflate anion.

The vibration region that indicates the salts content of the ($CF_3SO_3^-$) triflate anion is between 1020 cm^{-1} and 1080 cm^{-1}, characteristic of the symmetric stretching modes of SO_3 in trifluoromethanesulfonate anion as is represented in the figure 7.3. The attribution of the vibration bands of the respective salts in this region is listed in the table 7.1. In figure 7.3, the solid line is the absorption profile for each salt and the dashed lines represent the deconvoluted spectra.

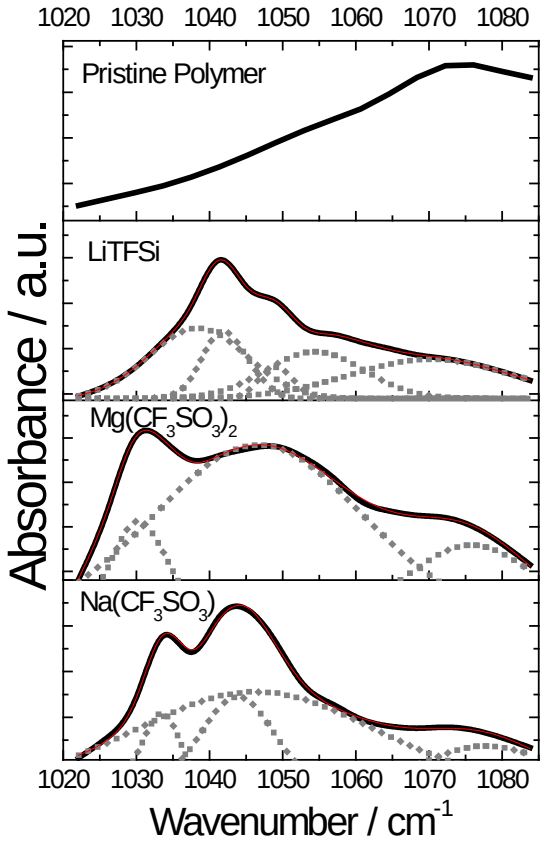

Figure 7.3 –FTIR spectrum and the curve-fitting results of the LiTFSi, $Mg(CF_3SO_3)_2$, $Na(CF_3SO_3)$ salts.

This region is divided in three parts corresponding to free triflate anions (1030-1034 cm^{-1}), ion-paired triflates (1040-1045cm^{-1}) and highly aggregated triflates (1049-1063 cm^{-1}) [5].

Figure 7.3 and table 7.1 show that the ion solvation ability of the polymer depends on the different cations (Li^+, Na^+ and $Mg2^+$) and anions ($CF_3SO_2^-$ and $CF_3SO_3^-$).

Table 7.1 - Characteristics vibration bands of the different salts in the ν_s SO_3 spectral region [6, 7].

LiTFSi	$Mg(CF_3SO_3)_2$	$Na(CF_3SO_3)$	Attribution
1038	1030	1032	ν_s SO_3 free region
1042	--------	1043	$Na^+(CF_3SO_3^-)$ /$Li^+(CF_3SO_3^-)$ and Na $(CF_3SO_3^-)_2$ /Li $(CF_3SO_3^-)_2$
1049	1046	1046	(Li^+ CF_3SO_3/Na^+ CF_3SO_3/$Mg^{2+}CF_3SO_3$
1054	--------	--------	$[Li_2(CF_3SO_3)]^+$
1070	1075	1077	---------

Taking account figure 7.3 for the same anion ($CF_3SO_3^-$) and different cations (Na^+ and Mg^{2+}), the position of the vibration peaks is the same but the intensity and the shape of these peaks is slightly different. The width is large for the Mg^{2+} cation in comparison to the Na^+ cation, related to a larger number of bonds.

Independently of the salts type (figure 3), it is identified two vibration peaks around 1035 cm^{-1} and 1046 cm^{-1} that represent the presence of free and highly aggregated triflates, respectively. In these salts, the contribution of "cross-link separated ion pairs" cannot be discarded as shown in the figure 7.3 [6].

The band at 1043 cm^{-1} is attributed of monodentate Na^+ ($CF_3SO_3^-$) /Li^+($CF_3SO_3^-$) ions pairs and negatively charged triplets $Na(CF_3SO_3^-)_2$ / $Li(CF_3SO_3^-)_2$ [6, 7].

The vibration band around 1075 cm^{-1} , present in all triflate salts, is related to higher ionic aggregates possibly associated to P(VDF-TrFE)/LiTFSi, P(VDF-TrFE)/$Mg(CF_3SO_3)_2$ and P(VDF-TrFE)/$Na(CF_3SO_3)$ crystalline complex in the samples [8].

7.2.2. Thermal and mechanical properties

The thermal and mechanical stability of the battery separator is very important for its performance. The thermal and mechanical properties were evaluated through DSC (figure 7.4) and stress-strain (figure 7.5) measurements, respectively as a function of the different electrolyte solutions.

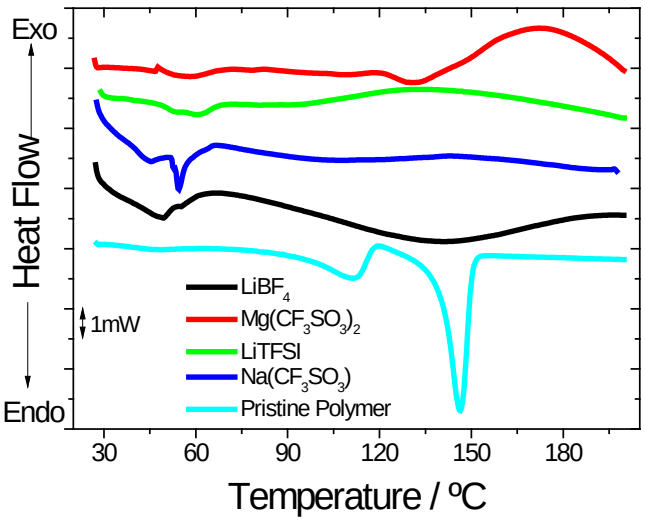

Figure 7.4 –DSC thermographs of the membrane immersed in the different electrolyte solution.

The DSC thermograms for the samples immersed in the different electrolyte solutions and the pristine P(VDF-TrFE) are shown in figure 7.4. The DSC thermograph of the pristine polymer shows the presence of two endothermic peaks, one representing the ferroelectric-paraelectric phase transition, T_{FP} ~112ºC, and the other representing the melting temperature of the polymer matrix, T_m ~146ºC.

The DSC thermographs of the membranes soaked in different electrolyte solutions do not show the two endothermic peaks characteristics of the P(VDF-TrFE) polymer as displayed of the figure 7.4. In turn, for all electrolyte solution one small endothermic peak is detected around 50ºC-60ºC, the intensity of the peak depending on the salt type present in the electrolyte solution. This peak is associated to the dynamic of the amorphous phase of the P(VDF-TrFE) in the present of the different salts [3, 9].

In PVDF-TrFEnLiClO43H2O composites, the degree of crystallinity of the samples decreases with increasing lithium ion content due to a more defective structural packing of the macromolecular chains [10].

The fact that the melting peak of the polymer is not observed in the thermographs of the membranes immersed in the electrolyte solution is due of the evaporation of the PC (TGA result) [3], which involve larger energies than any other effect at that temperature region.

The mechanical properties of the battery separator depend of the morphology and geometry of the membranes [11].

The stress-strain curves of the different samples are represented in figure 7.5 and table 7.2 shows the elastic modulus and yielding stress.

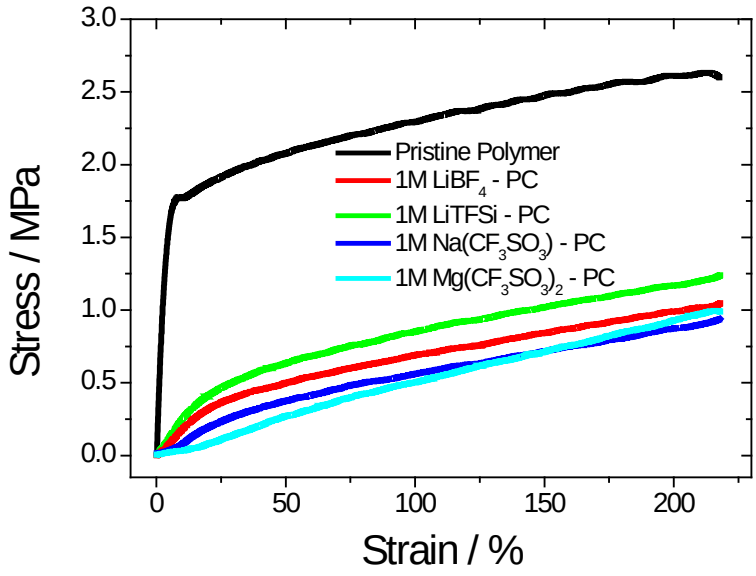

Figure 7.5 –Stress-strain curves of the membrane immersed in the different electrolyte solution and the pure polymer

All stress-strain curves (figure 7.5) show the characteristic thermoplastic behavior of the pristine polymer independently of being immersed in the different electrolytes.

Independently of electrolyte solution, the mechanical properties of the membranes soaked in the electrolyte solution decrease in comparison with the pristine polymer.

Table 7.2- Mechanical properties of the pristine polymer and the polymer oaked in the different salts.

Sample	Pristine polymer	$LiBF_4$	LiTFSI	$Na(CF_3SO_3)$	$Mg(CF_3SO_3)_2$
Yielding stress (MPa)	2.1	0.37	0.50	0.22	0.10
Elastic Modulus (MPa)	40	1.90	2.40	1.14	0.60

Table 7.2 shows that the mechanical properties (yielding stress and elastic modulus) for the samples with electrolyte solution decrease in the following order of LiTFSI > $LiBF_4$ > $Na(CF_3SO_3)$ > $Mg(CF_3SO_3)_2$. This observation follows the same behavior of the uptake value (figure 7.2a), i.e, can be concluded that there is a correlation between uptake value and mechanical properties. The mechanical properties of the P(VDF-TrFE) decreases with increase of the uptake value.

7.2.3. Electrical properties

Table 7.3 shows the room temperature effective conductivity, the tortuosity value and the MacMullin number (N_M) calculated by equation 6, 7 and 8 (chapter 2) respectively.

Table 7.3 - Room temperature effective conductivity, tortuosity value and MacMullin number (N_M) of the separator membranes soaked in the different electrolytes.

Sample	σ_o (mS/cm)	σ_{eff} (mS/cm)	τ	N_m
$LiBF_4$	4.5	0.19	4.1	23
LiTFSI	6.5	0.32	3.8	20
$Na(CF_3SO_3)$	4.1	0.27	3.3	15
$Mg(CF_3SO_3)_2$	1.6	0.102	3.4	16

The effective conductivity of the membrane soaked in the different salts show a high ionic conductivity independently of the salts.

The tortuosity value describes the average pore connectivity of a solid, which is related with the ionic transport and provides information about pore blockage. A tortuosity value of 1 describes an ideal porous body with cylindrical and parallel pores. The value of tortuosity of the membranes is between 4.1 at 3.1 and reveals that a major contribution for the conduction process is the swollen phase. With respect to $Na(CF_3SO_3)$ salts it is observed a low tortuosity value and supports better pore connectivity [12] due of the affinity between salt and polymer. It is also observed that the MacMullin number is dependent on the salt type and is correlated to the tortuosity value and the affinity between membrane and electrolyte solution [13]. The lowest value of the MacMullin number obtained for these membranes was for the electrolyte solution containing $Na(CF_3SO_3)$ salt in its constitution, the Na^+ cation showing the higher ionic radius (0.102nm) in comparison of the other cations presents in the different salts. The room temperature, ionic conductivity (table 7.3) is very similar to the values founds in the literature for other developed separators, as for example, σ_i = 0.7mS/cm for PMMA in EC-DMC-$LiN(SO_2CF_3)_2$ [14].

The Nyquist plot, i.e., imaginary impedance Z'' against real impedance Z' and Bode diagrams for all membranes with the different electrolyte solutions were determined between 25ºC and 100ºC. The Nyquist plots at 50ºC is represented in figure 7.6 a) for all membranes immersed in the electrolyte solution.

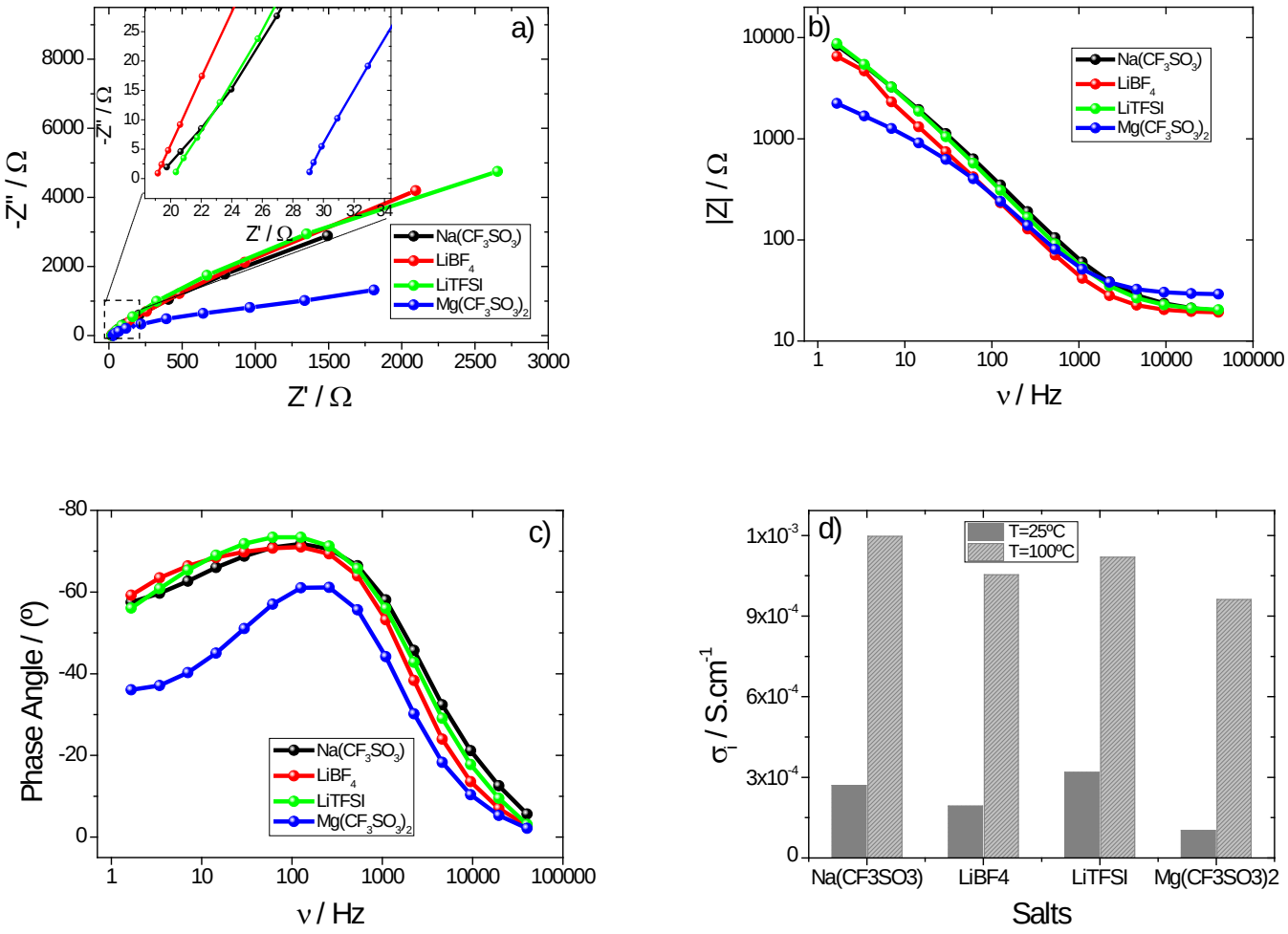

Figure 7.6 - a) Nyquist plots of the membrane soaked in different electrolyte solution at 50 ºC, b-c) Bode diagram of the membranes soaked in different electrolyte solution at 50 ºC and d) ionic conductivity of the membranes soaked in the different salt at 25ºC and 100ºC.

It is observed a partial small semicircle at high frequencies for all electrolyte solutions. The insert of figure 7.6 a) represents the ionic conductivity at low frequencies and shows an inclined straight-line, typical of the blocking electrode capacitive behavior [15], which depends on the anion size of the salts presents in the electrolyte solution. The ionic conductivity shown in figure 7.6 a) increases with decreasing anion size and follows of the following order: $BF_4^- < CF_3SO_3^- < (CF_3SO_2)_2N^-$ [16].

The anions are counter ions of strong acids and the difference observed in the ionic conductivity is presumably due to the difference in lattice energies [17].

For the same anion ($CF_3SO_3^-$), the ionic conductivity depends on the cation type, increasing with increasing ion radius ($Na^+ > Mg^{2+}$).

In relation for the same cation (Li^+) and different anion radius (BF_4^- and $CF_3SO_2)_2N^-$), the dissociation of lithium salts depend on their size, the ionic conductivity increasing with increasing anion radius.

Figures 7.6 b) and c) show Bode diagram (impedance modulus and phase angle as a function of frequency, respectively) for all electrolyte solution at 50ºC. The impedance modulus (figure 7.6 b) decreases with increasing the frequency, being the decrease more marked for the lower frequencies up to 1 kHz. This behavior is independent of the electrolyte solution and is ruled by the restricted dynamics of ion mobility within the porous membranes.

Figure 7.6 c) shows the phase angle as a function of the frequency and is detected that the maximum phase angle occurs at 70º except of the electrolyte solution containing $Mg(CF_3SO_3)_2$ salt. For this salt, the maximum phase angle is around 60º, and corresponds to the cation (Mg^{2+}) with the lowest ion radius (0.072nm) in comparison with the other cations (Li^+ and Na^+). Independently of the electrolyte solution, the maximum of the phase angle is lower than 90º, the behavior being therefore better represented by a constant phase element (CPE) [18].

The effect of temperature in the ionic conductivity of the membranes is reported in figure 7.6d) and figure 7.9. The ionic conductivity of the membrane with different electrolyte solutions increases with increasing temperature due to increased mobility of the ionic charge carriers [3]. This behavior is observed in all electrolyte solution (figure 7.6d). For example, in the $LiBF_4$ salt, the ionic conductivity increases from 0.2 to 1 mS/cm when the temperature is increased from room temperature to 100ºC. The most commonly equivalent electric circuit that describes the electrical behavior observed in this work, as shown in figures 7.7 and 7.8, is the Randles circuit [19]. This circuit can be used to describe electrode processes when both kinetics and diffusion processes are present.

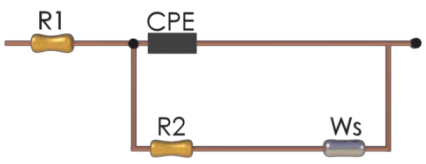

Figure 7.7 - Illustration of Randles circuit

The Randles circuit, takes into account the resistance to ionic migration current in the aqueous bulk solution by the solution resistance (R_1), the double-layer capacitance, i.e, the charges of the ions localized at the electrode interface (CPE) here a parameter *n* is used in order to accommodate the nonideal behavior, showing *n* a value of zero for pure resistive behavior and the value of one for capacitive behavior, and the Faraday impedance, i.e., charge-transfer resistance (R_2) in parallel to Warburg impedance (Z_w) [20] (Figure 7.7). The charge transfer resistance (R_2) in parallel to the Warburg impedance (Z_w) reflects the influence of the mass transport of electroactive species on the total impedance of the electrochemical cell [21].

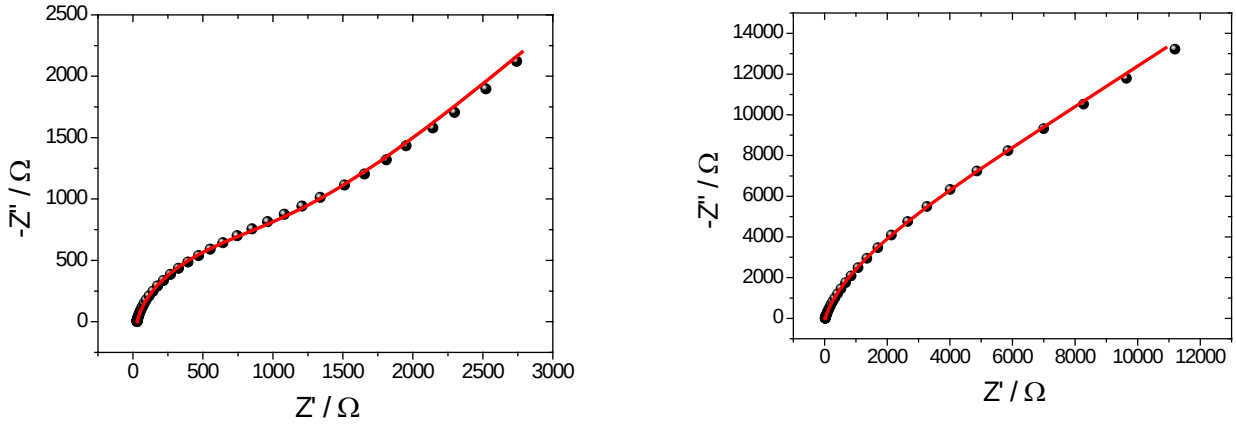

Figure 7.8 – Schematic representation of the equivalent circuit model used for the P(VDF-TrFE) membrane soaked in $Mg(CF_3SO_3)_2$ and LiTFSi at 50ºC.

The red solid lines in figure 7.8 indicates the good agreement between the experimental data and the results obtained by fitting the equivalent circuit to the experimental results obtained at 50ºC for the membranes soaked with $Mg(CF_3SO_3)_2$ and LiTFSi. Similar results are obtained for the other salts.

Table 7.4 shows the parameters obtained by the fitting with the equivalent circuit for all P(VDF-TrFE) membranes immersed in the electrolyte solution.

Table 7.4 - Parameters obtained by fitting the experimental values at 50 ºC to the equivalent circuit represented in figure 7.8.

	Samples			
Parameter	**$Na(CF_3SO_3)$**	**$LiBF_4$**	**LiTFSI**	**$Mg(CF_3SO_3)_2$**
$R_1(\Omega)$	20	19	20	29
$R_2(\Omega)$	4439	11049	8453	1056
$Z_w(\Omega.s^{-0.5})$	31397	18762	24832	3811
$CPE(F)$	$9.2x10^{-6}$	$1.5x10^{-5}$	$9.3x10^{-6}$	$1.2x10^{-5}$
n	0.86	0.86	0.88	0.87

The parameter n shows a high value close to 1 for all membranes, indicating a mainly capacitive behavior independent of the salts present in the electrolyte solution.

Analyzing the R_1 value, it is observed a low value around 20 Ω due of the low resistance to ionic migration current in the aqueous bulk solution for the different salts.

The charge-transfer resistance, R_2, is proportional of the uptake value, i.e, decreases with increasing uptake and follows this order: $Mg(CF_3SO_3)_2$ < $Na(CF_3SO_3)$ < LiTFSI < $LiBF_4$.

It is observed that the Warburg impedance (Z_w) and the capacitance (CPE) depend on the ion size as verified in table 4. Both parameters decrease with decreasing cation size present in the salt: Mg^{2+} (0.072nm) < Li^+ (0.076nm) < Na^+ (0.102nm).

The temperature dependence of the ionic conductivity calculated from equation 6 (chapter 2) for the different membranes is shown in figure 7.9.

Figure 7.9 shows that the ionic conductivity increases with increasing temperature due to the increase of the free volume and segmental mobility of the polymer with increasing temperature [22] and the larger concentration of ionic charge carriers and their mobility [3].

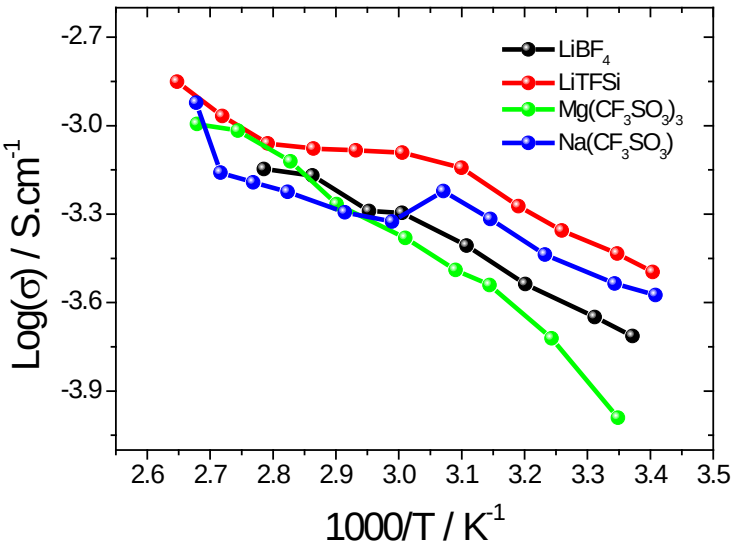

Figure 7.9 - Log σ as a function of 1000/T for the different membranes.

These both effects are observed for all electrolyte solutions.

Figure 7.9 also shows that ionic conductivity as a function of temperature does not obey the Arrehenius behavior and it is evident a slight curvature better described by the Vogel-Tamman-Fulcher (VTF) equation (equation 1, chapter 6).

Table 7.5 represents the VFT parameters obtained from the fittings of the data of figure 7.9 for the different membranes with the electrolyte solution.

Table 7.5 – Fitting parameters obtained by VFT equation for membranes with the different electrolyte solution.

Sample	Ea / eV	T_0 / K
$LiBF_4$	0.015	190
LiTFSI	0.007	216
$Na(CF_3SO_3)$	0.002	256
$Mg(CF_3SO_3)_2$	0.030	165

The value obtained for T_0 (table 7.5) depends on the different salts present in the electrolyte solution, i.e, depend on the interactions with polymer chain. Independently of the electrolyte solution, the value for the activation energy is low due to the high number and mobility of the ionic charge carriers present in the membranes soaked in the electrolyte solution.

The electrochemical window of the membranes soaked in the electrolyte solutions was determined by cyclic voltammetry over the potential range -2.0V to 6.0 V (figure 7.10).

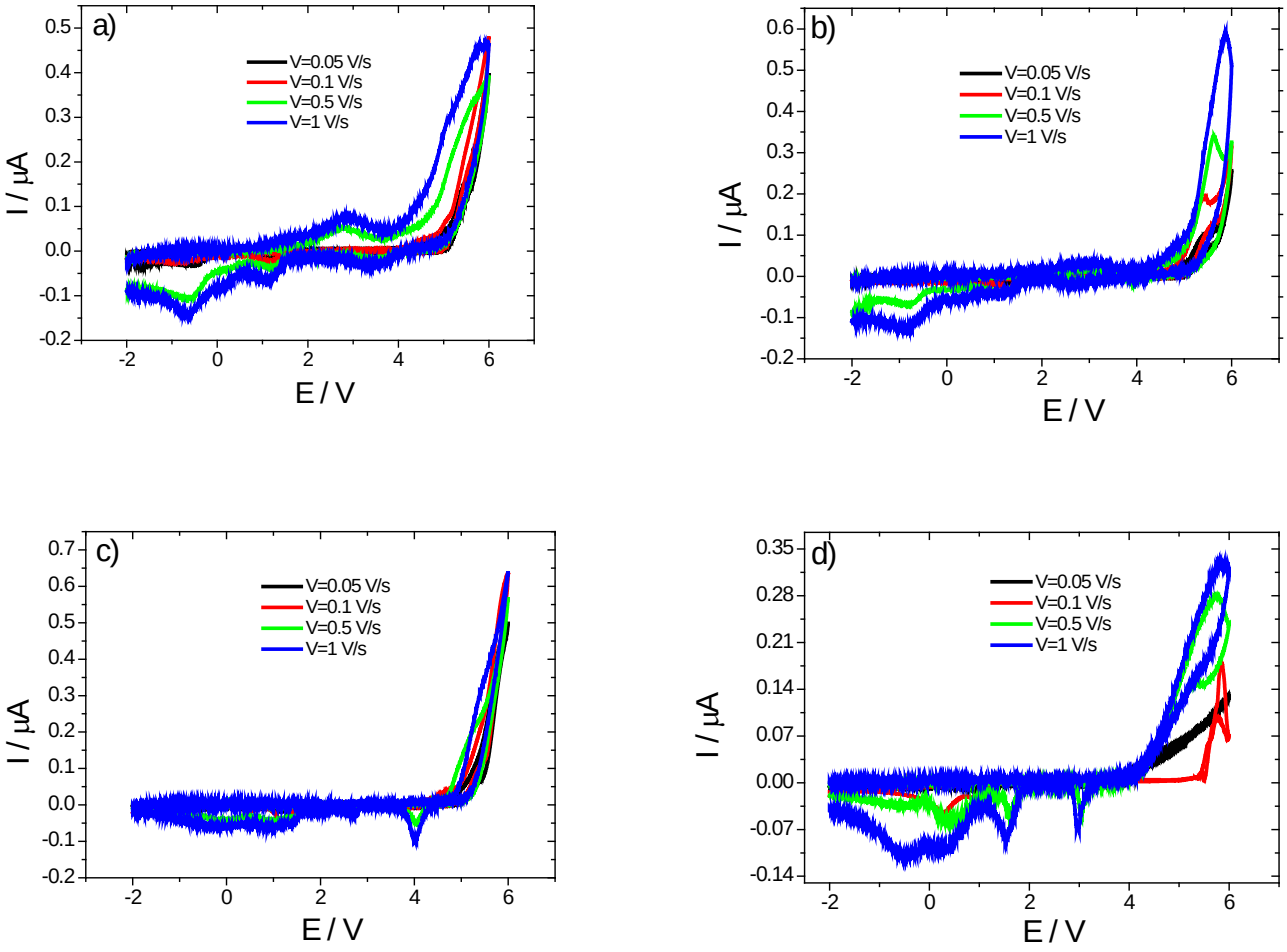

Figure 7.10 - Voltammogram of the membranes at different scanning rates for: a)$LiBF_4$, b) LiTFSI, c) $Na(CF_3SO_3)$ and d) $Mg(CF_3SO_3)_2$.

The voltammograms of figure 7.10 reflect a wide voltage window of electrochemical stability of the membranes immersed in the different electrolyte solutions.

Both cathodic and anodic current peaks are present in the voltammograms as illustrated in figure 7.10.

In figures 7.10 a) and b) it is observed good electrochemical stability independently of scanning rate, with anodic potentials higher than 4.0V (Li^+/Li) and oxidation peak around 0.0V (Li^+/Li). The anodic current onset may be associated with the decomposition of the polymer electrolyte.

The electrochemical deposition of lithium salts is observed in the cathodic current onset at about 0.0V in figure 7.10 a) and b) [23].

Increasing potential sweeping rate shifts the cathodic peak potential in the negative direction in all voltammograms (figure 7.10) independently of the salts present in the electrolyte solution.

The voltammograms (figure 10) do not close at -2V due of the reversibility of redox species and their dependence on the scan rate [24].

In relation of the salts with of Na^+ (figure 7.10c) and Mg^{2+} (figure 7.10d), it is observed existence of multiples cathodic peaks starting from 4.0V (Li^+/Li) due to the electrodeposition of the cation on the lithium substrate.

The voltammograms of the membranes (figure 7.10) are correlated to the different electrolyte solution as verified through the diffusion coefficient calculated from equation 9 (chapter 2). The diffusion coefficients being $9.0x10^{-5}$ cm^2/s for $LiBF_4$, $8.0x10^{-5}$ cm^2/s for LiTFSi, $1.1x10^{-4}$ cm^2/s for $Na(CF_3SO_3)$ and $7.7x10^{-5}$ cm^2/s $Mg(CF_3SO_3)_2$.

Through the electrochemical potential windows range and the diffusion coefficient determined for these membranes it is shown that these P(VDF-TrFE) membrane soaked with electrolyte solution of different salts are adequate and can be useful for separator in battery applications. Relatively the salts for lithium-ion battery applications ($LiBF_4$ and LiTFSI) it can be verified that the LiTFSI is more adequate and shows high ionic conductivity in comparison with $LiBF_4$ due the highest anion size present in the LiTFSI salt. In relation of the other salts for sodium ($Na(CF_3SO_3)$) and magnesium ($Mg(CF_3SO_3)_2$) battery applications are observed good compatibilization and affinity between salts and porous membrane adequate for this application.

7.3. Conclusions

Polymer porous membrane based on poly(vinylidene fluoride-trifluoroethylene), P(VDF-TrFE) have been developed and soaked with electrolyte solution different for Li-ion battery separator applications as well as for sodium and magnesium based batteries applications. The porous microstructure of the membrane is not influenced by the electrolyte solution.

The high uptake value of 529% is obtained for the $Mg(CF_3SO_3)_2$ electrolyte solution, and increases in the following order: LiTFSI, $LiBF_4$, $Na(CF_3SO_3)$ and $Mg(CF_3SO_3)_2$ demonstrating that electrolyte uptake depends on the anion size present in the salt.

The thermal and mechanical properties of the membranes are influenced by the presence of the electrolyte solution in the membrane due of the interaction/affinity between polymer and solvent.

Independently of the electrolyte solution, LiTFSI, $LiBF_4$, $Na(CF_3SO_3)$ or $Mg(CF_3SO_3)_2$, high ionic conductivity is obtained and for LiTFSI salt the ionic conductivity increases from 0.32 to 1.2 mS/cm when the temperature is increased from room temperature at 100ºC.

The equivalent circuit of these membranes is the Randles circuit that describes the kinetics and diffusion processes. The electrical results obtained by impedance spectroscopy and cyclic voltammetry confirm that the polymer membranes soaked in the different electrolyte solution are adequate for battery applications.

7.4. References

1. Ferreira, A., et al., *Poly[(vinylidene fluoride)-co-trifluoroethylene] Membranes Obtained by Isothermal Crystallization from Solution.* Macromolecular Materials and Engineering, 2010. 295(6): p. 523-528.
2. California, A., et al., *Tailoring porous structure of ferroelectric poly(vinylidene fluoride-trifluoroethylene) by controlling solvent/polymer ratio and solvent evaporation rate.* European Polymer Journal, 2011. 47(12): p. 2442-2450.
3. Costa, C.M., et al., *Effect of degree of porosity on the properties of poly(vinylidene fluoride–trifluorethylene) for Li-ion battery separators.* Journal of Membrane Science, 2012. 407–408(0): p. 193-201.
4. Fernandes, M., et al., *Di-ureasil hybrids doped with LiBF4: Spectroscopic study of the ionic interactions and hydrogen bonding.* Materials Chemistry and Physics, 2011. 129(1–2): p. 385-393.
5. Kim, C.S. and S.M. Oh, *Importance of donor number in determining solvating ability of polymers and transport properties in gel-type polymer electrolytes.* Electrochimica Acta, 2000. 45(13): p. 2101-2109.
6. Nunes, S.C., et al., *Ionic environment and hydrogen bonding in di-ureasil ormolytes doped with lithium triflate.* Journal of Molecular Structure, 2004. 702(1–3): p. 39-48.
7. Gonçalves, M.C., et al., *Cation coordination in mono-urethanesil hybrids doped with sodium triflate.* Electrochimica Acta, 2003. 48(14–16): p. 1977-1989.
8. Nunes, S.C., et al., *Di-ureasil ormolytes doped with Mg2+ ions: Part 2. Cationic and anionic environments.* Solid State Ionics, 2005. 176(17–18): p. 1601-1611.
9. Tian, L.-y., X.-b. Huang, and X.-z. Tang, *Study on morphology behavior of PVDF-based electrolytes.* Journal of Applied Polymer Science, 2004. 92(6): p. 3839-3842.
10. Costa, C.M., et al., *Effect of the microsctructure and lithium-ion content in poly[(vinylidene fluoride)-co-trifluoroethylene]/lithium perchlorate trihydrate composite membranes for battery applications.* Solid State Ionics, 2012. 217(0): p. 19-26.

11. Tian, Z., et al., *Preparation of poly(acrylonitrile–butyl acrylate) gel electrolyte for lithium-ion batteries.* Electrochimica Acta, 2006. 52(2): p. 688-693.
12. Quartarone, E., P. Mustarelli, and A. Magistris, *Transport Properties of Porous PVDF Membranes.* The Journal of Physical Chemistry B, 2002. 106(42): p. 10828-10833.
13. Djian, D., et al., *Macroporous poly(vinylidene fluoride) membrane as a separator for lithium-ion batteries with high charge rate capacity.* Journal of Power Sources, 2009. 187(2): p. 575-580.
14. Appetecchi, G.B., F. Croce, and B. Scrosati, *Kinetics and stability of the lithium electrode in poly(methylmethacrylate)-based gel electrolytes.* Electrochimica Acta, 1995. 40(8): p. 991-997.
15. Chang, B.-Y. and S.-M. Park, *Electrochemical Impedance Spectroscopy.* Annual Review of Analytical Chemistry, 2010. 3(1): p. 207-229.
16. Park, J.K., *Principles and Applications of Lithium Secondary Batteries*2012: Wiley.
17. Ulaganathan, M., C.M. Mathew, and S. Rajendran, *Highly porous lithium-ion conducting solvent-free poly(vinylidene fluoride-co-hexafluoropropylene)/poly(ethyl methacrylate) based polymer blend electrolytes for Li battery applications.* Electrochimica Acta, 2013. 93(0): p. 230-235.
18. Zelinka, S.L., et al., *Electrochemical impedance spectroscopy (EIS) as a tool for measuring corrosion of polymer-coated fasteners used in treated wood.* . Forest products journal, 2009. 59(1-2): p. 77-82.
19. Fernández-Sánchez, C., C.J. McNeil, and K. Rawson, *Electrochemical impedance spectroscopy studies of polymer degradation: application to biosensor development.* TrAC Trends in Analytical Chemistry, 2005. 24(1): p. 37-48.
20. Lasia, A., *Electrochemical Impedance Spectroscopy and its Applications*, in *Modern Aspects of Electrochemistry*, B.E. Conway, J.O.M. Bockris, and R. White, Editors. 2002, Springer US. p. 143-248.
21. Croce, F., et al., *A safe, high-rate and high-energy polymer lithium-ion battery based on gelled membranes prepared by electrospinning.* Energy & Environmental Science, 2011. 4(3): p. 921-927.

22. Gray, F.M. and R.S.o. Chemistry, *Polymer electrolytes*1997: Royal Society of Chemistry.

23. Cheng, H., et al., *Synthesis and electrochemical characterization of PEO-based polymer electrolytes with room temperature ionic liquids.* Electrochimica Acta, 2007. 52(19): p. 5789-5794.

24. Harnisch, F. and Freguia, S., *A basic tutorial on cyclic voltammetry for the investigation of electroactive microbial biofilms.* Chemistry – An Asian Journal, 2012. 7(3): p. 466-475.

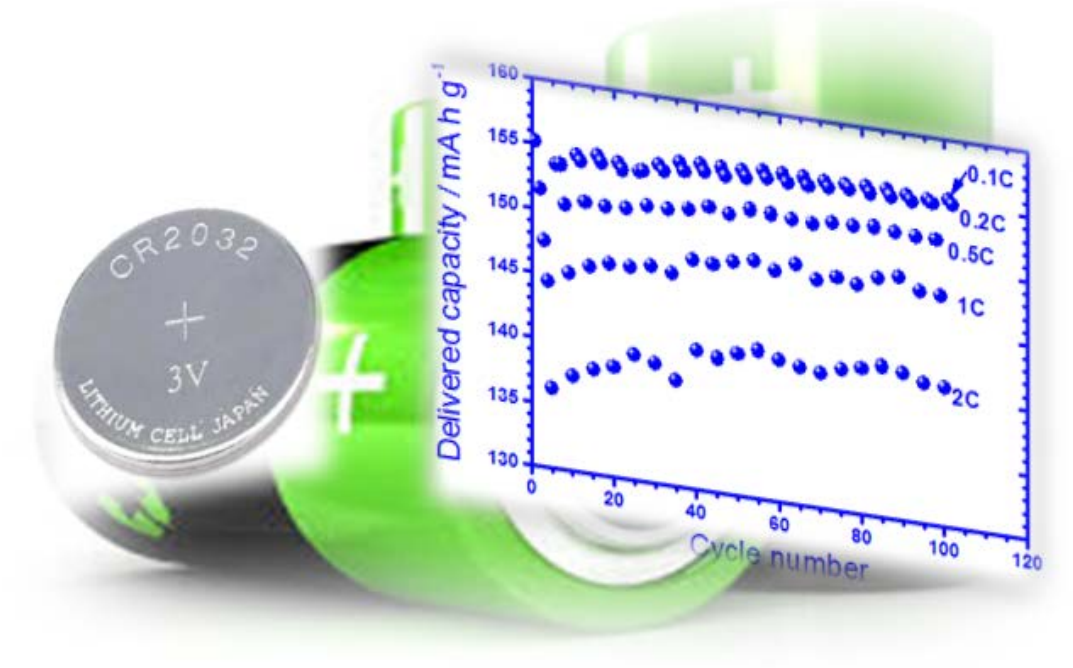

8. *Lithium-ion batteries with separator membranes based on PVDF co-polymers and blends*

This chapter report and discuss the physicochemical properties of the novel electrolyte membranes based on poly(vinylidenefluoride-co-trifluoroethylene), P(VDF-TrFE), and poly(vinylidenefluoride-co-hexafluoropropylene), P(VDF-HFP), co-polymer hosts and the P(VDF-TrFE)/poly(ethylene oxide (PEO) blend as separators for lithium-ion battery systems.

This chapter is based on the following publication:

"Poly(vinylidene fluoride)-based, co-polymer separator electrolyte membranes for lithium-ion battery systems", C. M. Costa, J. L. Gomez Ribelles, S. Lanceros-Méndez, G. B. Appetecchi, B. Scrosati, Journal of Power Sources 245 (2014) 779-786

8.1. Samples

The samples used in this chapter are P(VDF-TrFE), P(VDF-HFP) and P(VDF-TrFE)/PEO (1/1 weight ratio) polymer blend prepared from a 15/85 polymer/solvent weight ratio. The electrolyte solutions used are 1 M $LiPF_6$ in EC-DMC (1/1 in weight) and the ionic liquid of LiTFSI/PYR_{14}TFSI (mole ratio fixed equal to 1/9).

8.2. Results and discussion

The swelling effect of the separator membrane size is evidenced in Figure 8.1 which shows a picture of a P(VDF-TrFE) sample before (panel A) and after (panel B) immersing in $LiPF_6$-EC/DMC electrolyte solution.

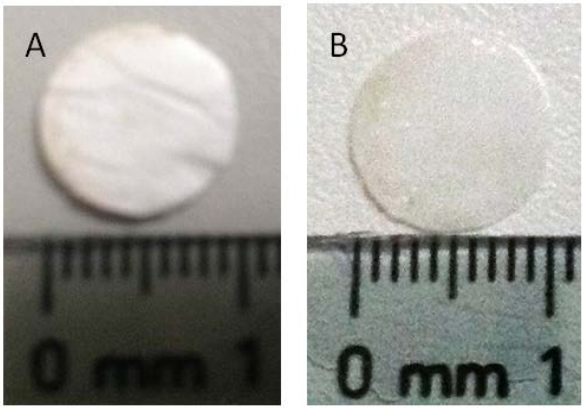

Figure 8.1 - Picture of a P(VDF-TrFE) membrane before (panel A) and upon (panel B) swelling in (1M)$LiPF_6$-EC/DMC(1/1 in weight) electrolyte solution at room temperature.

The loading with liquid electrolyte is witnessed by a slight increase in size of the sample and the turning of the membrane appearance from white to translucent. This latter behavior supports for interactions among the polymer chains and the solvent molecules. Also, the mechanical stability of the membranes is not influenced by the uptake process in the sense that no fragmentation was observed.

The morphology of the PVDF separator membranes is presented in Figure 8.2 (panels from A through C) as SEM images.

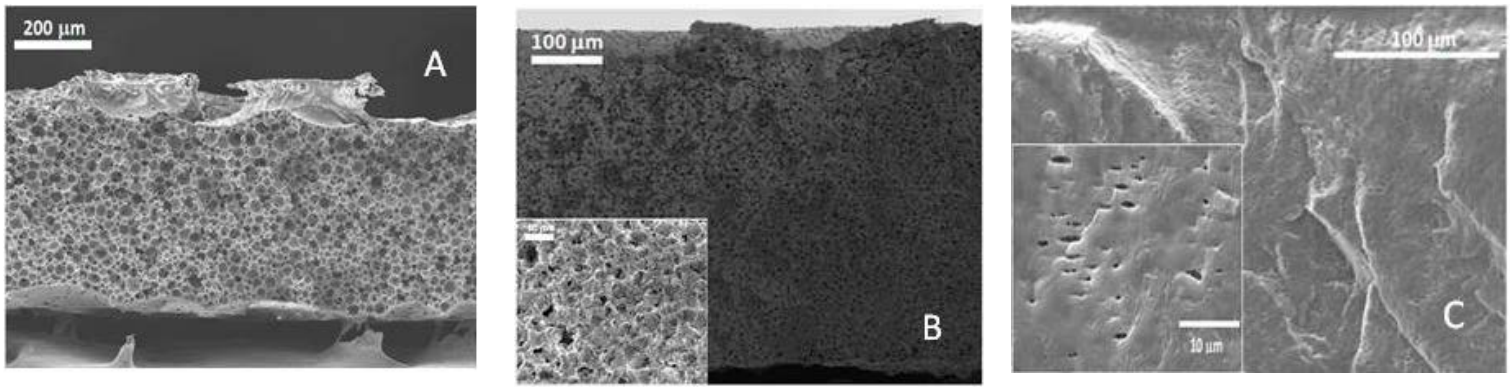

Figure 8.2 - Cross-section SEM images of different battery separator membranes. Panel A: P(VDF-TrFE); panel B: P(VDF-HFP); panel C: P(VDF-TrFE/PEO). Magnifications are depicted in the inserts.

The presence of open porosity with interconnected pathways is observed in all co-polymer samples, being the pores smaller and dispersed in the blend samples. The porosity of the P(VDF-TrFE) (panel A) and P(VDF-HFP) (panel B) membranes is the result of the polymer-solvent interaction in the phase diagram of binary systems [1] and has been explained as a liquid-liquid phase separation and consequent crystallization of the copolymer rich phase [2]. For the P(VDF-TrFE)/PEO blend (panel C), the microstructure also is determined by the crystallization process, in which PEO polymer shows large spherulites (having a diameter larger than 50 µm, images not shown [3]). In panel C of Figure 8.2 it is evidenced the roughness of the sample cross-sections, allowing to detect presence of crystalline PEO and small pores in the surface probably due to solvent evaporation (during drying at 70ºC). P(VDF-TrFE) crystallizes from solution during the drying process (70°C), thus promoting diffusion of amorphous PEO chains through the porous structure [3].

The thermal behavior of selected membranes is reported as DSC traces in Figure 8.3.

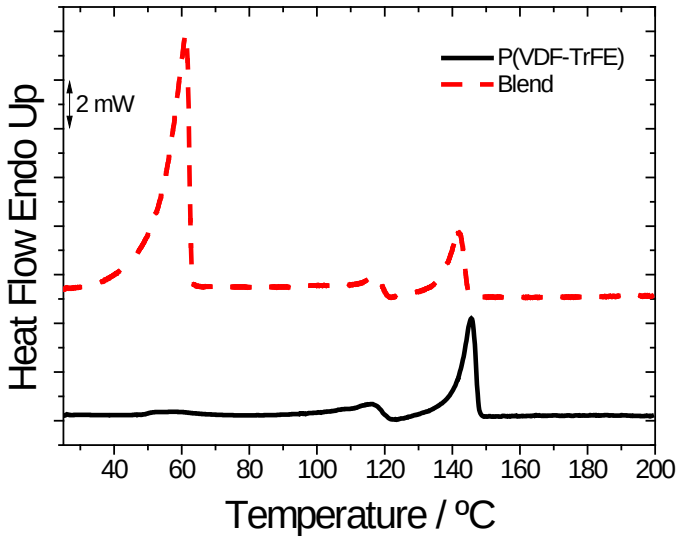

Figure 8.3 - DSC trace of selected electrolyte membranes based on different PVDF hosts. Scan rate: 10°C min^{-1}.

For the P(VDF-TrFE) sample (solid line) two endothermic peaks are observed, the first one corresponding to the ferroelectric–paraelectric phase transition (T_{FP}) identified around 117ºC whereas the second one (145ºC) represents the melting temperature. The P(VDF-HFP) sample (data not reported) displays just one peak around 135ºC which corresponds to the fusion of the polymer. The DSC trace (dotted line) of the P(VDF-TrFE)/PEO blend evidences three peaks, the first one (around 61ºC) corresponding to the PEO melting and the other ones corresponding to the fusion of the PVdF-TrFE co-polymer.

The liquid electrolyte uptake vs. dipping time dependence is illustrated in Figure 8.4 and summarized in Table 8.1.

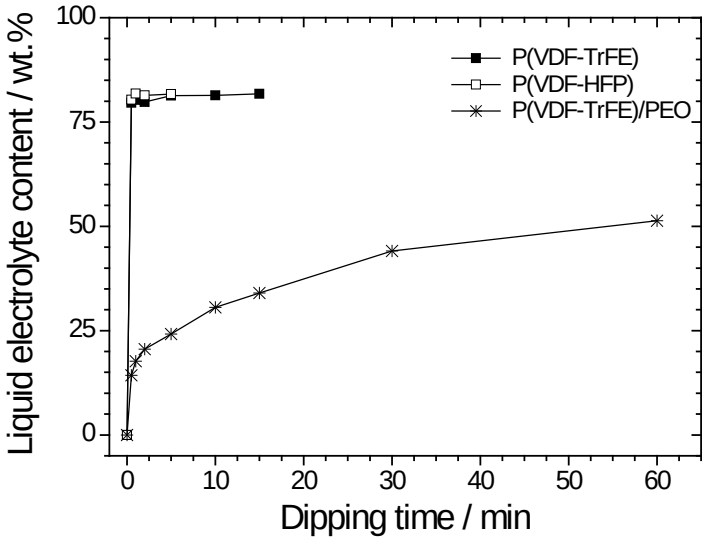

Figure 8.4 - Liquid electrolyte content vs. dipping time dependence (at room temperature) for Li+-conducting, polymer membranes based on P(VDF-TrFE), P(VDF-HFP) and P(VDF-TrFE)/PEO hosts during immersing in (1M)LiPF6-EC/DMC(1/1 in weight) electrolyte solution.

Table 8.1 - Porosity, liquid content and ionic conductivity of electrolyte membranes based on different PVDF hosts. Organic = (1M)$LiPF_6$ in EC/DMC (1/1 in weight) organic electrolyte. RTIL = (0.1)LiTFSI-(0.9)PYR_{14}TFSI ionic liquid electrolyte (0.1 and 0.9 represent the mole fractions).

Polymer host	**Porosity / % in volume**	**Liquid content / wt.%**		**Conductivity (24°C) / mS cm^{-1}**		**Conductivity (50°C) / mS cm^{-1}**	
		organic	**RTIL**	**organic**	**RTIL**	**organic**	**RTIL**
P(VDF-TrFE)	72	84	71	2.6	0.4	4.9	0.9
P(VDF-HFP)	60	81	75	3.5	0.4	4.8	1.2
P(VDF-TrFE/PEO	30	45	24	2.3	0.006	3.8	0.015

The P(VDF-TrFE) and P(VDF-HFP) membrane samples achieve saturation after approximately 6 min with a $LiPF_6$-EC-DMC content (with respect to the overall weight of the swollen membrane samples) equal to 84 wt.% and 81 wt.%, respectively, indicating that the (open) void volume was fully filled. Conversely, the P(VDF-TrFE/PEO) blend required much longer dipping times (one hour) to be saturated with a liquid electrolyte content not exceeding 45 wt.%. This larger necessary dipping time is

to be attributed to the stronger interactions of the organic electrolyte (e.g., solvent molecules and lithium salt) with the PEO host compound. In addition, despite its swelling ability in alkyl carbonate-based electrolyte solutions [4], PEO is not allowed to largely swell when constricted in a blend with other polymeric materials (e.g., PVDF). The lower porosity exhibited by the P(VDF-TrFE/PEO) blends with respect to the neat P(VDF-TrFE) membranes is indicated by their less remarkable liquid uptake (Figure 8.4).

The dipping tests in LiTFSI-$PYR_{14}TFSI$ led to lower electrolyte content, e.g., 71 wt.%, 75 wt.% and 24 wt.% for P(VDF-TrFE), P(VDF-HFP) and P(VDF-TrFE)/PEO, respectively, despite the higher density of the ionic liquid electrolyte (1.4 g cm^{-3}) with respect to the organic solution (1.2 g cm^{-3}), thus suggesting a lower wettability of the LiTFSI-$PYR_{14}TFSI$ mixture towards the PVDF polymer hosts. The results of the swelling tests are in agreement with the porosity measurements (Table 8.1), which have shown higher void volume fraction for the PVDF co-polymer (72% and 60% for P(VDF-TrFE) and P(VDF-HFP), respectively) with respect to the P(VDF-TrFE)/PEO blend (30%). This fact is strongly dependent on the membrane processing conditions [4, 5].

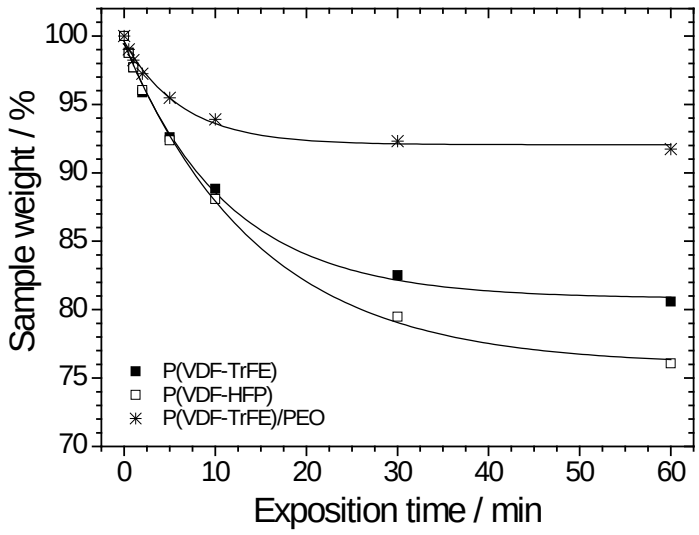

Figure 8.5 - Retention of liquid electrolyte as a function of the exposition time (at room temperature) for Li^+-conducting, polymer membranes, based on P(VDF-TrFE), P(VDF-HFP) and P(VDF-TrFE)/PEO hosts, upon swelling in (1M)$LiPF_6$-EC/DMC(1/1 in weight) electrolyte solution.

In Figure 8.5 it is displayed the weight variation (recorded at room temperature) as a function of the storage time (in glove box atmosphere) of the swollen PVDF-based separator membranes immediately after electrolyte uptake. An exponential decay in weight was detected for all investigated samples until leveling time-stable mass values upon one hour. This behavior is related to the different volatility of the solvents (EC and DMC) present in the electrolyte solution. Therefore, the weight decrease detected in the separator membranes is practically ascribed to the evaporation of DMC (boiling temperature equal to 90ºC) instead EC (248°C) [6]. Weight losses equal to 30 wt.% and 25 wt.% were observed for the P(VDF-TrFE) (solid squares) and P(VDF-HFP) (open squares) samples, respectively, after one hour evaporation whereas only a decrease in weight around 7% was recorded for the P(VDF-TrFE/PEO) blend (star). This fact is explained by the lower initial content in liquid electrolyte (Table 8.1) and to stronger interactions of the solution components with PEO.

The ionic conductivity of the PVDF-based electrolyte membranes was determined by impedance spectroscopy measurements taken on symmetric two steel electrode cells at 24°C and 50°C, which are represented in Figure 8.6 as Nyquist plots.

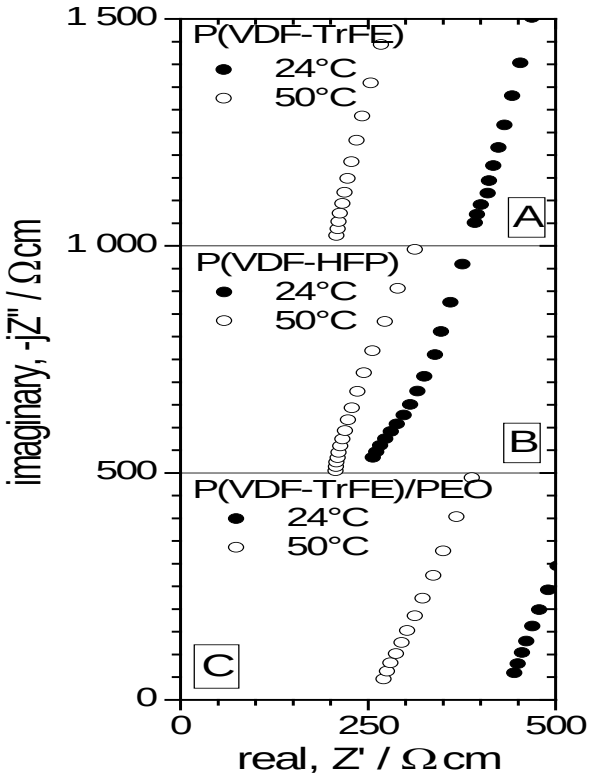

Figure 8.6 - AC response, taken at different temperatures, of Li^+-conducting, polymer membranes based on P(VDF-TrFE) (panel A), P(VDF-HFP) (panel B) and P(VDF-TrFE)/PEO (panel C) hosts upon swelling in (1M)$LiPF_6$-EC/DMC(1/1 in weight) electrolyte solution.

The AC responses, normalized toward the area and the thickness of each sample, show an inclined straight-line (typical of the blocking electrode capacitive behavior) whose intercept with the real axes, Z', gives the PVDF-based electrolyte membrane ionic resistance [7, 8]. At 24°C the P(VDF-HFP) electrolyte sample (panel B) exhibits a partial small semicircle (at high frequencies) which does not fall into the origin of the axes. This is likely to be associated to a grain boundary resistance contribution [7, 8] as also confirmed by the NLLSQ analysis of the AC responses. At medium temperature (50°C), a shift of the high frequency intercept inclined straight-line is observed, indicating a decrease of the electrolyte membrane ionic resistance. The ionic conductivity of the PVDF-based electrolyte membranes is depicted in Table 8.1, which

denotes how conduction values above 10^{-3} S cm^{-1} are already exhibited at room temperature (24°C). Also, it is to note that the P(VDF-TrFE)/PEO blend sample, even if able to retain reduced liquid electrolyte amounts (Table 8.1), shows conduction values only slightly lower with respect to the PVDF co-polymer electrolytes. This behavior may be ascribed to a optimal pore size and interconnection, thus allowing a better distribution of the liquid electrolyte. In Table 8.1 are also compared the conduction values determined after dipping the PVDF co-polymer separator membranes in (0.1)LiTFSI-(0.9)PYR_{14}TFSI, non-volatile, ionic liquid electrolyte. Conductivities one order of magnitude lower are observed, even still of interest for practical applications (≥ 10^{-4} S cm^{-1}) [9-14], mainly attributed to the lower viscosity of the ionic liquid electrolyte with respect the organic one [15].

Table 8.2 - Comparison among the liquid uptake and ionic conductivity values of the PVdF-based copolymer electrolyte membranes with those of various gel polymer electrolytes reported in literature.

Polymer host	Electrolyte solution	Liquid content / wt.%	Conductivity / mS cm^{-1}
PAN [16]	EC-DMC-$LiPF_6$	91	3.1 (25°C)
PMMA [17]	EC-DMC-$LiN(SO_2CF_3)_2$	78	0.7 (25°C)
PolyFluoroSilicone/PEO [18]	EC-DMC-$LiPF_6$	57	1.9 (20°C)
PVDF/CTFE [19]	PC-EC-$LiC(SO_2CF_3)_3$	79	0.7 (30°C)
PEO [4]	EC-DMC-$LiClO_4$	80	2.5 (25°C)
P(VDF-TrFE)	EC-DMC-$LiPF_6$	84	2.6 (24°C)
P(VDF-HFP)	EC-DMC-$LiPF_6$	81	3.5 (24°C)
P(VDF-TrFE)/PEO	EC-DMC-$LiPF_6$	45	2.3 (24°C)

The physicochemical properties of various gel polymer electrolytes, previously reported in literature, are compared in Table 8.2 with those of the investigated PVdF-based copolymer electrolyte membranes [4, 16-19]. The latter show analogous or superior ion conduction values despite comparable liquid uptake values are displayed. This behavior is to be ascribed to weaker interactions between the PVDF copolymer host and the liquid electrolyte (i.e., mainly solvent molecules), thus allowing faster ion transport through the membranes, even if analogous liquid retention is exhibited [4, 16-19]. It is to note that simpler and cheaper swelling process was adopted for PVDF copolymer with respect to other gel polymer electrolyte systems [4, 16-19].

The performance of $Li/LiFePO_4$ cathode half-cells, preliminarily investigated in PVDF-HFP electrolyte membranes at room temperature, is reported in Figures 8.7 and 8.8.

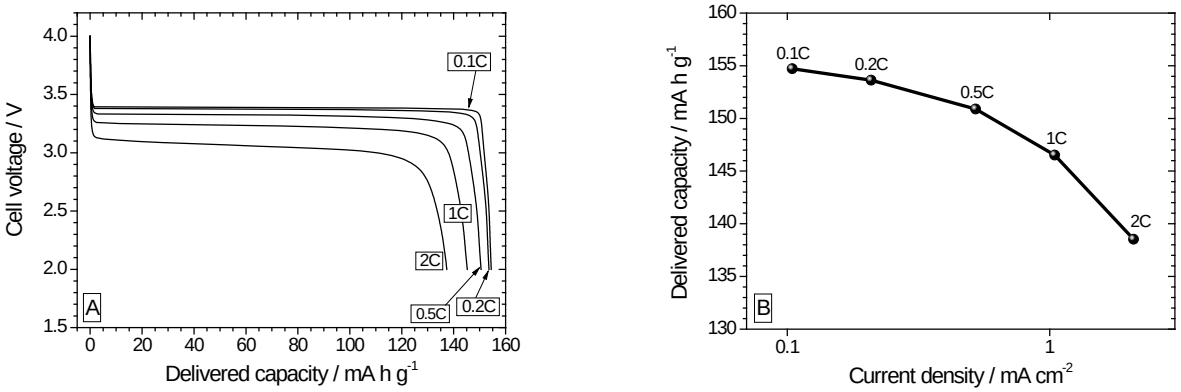

Figure 8.7 - Voltage vs. capacity discharge profiles (panel A) and capacity vs. current density dependence (panel B) of $Li/LiFePO_4$ cathode half-cells containing Li^+-conducting, P(VDF-HFP) separators swollen in (1M)$LiPF_6$-EC/DMC(1:1 in weight) electrolyte solution. Discharge rate: C/10 – 2C. Charge rate: C/10. Room temperature.

Panel A of Figure 8.7 illustrates the voltage vs. capacity profile of selected discharge half-cycles obtained at various current rates, revealing a well-defined voltage curve typical of $LiFePO_4$ cathodes [20] even at high current densities. A moderate increase in ohmic drop, e.g., from 0.6 V to 0.9 V, is detected with increasing the discharge rates from 0.1C to 2C, this supporting for high conduction of the electrolyte membrane (e.g., high mobility of the Li^+ cation). In panel B of Figure 8.7 is reported the discharge capacity vs. current rate dependence. A nominal capacity equal to 155 mA h g^{-1} (91.2 % of the theoretical value) is delivered, approaching the performance achieved in $LiPF_6$-EC-DMC liquid electrolytes supported by glass fiber separators, (e.g., 155 mA h g^{-1} at 0.1C) [21-23]. It is worth noticing that at 2C (corresponding to 2.0 mA cm^{-2}) the cells are still able to deliver above 89% (corresponding to 138 mA h g^{-1}) of the capacity (155 mA h g^{-1}) discharged at 0.1C (0.1 mA cm^{-2}, e.g., at a current density twenty times lower). Such an excellent rate capability, comparable with that detected in liquid electrolyte solutions [21-23], supports, once more, for fast transport properties of the PVDF-HFP electrolyte membrane, indicating that negligible diffusive phenomena occur

up to 2.0 mA cm^{-2}. These promising results suggest that: *ii*) the liquid $LiPF_6$-EC-DMC solution, even if well confined within the PVDF-HFP host, is free to move through the membrane, thus quickly conducting Li^+ electrochemically active species; *ii*) fast ion transport also within the composite cathode (due to adequate and well interconnected pores through the electrode).

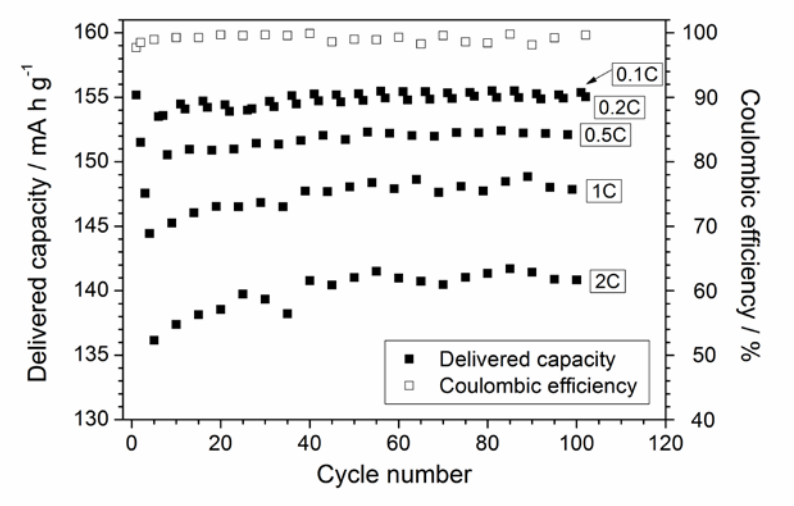

Figure 8.8 - Cycling performance (delivered capacity: solid squares; coulombic efficiency: open squares) of Li/$LiFePO_4$ cathode half-cells containing Li^+-conducting, P(VDF-HFP) separators swollen in (1M)$LiPF_6$-EC/DMC(1/1 weight) electrolyte solution at room temperature. Discharge rate: C/10 – 2C. Charge rate: C/10. Room temperature.

The results plotted in Figure 8.8 show a very good cycling behavior (delivered capacity: solid squares; coulombic efficiency: open squares) with large capacities even at high current rates (2C) and upon prolonged charge/discharge cycles run at 100% of DOD. For instance, above 99% of the initial capacity is still discharged after 100 cycles run within the full voltage range (100% DOD), thus highlighting an excellent capacity retention. This and the about 100% coulombic efficiency achievements even at high rates and upon prolonged cycling tests (Figure 8.8) are certainly related to the very good electrolyte/electrode compatibility, which results from the high purity of the electrolyte materials and the cell manufacturing besides the high stability of the cathode material.

Figures 8.9 and 8.10 illustrate the preliminary performance of Li/Sn-C anode half-cells investigated in P(VDF-TrFE) electrolyte membranes at room temperature.

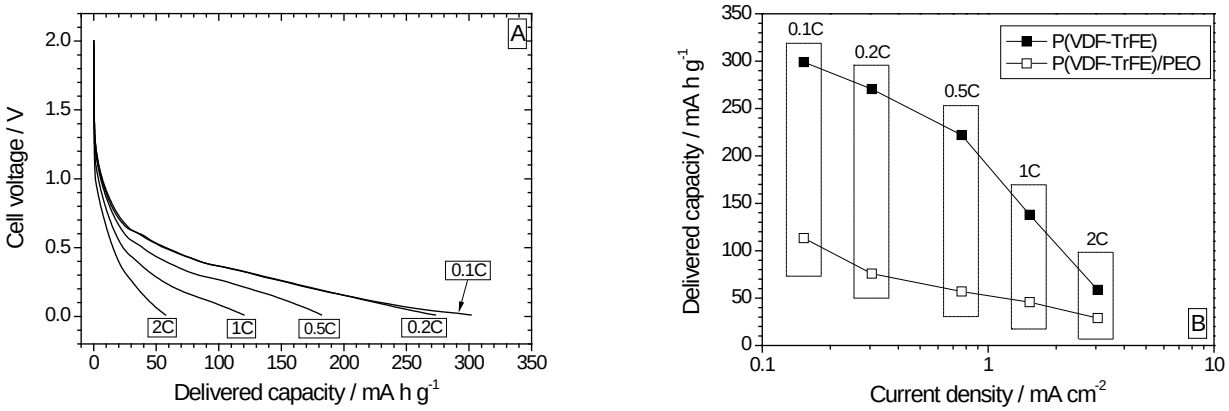

Figure 8.9 - Voltage vs. capacity discharge profiles (panel A) and capacity vs. current density dependence (panel B) of Li/Sn-C anode half-cells containing Li^+-conducting, P(VDF-TrFE) separators swollen in (1M)$LiPF_6$-EC/DMC(1/1 in weight) electrolyte solution. Discharge rate: C/10 – 2C. Charge rate: C/10. Room temperature. The rate capability referred to Sn-C anodes in P(VDF-TrFE)/PEO-based electrolyte membranes is reported in panel B for comparing purpose.

Panel A of Figure 8.9 shows the voltage vs. capacity profiles, typical of tin anodes [21-23], referred to selected discharge half-cycles run at various current rates. A moderate ohmic drop increase, e.g., from 0.7 V to 0.95 V, is recorded with increasing the discharge rates from 0.1C to 2C, once more indicating fast Li^+ ion conduction for the P(VDF-TrFE) electrolyte membrane. In panel B of Figure 8.9 is depicted the discharge capacity vs. current density behavior. A nominal capacity equal to 300 mA h g^{-1} is delivered, which is found to decrease with the current rate. Large capacity values are observed up to 0.5C (about 0.8 mA cm^{-2}), e.g., 300 mA h g^{-1}, 270 mA h g^{-1} and 230 mA h g^{-1} are discharged at 0.1C, 0.2C and 0.5C, respectively. Appreciable capacities (about 140 mA h g^{-1} and 60 mA h g^{-1}) are still delivered at higher rates (1C and 2C, respectively). Differently to that recorded for the P(VDF-HFP) membrane adopted as the electrolyte separator in Li/$LiFePO_4$ cells (e.g., analogous performance with respect to the one observed in $LiPF_6$-EC-DMC solutions), these values are, however, lower than the results observed in liquid electrolyte (e.g., 450 mA h g^{-1} at 0.2C) [21-23], which is to be ascribed to the inferior ion conduction of the P(VDF-TrFE) polymer electrolyte

(2.6 mS cm^{-1} at 24°C) with respect to the P(VDF-HFP) (3.5 mS cm^{-1} at 24°C) membrane (Tables 8.1 and 8.2). This behavior, taking also into account that the P(VDF-TrFE) membranes showed a higher liquid uptake (84 wt.%) with respect to the P(VDF-HFP) (81 wt.%), is to be ascribed to higher interactions of the P(VDF-TrFE) host with the $LiPF_6$-EC-DMC solution, thus leading to slower transport properties.

The data plotted in panel B of Figure 8.9 show two well-defined linear trends with a knee at 0.8 mA cm^{-2} (0.5C), due to the delivered capacity limitation originating from different diffusive phenomena taking place in the electrolyte membrane (higher rates) and in the anode active material phase (lower rates).

For instance, the value of 0.8 mA cm^{-2} may be taken as the current density limit for the P(VDF-TrFE) electrolyte separator.

The lower rate capability with respect to the Li/$LiFePO_4$ half-cells is likely addressed to the less conductive P(VDF-TrFE) electrolyte membrane (in comparison to the P(VDF-HFP) electrolyte separator) and more marked diffusive phenomena within the Sn-C active material (with respect to $LiFePO_4$ [20-23]).

Finally, the capacity vs. current rate dependence of Li/Sn-C half-cells in P(VDF-TrFE)/PEO blend electrolyte (open square markers) is reported for comparison purpose.

As clearly evidenced from panel B of Figure 8.9, reduced capacity values are observed, likely due to the remarkably lower ion conduction of the P(VDF-TrFE)/PEO membrane (Table 8.1).

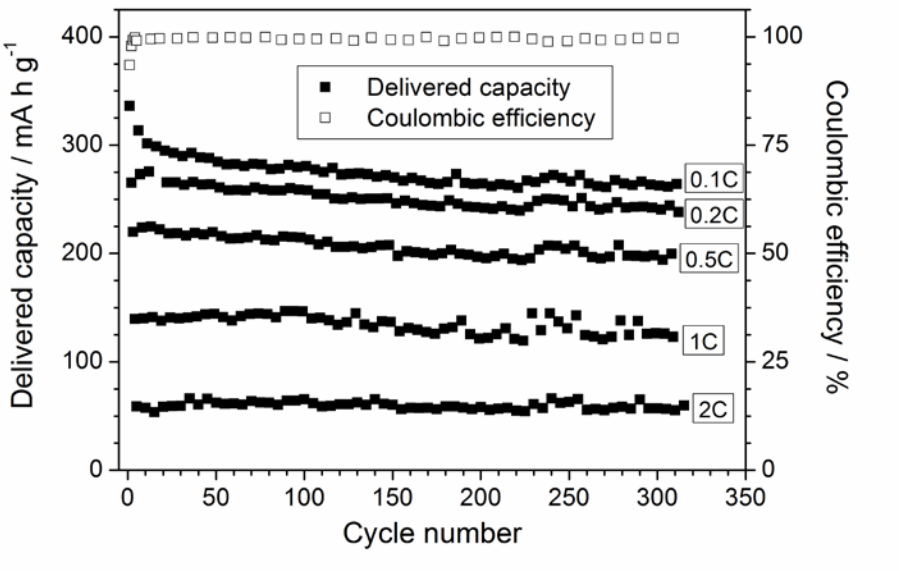

Figure 8.10 - Cycling performance (delivered capacity: solid squares; coulombic efficiency: open squares) of Li/Sn-C anode half-cells containing Li^+-conducting, P(VDF-TrFE) separators swollen in (1M)$LiPF_6$-EC/DMC(1:1 in weight) electrolyte solution at room temperature. Discharge rate: C/10 – 2C. Charge rate: C/10. Room temperature.

The rate performance of the Li/Sn-C half-cells in P(VDF-TrFE) electrolyte membrane is also observed in Figure 10 where are displayed the delivered capacity vs. cycle trend (solid squares) and the coulombic efficiency evolution (open squares) at increasing current rates from 0.1C (0.15 mA cm^{-2}) to 2C (3.0 mA cm^{-2}). A very good cycling behavior is shown even upon prolonged charge/discharge cycles run at 100% of DOD. It is to note that a better capacity retention is observed at high instead at low rates. At 0.1C, upon an initial value equal to 336 mA h g^{-1}, the capacity is seen to leveling at 300 mA h g^{-1} after 10 cycles and, then, almost linearly decreasing down to 264 mA h g^{-1} upon further 165 consecutive cycles, corresponding to a fade equal to 0.05% per cycle, due to the intrinsic fading of deeply discharged Sn-C anodes [21-23] rather than to P(VDF-TrFE) electrolyte misbehavior and/or cell design. Conversely, above 99% of the capacity initially delivered at 2C was discharged after 180 cycles, corresponding to a fade lower than 0.002% per cycle. This behavior can be mainly ascribed to the intercalation of the Li^+ ion present in the pores of the tin electrodes only. Nominally, no contribution from the Li^+ ion diffusion in the bulk electrolyte is existing in this current regime. These results and the leveled 100% coulombic efficiency value

even at high current densities and after prolonged tests (Figure 8.10) witness very good electrolyte/electrode compatibility, deriving from the high purity of the materials and cell manufacturing.

8.3. Conclusions

The physicochemical properties of electrolyte membranes based on the P(VDF-TrFE) and P(VDF-HFP) copolymers, and the P(VDF-TrFE)/PEO blend, as separators for lithium battery systems, were investigated in organic electrolytes and non-volatile, non-flammable ionic liquid-lithium salt solutions. The results have shown that the examined membranes, particularly those based on the PVDF co-polymers, are able to uptake large liquid amounts, e.g., above 80% with respect to the overall weight of the swollen sample, due to their high interconnected porosity (60-70% in volume), leading to ionic conductivity values of the order to 10^{-3} S cm^{-1} at room temperature.

Cycling tests performed on Li/$LiFePO_4$ and Li/Sn-C half-cells have revealed very good capacity retention even upon prolonged charge/discharge cycles run at high current rates and 100% of DOD. A capacity fading lower than 0.002% per cycle was observed. Particularly, the Li/$LiFePO_4$ cathode cells have exhibited excellent rate capability, being still able to deliver at 2C above 89% of the capacity discharged at 0.1C. These results, in conjunction with the about 100% coulombic efficiency, suggest very good electrolyte/electrode compatibility, which results from the high purity of the electrolyte materials and the cell manufacturing besides the high stability of the electrode active materials.

8.4. References

1. California, A., et al., *Tailoring porous structure of ferroelectric poly(vinylidene fluoride-trifluoroethylene) by controlling solvent/polymer ratio and solvent evaporation rate.* European Polymer Journal, 2011. 47(12): p. 2442-2450.
2. Ferreira, A., et al., *Poly[(vinylidene fluoride)-co-trifluoroethylene] Membranes Obtained by Isothermal Crystallization from Solution.* Macromolecular Materials and Engineering, 2010. 295(6): p. 523-528.
3. Costa, C.M., et al., *Composition-dependent physical properties of poly[(vinylidene fluoride)-co-trifluoroethylene]–poly(ethylene oxide) blends.* Journal of Materials Science, 2013. 48(9): p. 3494-3504.
4. Aihara, Y., G.B. Appetecchi, and B. Scrosati, *A New Concept for the Formation of Homogeneous, Poly(ethylene oxide) based, Gel-Type Polymer Electrolyte.* Journal of The Electrochemical Society, 2002. 149(7): p. A849-A854.
5. Gray, F.M., *Solid Polymer Electrolytes: Fundamentals and Technological Applications*1991: Wiley.
6. Xu, K., *Nonaqueous Liquid Electrolytes for Lithium-Based Rechargeable Batteries.* Chemical Reviews, 2004. 104(10): p. 4303-4418.
7. Barsoukov, E. and J.R. Macdonald, *Impedance Spectroscopy: Theory, Experiment, and Applications*2005: Wiley.
8. Chang, B.-Y. and S.-M. Park, *Electrochemical Impedance Spectroscopy.* Annual Review of Analytical Chemistry, 2010. 3(1): p. 207-229.
9. Balbuena, P.B. and Y. Wang, eds. *Lithium-Ion Batteries: Solid-Electrolyte Interphase*. 2004, Imperial College Press: London.
10. Nazri, G.A. and G. Pistoia, *Lithium Batteries: Science and Technology*2009: Springer.
11. Whittingham, M.S., *Lithium Batteries and Cathode Materials.* Chemical Reviews, 2004. 104(10): p. 4271-4302.
12. Scrosati, B. and J. Garche, *Lithium batteries: Status, prospects and future.* Journal of Power Sources, 2010. 195(9): p. 2419-2430.
13. Etacheri, V., et al., *Challenges in the development of advanced Li-ion batteries: a review.* Energy & Environmental Science, 2011. 4(9): p. 3243-3262.
14. Daniel, C. and J.O. Besenhard, *Handbook of Battery Materials*2012: Wiley.

15. Rogers, R.D., et al., *Ionic liquids: industrial applications for green chemistry*2002: American Chemical Society.
16. Appetecchi, G.B., P. Romagnoli, and B. Scrosati, *Composite gel membranes: a new class of improved polymer electrolytes for lithium batteries.* Electrochemistry Communications, 2001. 3(6): p. 281-284.
17. Appetecchi, G.B., F. Croce, and B. Scrosati, *Kinetics and stability of the lithium electrode in poly(methylmethacrylate)-based gel electrolytes.* Electrochimica Acta, 1995. 40(8): p. 991-997.
18. Appetecchi, G.B., et al., *Novel polymeric systems for lithium ion batteries gel electrolytes: II. Hybrid cross-linked poly(fluorosilicone-ethyleneoxide).* Electrochimica Acta, 2005. 50(22): p. 4396-4404.
19. Appetecchi, G.B., et al., *A poly(vinylidene fluoride)-based gel electrolyte membrane for lithium batteries.* Journal of Electroanalytical Chemistry, 1999. 463(2): p. 248-252.
20. N. Ravel, J.B.G., S. Besner, M. Gauthier, M. Armand. in *Electrochemical Society and the Electrochemical Society of Japan Meeting*. 1997. Honolulu.
21. Brutti, S., et al., *A high power Sn–C/C–LiFePO4 lithium ion battery.* Journal of Power Sources, 2012. 217(0): p. 72-76.
22. Elia, G.A., et al., *Mechanically milled, nanostructured SnC composite anode for lithium ion battery.* Electrochimica Acta, 2013. 90(0): p. 690-694.
23. Scrosati, B., *Recent advances in lithium ion battery materials.* Electrochimica Acta, 2000. 45(15–16): p. 2461-2466.

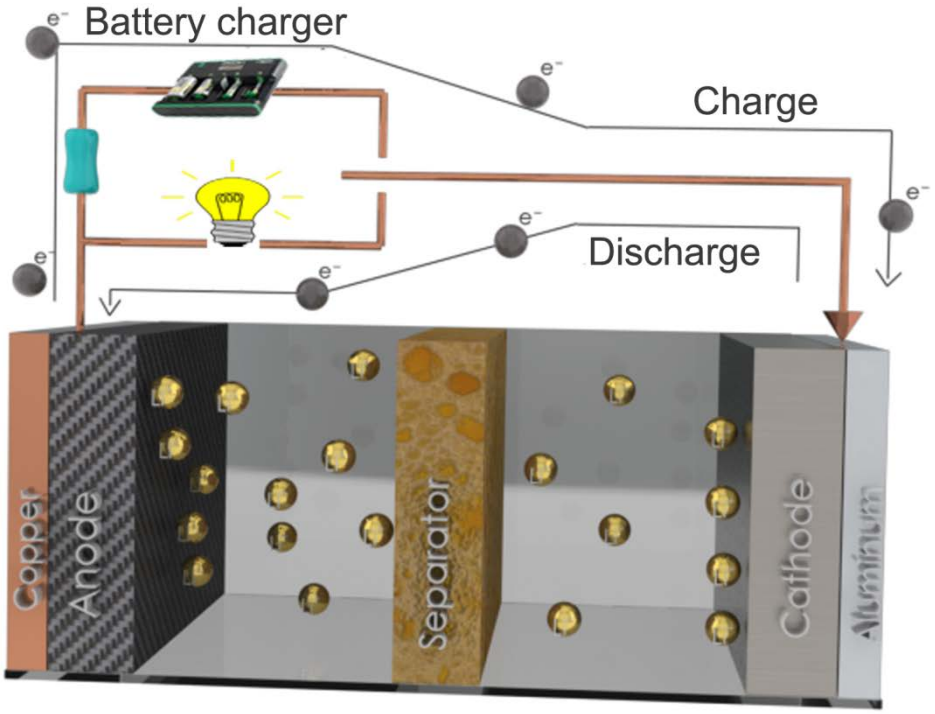

9. *Conclusions and future works*

The battery separator membrane is critical in determining the operation of a battery.

This chapter presents the main conclusions of the present work, devoted to the development of P(VDF-TrFE) co-polymer separator membranes, as well as the main challenges for future work.

9.1. Conclusion

Technological development and the constant mobility of society also lead to the question of how to generate and store energy. Energy storage is critical, in particular in the field of mobile applications and transportation.

For lithium-ion batteries, the ionic conductivity of the battery separator, related to membrane porosity, pore size and electrolyte uptake, among others, strongly influences the performance of the battery. The correlation between the membrane properties and the fabrication methods is fundamental in order to achieve adequate battery separators. It is essential the knowledge and control of their structure, stability and ionic conductivity in order to increase performance of the materials as battery separators.

In this work it has been shown that the P(VDF–TrFE) copolymer shows adequate properties for battery separator application through the control of the porosity of the membranes. By solvent evaporation at room temperature, membranes with degrees of porosity from 70% to 80% were obtained leading to the electrolyte solution uptakes from 250% up to 600%.

In relation of the composites of P(VDF-TrFE) with lithium salts, lithium salt concentration influences the ionic conductivity of the electrolytes and the best values of 2.3×10^{-6} S/cm at 120 °C were obtained. These composites show good overall electrochemical stability.

It is concluded that the best membranes for lithium ion applications are the ones with high degrees of porosity and loaded by electrolyte uptake.

Novel polymer blends based on poly(vinylidene fluoride-trifluoroethylene)/poly(ethylene oxide) were produced. In this blend, the ionic conductivity has a maximum in the samples containing 60% PEO, reaching a value of 0.25 mS cm^{-1}.

The effect of the electrolyte solution uptake in the P(VDF-TrFE) membranes was studied, the ionic conductivity of the membrane being dependent on the anion size of the salts present in the electrolyte.

The performance of the battery was evaluated in anodic (Li/Sn-C) and cathodic ($Li/LiFePO_4$) half cells.

Independently of the half-cell type, these battery separators revealed very good cycling performance even at high current rates and 100% of depth of discharge (DOD), approaching the results achieved in liquid electrolytes.

For P(VDF-TrFE) in anodic half-cell, the initial value for 0.1C is equal to 336 mA h g^{-1} and the capacity decreases to 264 mA h g^{-1} upon 165 consecutive cycles, corresponding to a fade equal to 0.05% per cycle.

In conclusion, P(VDF-TrFE) copolymer based polymer electrolytes offer broad engineering possibilities for membrane preparation with tailored microstructure and physicochemical properties, showing therefore large potential for a new generation of more efficient battery separator membranes.

9.2. Future works

The battery separator determined the safety of lithium-ion batteries and represents a strong growing research field. With respect to the future trends, membranes have to be achieved with similar large degrees of porosity (80%) but with hierarchical pore size structures down to pore sizes below 1 μm in an up-scalable way. This will allow to improve uptake without compromising mechanical properties and to obtain larger batch productions.

The incorporation of ionic liquids in the single polymer membranes is a promising field for more environmental friendly battery separators with high ionic conductivity at room temperature and wider electrochemical windows.

It can be also explored the performance of new types of battery separators through the fabrication of multilayers, coated or hierarchical pore structures to enhance the thermal, electrical, mechanical and electrochemical properties of the battery separators and to improve compatibility with electrodes.